NATIONAL ADVISORY COMMITTEE FOR AERONAUTICS

WARTIME REPORT

ORIGINALLY ISSUED
May 1941 as
Advance Confidential Report

EFFECT OF PROPELLER OPERATION ON THE PITCHING MOMENTS OF SINGLE-ENGINE MONOPLANES

By Harry J. Goett and H. R. Pass

Langley Memorial Aeronautical Laboratory
Langley Field, Va.

NACA

WASHINGTON

NATIONAL ADVISORY COMMITTEE FOR AERONAUTICS

EFFECT OF PROPELLER OPERATION ON THE PITCHING MOMENTS OF SINGLE-ENGINE MONOPLANES

By Harry J. Goett and H. R. Pass

SUMMARY

An investigation of the effects of propeller operation on pitching moments has been made with particular reference to the effect of propeller forces, the field of flow in the slipstream, and the increments of lift on the wing and the tail. Two single-engine monoplanes without flaps were tested in the full-scale wind tunnel and efforts were made to correlate the results with the available theory of the phenomena involved.

A procedure, directly applicable only to single-engine monoplanes without flaps, has been set up for predicting the effect of propeller operation on pitching moments. This procedure is, at least for the present, a satisfactory engineering approximation, as indicated by the checks obtained for the two airplanes tested. An example illustrating the procedure has been included.

INTRODUCTION

The effects of propeller operation on the longitudinal-stability characteristics of modern airplanes are becoming increasingly important as the airplanes become more highly powered. As part of a general investigation directed toward an improved understanding of stability and control, some preliminary theoretical and experimental studies have been made of the effects of propeller operation with particular reference to the single-engine monoplane without flaps. The experimental work consisted mainly of full-scale wind-tunnel tests of two airplanes and included not only force measurements but also numerous surveys of the air flow in the region of the tail. In the analysis, an effort was made to correlate the results with the available theory of the phenomena involved.

The correlation between experiments and theory was considered to be sufficiently good to justify a general procedure for calculating the effects of propeller operation for single-engine monoplanes. The method utilizes simplified concepts and generalizations for which the data

may be considered meager. It was believed, however, that an engineering approximation would be of some use for the present, at least until a more precise and complete treatment is developed.

The first part of this paper contains a résumé of the theory, together with comparisons between the theory and the subject experiments; the second part summarizes the proposed procedure for predicting the effects of propeller operation and illustrates, by an example, the method of application.

SYMBOLS

L	lift
C_L	lift coefficient
C_D	drag coefficient
M	pitching moment
C_m	pitching-moment coefficient
c_{d_o}	section profile-drag coefficient
T	axial propeller thrust
N_P	normal force acting on a propeller inclined to the air stream
D	propeller diameter unless subscripted
V	air speed
n	revolutions per second
ρ	air density
C_T	thrust coefficient $\left(\frac{T}{\rho n^2 D^4}\right)$
T_c	thrust coefficient $\left(\frac{T}{\rho V^2 D^2}\right)$
$\frac{8}{\pi} T_c$	thrust disk-loading coefficient $\left(\frac{2T}{\rho V^2 \text{ (disk area)}}\right)$

C_{N_P}	propeller normal-force coefficient $\left(\frac{N_P}{\rho n^2 D^4}\right)$
C_P	power coefficient $\left(\frac{P}{\rho n^3 D^5}\right)$
P	power input to propeller
q	local dynamic pressure $(\frac{1}{2} \rho V^2)$
q_o	free-stream dynamic pressure
q/q_o	ratio of local dynamic pressure of air stream to free-stream dynamic pressure
a	velocity-increment factor at propeller disk
V(1+a)	air velocity through propeller disk
s	velocity-increment factor back of propeller disk
V(1+s)	air velocity back of propeller disk in the slip-stream
K	function of V/nD and blade angle for an inclined propeller for determining normal force acting on propeller $(C_{N_P}/\sin \alpha_T)$
k	parameter for determining downwash behind an inclined propeller $\left(\frac{K}{T_c (V/nD)^2}\right)$
C	function of thrust distribution in normal-force equation
u	velocity inside boundary layer
a_o	lift-curve slope for infinite aspect ratio
S	area
b	span
c	chord
$\bar{c}$	mean geometric chord
l_1	distance from propeller disk to center of gravity of airplane (measured parallel to thrust line)

l_a distance from center of gravity to elevator hinge line (measured parallel to thrust line)

l_3 distance from trailing edge of root chord to elevator hinge line (measured parallel to thrust line)

d_w distance from quarter-chord point of wing to thrust line (measured perpendicular to thrust line)

d_t distance from elevator hinge line to thrust line (measured perpendicular to thrust line)

h_w distance from quarter-chord point of wing to center line of slipstream (measured perpendicular to thrust line)

h_t distance from elevator hinge line to center line of slipstream (measured perpendicular to thrust line)

z distance from center of gravity of airplane to thrust line; negative when the center of gravity is below thrust line (measured perpendicular to thrust line)

m distance above wake center line (measured perpendicular to wake center line)

x radial distance from center line of fuselage to a point in the boundary layer

R propeller radius unless subscripted

α_T angle of attack of thrust axis

β propeller blade angle

i_t angle of tail setting relative to thrust axis

γ angle between thrust line and line joining trailing edge of root chord and elevator hinge
(When the thrust line is used as a reference, the angle is positive if the tail is above the trailing edge.)

δ control-surface deflection (with subscripts); boundary-layer thickness

ϵ downwash angle

λ empirical factor used in determining increase in lift due to slipstream velocity

λ' empirical constant for wing lift due to slipstream inclination

λ_t theoretical factor used in determining increase in tail lift due to slipstream

ϕ angle of inclination of wing wake, radians

Subscripts:

o propeller-removed condition

p propeller-operating condition

P propeller

w wing

t horizontal tail

f fuselage

A airplane

e elevator

r station at intersection of wing and fuselage

i portion immersed in slipstream

is isolated

s slipstream

TESTS

The airplanes used for the tests were the Brewster XSBA-1 and the North American BT-9B; their principal dimensions are given in figures 1 and 2, respectively. A description of the NACA full-scale wind tunnel and the method of correcting the data are given in references 1, 2, and 3. The tests consisted of extensive velocity and stream-angle surveys in the region of the airplane tail and force meas-

urements on the airplane with and without the horizontal tail. These measurements were made over a range of propeller-operating conditions. The tunnel air speed for these tests was about 60 miles per hour except for a few cases in which it was varied in order to attain desired values of V/nD. Force tests of the isolated horizontal tail surfaces were also made for a range of angles of attack and elevator angles.

I. THEORY AND DISCUSSION OF RESULTS

In the analysis, the effects of propeller operation on longitudinal-stability characteristics have been considered in three parts: (1) the direct effect of the propeller forces on the lift and the pitching moment, (2) the changes imposed by the slipstream on the field of flow at the wing and at the tail, and (3) the increments of lift on both the wing and the tail resulting from these changes. These factors are discussed in the following sections.

Effect of Propeller Forces on Lift and Pitching Moment

The resultant force exerted by a propeller with its axis inclined, may be divided into two components in the vertical plane: the thrust acting along the propeller axis and the force normal to this axis at the propeller disk. The resultant lift and pitching-moment increments are:

$$\Delta L = T \sin \alpha_T + N_P \cos \alpha_T \qquad (1)$$

$$\Delta M = Tz + N_P l_1 \qquad (2)$$

The value of T in this equation, as shown in reference 4, may be obtained from propeller data for an uninclined propeller. Glauert has shown (references 5 and 6) the normal force on an inclined propeller N_P to be a function of the angle of inclination, of V/nD, of C_P, and of the thrust distribution along the blade. The normal force may be expressed as

$$N_P = C_{N_P} \rho n^2 D^4 \qquad (3)$$

where

$$C_{N_P} = K \sin \alpha_T \qquad (4)$$

From Glauert's equations,

$$K = C\, C_P \left(\frac{V}{nD}\right)\left(1 - \frac{V}{nD}\,\frac{1}{2C_P}\,\frac{dC_P}{d\frac{V}{nD}}\right) \qquad (5)$$

where C is a function of the thrust distribution. According to reference 6, $C = 0.365$ and, according to reference 5, C varies with V/nD. The correspondence of Glauert's theory with the experimental results of Lesley (reference 4) is shown in figure 3. With $C = 0.365$, excellent agreement is obtained, as noted by Millikan in reference 7.

The average variation of K, when $C = 0.365$, with the parameters V/nD and β, is shown in figure 4 for the three-blade propellers of references 8 and 9. Up to blade angles of 45° and values of V/nD of 2.0, the various propellers showed little difference so that the plotted value may be used for preliminary estimates of the vertical force on any conventional inclined propeller within these limits. The data of reference 4 were taken for blade angles up to 28.6°; there exists no known experimental verification of the theory for the higher blade angles. In addition, plots of K against V/nD for the various propellers are very erratic at values of V/nD greater than 2.0. These limitations of the data are not considered important because these high values of blade angle and V/nD are encountered at a high speed where the angle of attack of the thrust axis is normally small. Figure 4 may be applied with sufficient accuracy to other than three-blade propellers by multiplying K by $N/3$, where N is the number of blades.

Equations (1) and (2) transformed to coefficient form with the coefficient based on the wing dimensions become

$$\Delta C_{L_P} = \frac{C_T}{(V/nD)^2}\left(\frac{2D^2}{S_W}\right)\sin \alpha_T \qquad (6)$$

(where the effect of the vertical force has been neglected because it is small) and

$$\Delta C_{m_P} = \left(\frac{2D^2}{S_W}\right)\frac{1}{(V/nD)^2}\left(C_T\,\frac{z}{c_W} + K \sin \alpha_T\,\frac{l_1}{c_W}\right) \qquad (7)$$

Comparisons between the calculated and the experimental effect of propeller operation on the pitching moment of the XSBA-1 and the BT-9B airplanes, horizontal tails removed, are given in figures 5 and 6. The agreement is considered satisfactory and indicates that the effect of propeller operation is accounted for by the propeller forces for the tail-removed condition; the effect of the slipstream on the wing-fuselage combination appears to be negligible.

The variables that determine the effect of the propeller, and which are under the control of the designer, are the vertical location of the center of gravity with respect to the thrust axis and the angle of incidence of the thrust axis with respect to the wing. It will be noted that these variables primarily control the value of $z/\bar{c}_w$. The distance of the propeller forward of the center of gravity has only a slight effect and will probably be established by other considerations. Figures 7, 8, and 9, in which only the propeller forces are varied, demonstrate the effect of the relative position of the center of gravity and the propeller on the pitching moment. In any practical application other factors, notably the flow at the tail, require consideration and would probably modify the results of these figures.

The calculated change in C_m caused by the normal force of the propeller over a normal range of $l_1/\bar{c}_w$ values, is shown in figure 7 for a conventional 1000-horsepower single-engine monoplane with characteristics the same as those of the airplane described in the illustrative example in the last section of the paper. The calculated variation due to the thrust component is shown in figure 8 and the effect of inclination of the propeller axis (the location of the propeller hub being unchanged) is shown in figure 9. It is evident that a marked change in dC_m/dC_L can be obtained by changing either $z/\bar{c}_w$ or the inclination of the propeller axis.

Field of Flow at the Tail

The velocity in the region of the horizontal tail may be considered as the resultant of three superimposed fields, namely, the fuselage wake, the wing wake, and the propeller slipstream. The separate velocity fields, shown in idealized form in figure 10, will be discussed in the following sections.

The results of the surveys of the air flow in the region of the tail are presented in figures 11 to 19 for the XSBA-1 airplane and in figures 20 to 26 for the BT-9B airplane. For the propeller-removed condition, the fuselage boundary layer, the wing wake, and the region where the two fields combine are evident. The strong local downwash fields above the fuselage are possibly associated with the flow breakdown over the cockpits. For the propeller-operating conditions, the slipstream limits are clearly defined; because of the interference from the wing and the fuselage, however, the slipstreams are not circular but generally have some other characteristic shape. The difference between the downwash angles on the two sides is due to rotation.

Fuselage wake.- The characteristics of the fuselage boundary layer are dependent upon the drag, the geometric characteristics of the fuselage, and the angle of attack. As a first approximation, however, it may be assumed that the fuselage boundary layer is symmetrical about the fuselage and that its velocity distribution varies according to the 1/7-power law (as suggested in reference 10 for fuselages):

$$\frac{u}{V} = \left(\frac{x - R_f}{\delta}\right)^{1/7} \qquad (8)$$

where R_f is the fuselage radius at the elevator hinge line and δ is the thickness of the boundary layer. It may be assumed that the momentum loss in the boundary layer near the rear of the fuselage corresponds to the entire fuselage drag D_f (reference 11); thus

$$\frac{D_f}{q_o} = 2 \iint \left[\frac{u}{V} - \left(\frac{u}{V}\right)^2\right] dS$$

$$= 4\pi \int_{R_f}^{R_f+\delta} \left[\left(\frac{x - R_f}{\delta}\right)^{1/7} - \left(\frac{x - R_f}{\delta}\right)^{2/7}\right] x\,dx$$

$$= \frac{7\pi}{60}\,\delta^2 + \frac{7\pi}{18}\,\delta\,R_f \qquad (9)$$

which may be solved for the boundary-layer thickness:

$$\delta = -1.67\, R_f + \sqrt{2.78\, R_f^2 + 2.72\, C_{D_f}\, S_w} \qquad (10)$$

where C_{D_f} is based on the wing area.

On most of the surveys behind the BT-9B airplane and on some of the surveys behind the XSBA-1 airplane, the fuselage wake was clearly defined and separated from the wing wake. For these cases the wake characteristics were in satisfactory agreement with equations (8) and (10), where C_{D_f} was the difference between the measured drag of the entire airplane and the computed drag of the wing. Both of the equations and the surveys indicate that, for the usual range of fuselage size and fuselage drag, the average velocity-increment factor in the fuselage boundary layer may be taken as -0.07.

Wing wake.- The theory describing the width and the velocity distribution of wing wakes is given in references 12 and 13, and charts are therein furnished from which the displacement of the wake below the wing trailing edge may be determined as a function of the wing lift coefficient, the plan form, and the aspect ratio.

The variation in dynamic pressure in the wing wake is given as a function of the profile drag of the wing, the distance behind the wing, and the distance above or below the wake center line. The profile drag of the inboard section of the wing, the wake of which passes over the tail, may be estimated from airfoil data. The distance behind the wing can be determined directly from the dimensions of the airplane. The distance of the tail above the wake center line may be expressed as follows (see fig. 27):

$$m = l_3 \left[\tan\left(\alpha_T - \epsilon_w\right) - \tan\gamma\right] \qquad (11)$$

which, for moderate angles, becomes

$$m = l_3 \left(\alpha_T - \epsilon_w - \gamma\right) \qquad (12)$$

The angle of downwash ϵ_w, in the center of the wake, will be approximately equal to $C_L\, \phi$, where ϕ is the angle of inclination of the wing wake (from reference 13). Table I

lists values of ϕ for wings of various taper ratios and aspect ratios.

The foregoing method was used to determine the values of q/q_0 due to the wing wake at the tail location of the XSBA-1 airplane and, because the average values of q/q_0 were also experimentally determined, a direct comparison was made. (See fig. 28.) The agreement between the experimental and the theoretical values is considered satisfactory. On the BT-9B airplane, which has a low wing and a comparatively high tail, the wing wake was below the tail throughout the flight range, as indicated by the foregoing theory.

Slipstream velocity.- The simple momentum theory indicates that the relation between the propeller thrust and the increment of dynamic pressure in the slipstream may be expressed as follows:

$$\frac{\Delta q}{q} = \frac{8}{\pi} T_c \quad \text{and} \quad a = \frac{s}{2} = \frac{1}{2}\left(-1 + \sqrt{1 + \frac{8}{\pi} T_c}\right) \qquad (13)$$

The simple theory assumes a uniform increment in velocity over the slipstream area. Owing to the nonuniform distribution of thrust along the propeller, the ratio $\Delta q/q_0$ varies considerably over the propeller-disk area; the theoretical expression, however, may be used as a good approximation of the average.

No allowance is made for the distortion of the slipstream caused by the fuselage or the wake. For the XSBA-1 and the BT-9B airplanes, the slipstream diameter in the region of the tail may be taken to be equal to the propeller diameter D instead of equal to 0.8D to 0.9D, as would be calculated from the momentum theory. A comparison between the calculated and the experimental dynamic pressure increment $\Delta q/q_0$, averaged over the propeller diameter at the slipstream center line, is given in figure 29 for the XSBA-1 and the BT-9B airplanes. It will be noted that the experimental points and the theoretical curve agree within 10 percent; it may therefore be concluded that the average characteristics of the slipstream correspond fairly well with those indicated by theory despite interference effects.

As the tail moves away from the center line of the idealized circular slipstream, the average value of $\Delta q/q_0$ taken over a span equal to the propeller diameter would

vary according to the following relation:

$$\frac{\left(\frac{\Delta q}{q_o}\right)_{h_t}}{\left(\frac{\Delta q}{q_o}\right)_{h_t=o}} = \frac{\sqrt{R^2 - h_t^2}}{R} \qquad (14)$$

where h_t is the distance of the tail above or below the slipstream center line. Actually, the slipstream is not circular but is considerably distorted by the induced sideward flow of the wing, by the fuselage, and by the propeller-slipstream rotation (reference 14). Comparison of the experimental surveys and the theory for the BT-9B and the XSBA-1 airplanes shown in figure 30 indicates that, in spite of these interference effects, equation (14) represents a fair average and the slipstream may therefore be considered cylindrical.

Increment of downwash due to the slipstream.- The theoretical angle of downflow of the slipstream behind an inclined propeller is given by Glauert (reference 5) as

$$\frac{\epsilon_P}{\alpha_T} = \frac{2a(1 + a)(1 + k)}{(1 + 2a)[1 + a(1 + k)]} \qquad (15)$$

where k is defined in terms of the normal-force constant of equation (5):

$$k = \frac{K}{T_c \left(\frac{V}{nD}\right)^2} \qquad (16)$$

Values of ϵ_P/α_T are given in figure 31 for various values of T_c and $K/(V/nD)^2$.

A further increment of downwash, corresponding to the increment of lift at the wing, exists in the slipstream; it has been assumed, as a rough approximation, to be equal to $\phi \Delta C_{L_W}$, where ϕ, given in table I, is based on the overall dimensions of the wing and ΔC_{L_W} will be discussed in a later section.

It appeared from the surveys at the tail that, to a first approximation, the downflow due to the propeller and that due to the wing are additive; that is, the average downwash angle at the tail is the sum of the wing downwash angle ϕC_L and the slipstream downwash angle averaged across the tail span $\left(\phi \Delta C_{L_w} + \epsilon_p\right) \frac{b_{t_i}}{b_t}$, where the factor b_{t_i} is the tail span immersed in the slipstream, as derived in the next section. In the theory, the downwash increment is assumed to be uniform and confined to the slipstream; actually, because of turbulence and interference, it appears to affect a considerable region outside the limits of the slipstream. For this reason the increment was averaged across the tail span when the surveys were evaluated. Comparisons of the average experimental downwash-angle increment due to the propeller across the tail with the calculated increment for the XSBA-1 and the BT-9B airplanes are shown in figures 32 and 33, respectively.

An illustration of the actual downwash-angle distribution across the span of the tail for a power-on condition is shown in figure 34. The extent to which such high rotations as shown here complicate the calculation of tail lift is unknown. The available data indicate that, unless the rotation is sufficient to cause stalling of the tail on the side where there is an upwash, it does not require separate consideration. In figure 35 are shown some results of unpublished tests of the XF4U-1 airplane in which similar thrust conditions were obtained with various values of β and V/nD, corresponding to various efficiencies and various amounts of rotation. From this figure the pitching-moment increment appears to be a function only of the thrust coefficient and is essentially independent of β.

The assumed slipstream characteristics at the tail location, together with the corresponding theoretical and experimental characteristics, are as follows:

Source	Shape of cylinder	Size	Velocity and downwash increments
Theory	Circular	0.8D to 0.9D	Uniform and confined to cylinder
Surveys	Distorted, usually with a characteristic shape	Spread over almost entire tail span (for the b_t/D ratios tested)	Nonuniform and spread over almost entire tail span (for the b_t/D ratios tested)
Assumption	Circular (fig. 30)	D (fig. 29)	Uniform and confined to cylinder (figs. 29, 32, 33)

Location of the slipstream with respect to the tail.- It is assumed (fig. 36) that the slipstream is inclined at an angle ϵ_p between the propeller and the wing and at an angle $\epsilon_p + \epsilon_w$ between the wing and the tail. The distance from the elevator hinge line to the center of the slipstream is then

$$h_t = (l_1+l_2) \tan \alpha_T - l_1 \tan \epsilon_p - l_2 \tan(\epsilon_w+\epsilon_p) - d_t \quad (17)$$

which, for small angles, reduces to

$$h_t = l_1 (\alpha_T - \epsilon_p) + l_2 (\alpha_T - \epsilon_w - \epsilon_p) - d_t \quad (18)$$

where ϵ_w is assumed to be equal to $\phi C_{L_{w_p}}$. The span of the tail immersed in the slipstream is

$$b_{t_i} = 2 \sqrt{R^2 - h_t^2} \quad (19)$$

Increments of Lift on the Wing and on the Tail

The problem of an airfoil immersed in an accelerated jet of air has been studied theoretically by Koning (reference 15) and experimentally by Smelt and Davies (reference 16).

Smelt and Davies present their results in the form (changed to NACA notation)

$$\Delta C_L = C_{L_{is}} \frac{b_i \bar{c}_i}{S} \lambda \, s - \frac{b_i \bar{c}_i}{S} \lambda' \, a_o \Delta \epsilon_s \qquad (20)$$

where $C_{L_{is}}$ is the lift coefficient of the isolated airfoil in the uniform field, λ is given by the experimental curve of figure 37 as a function of $b_i/\bar{c}_i$, and λ' is 0.6. As a matter of interest, the corresponding theoretical curve, based on Koning's results, is also shown in the figure. The first term of equation (20) corresponds to the increased velocity in the slipstream (or decreased velocity in a wake) and the second term corresponds to the change in the local angle of attack. The present discussion is concerned mainly with the application of this equation.

Increment of lift on the wing.- Inasmuch as no fuselage was used in the tests of reference 16, direct application of the results to the wing of a single-engine monoplane may appear questionable. Comparison of the calculated results from reference 16 with the results of the present tests (figs. 38 and 39) and also with the results of a P-36A model tested in the NACA 7- by 10-foot wind tunnel (fig. 40), however, showed satisfactory agreement; none of the more obvious modifications of the method to take care of the presence of the fuselage seemed to improve the agreement. Accordingly, it appears that the methods of reference 16 may be directly applied without regard to the presence of the fuselage. The methods of estimating the constants of equation (20) are here summarized:

The angle of inclination of the slipstream ϵ_p is found from figure 31 for the given values of T_c and $K/(V/nD)^2$. The velocity-increment factor back of the propeller disk s is taken as twice the velocity-increment factor at the propeller:

$$s = 2a \qquad (21)$$

The distance of the wing lifting line from the axis of the slipstream is

$$h_w = l_1 (\alpha_T - \epsilon_p) - d_w \qquad (22)$$

where the angles are in radians. The span of the part of the wing that is immersed in the slipstream is

$$b_{w_i} = \sqrt{D_1^2 - 4h_w^2} \qquad (23)$$

where

$$D_1 = D\sqrt{\frac{1 + a}{1 + s}} \qquad (24)$$

The factor λ is 1.0 for single-engine monoplanes.

The increment of lift on the wing may affect the pitching moment, depending on the location of its point of application relative to the center of gravity. The direct effect of the propeller forces, however, accounted for essentially all of the observed effect of power on the pitching moments for the tail-removed condition (figs. 5 and 6). Accordingly, for a single-engine monoplane, it appears that the change in pitching moment of the wing-fuselage combination may be neglected.

Increments of lift on the tail.- For the power-off condition, the tail suffers a loss of lift and of elevator effectiveness due to the passage of the fuselage wake over it. The effect is relatively small. It could be calculated with satisfactory accuracy by applying the methods of the preceding section, the slipstream now being replaced by the fuselage wake and the wing being replaced by the tail. The term b_{t_i} is here the diameter of the wake, which may be taken as $2(R_f + \delta)$, where δ is given by equation (10), λ is still 1.0, and s corresponds to the average velocity change in the boundary layer and may be taken as -0.07 unless the wing wake also passes over the tail, in which case s is further reduced.

Table II shows the agreement between the elevator effectiveness calculated by this method and the experimental values of the elevator effectiveness.

For the power-on condition, the increment of lift and the elevator effectiveness due to the slipstream is superimposed on the (negative) increment just discussed. Calculation of the change in elevator effectiveness by the preceding method, however, gave results much lower than the experimental results. (See table III.) The discrep-

ancy apparently comes from the use of the experimental λ-curve of figure 37, which is probably not applicable to this case because ratios of b/D covering tail planes were not tested and Koning's theory indicates that this parameter requires consideration. Koning's theoretical results (reference 15) were therefore worked up for a range of b/D covering tail planes, and a λ_t-curve was obtained (fig. 41). The agreement between the experimental elevator effectiveness and the calculated values based on this curve is much better than before (see last two columns of table III), although it is not clear why the theory should be applicable at the tail and yet give definitely high results at the wing. The value of b_{t_i} used in these calculations was derived from equation (19); it was practically equal to the propeller diameter in nearly every case.

The data were not adapted to the direct evaluation of the factor λ' (equation (20)) for the case of the tail in the slipstream. Some calculations of this parameter were made, however, by comparing the tail-on and the tail-removed data on the basis of values of s, λ_t, and $\Delta\epsilon$ values determined by the method already discussed. The best of the values thus obtained was between 0.7 and 0.9. Although, as with λ, it might be expected that λ' would be increased for the case of the tail, the data are hardly sufficient to justify a revision of its value.

All the important effects of propeller operation on the complete airplane, flaps up, have now been evaluated to at least a first approximation. As a check on the general applicability of these approximations, the effects of propeller operation on the pitching moments, and hence on the stability, were calculated for the XSBA-1 and the BT-9B airplanes. The comparison between the calculated and the experimental effects of propeller operation, together with values for the propeller-removed condition, are presented in tables IV and V and in figures 42 and 43. For the two airplanes tested, the difference between propeller-removed and propeller-operating conditions is not very marked; the largest difference shown is equivalent to about 2° of elevator deflection. The slipstream increases both the velocity of the stream and the downwash at the tail. The corresponding effect of each change on the pitching moment is considerable; these changes act in opposite ways, however, and tend to cancel, although the difference between them is still important. The difference between

the calculated and the experimental pitching moments for the XSBA-1 airplane (fig. 42) could be accounted for by a discrepancy of only approximately 1° in the downwash angle.

II. APPLICATION TO DESIGN

In this part of the paper a step-by-step method of predicting the effect of propeller operation on the pitching moment of a single-engine monoplane without flaps is outlined and illustrated by an example. It is assumed that the geometrical characteristics of the airplane are given, together with lift, drag, and pitching-moment curves for the power-off condition with tail on and off, propeller charts, and engine characteristics. A constant-speed propeller operating at constant power was chosen to simplify the demonstration. The angle of attack of the thrust axis will be taken as the independent variable throughout the calculations.

Detailed Procedure

A. Determination of propeller-operating characteristics

1. Calculate V from values of C_{L_o} obtained from wind-tunnel data.

2. Calculate V/nD and C_p from the engine characteristics.

3. Pick off values of β and C_T from appropriate propeller charts (reference 17).

B. Effect of thrust and normal force of the propeller on the lift and the pitching moment

1. Calculate $T_c = \frac{C_T}{(V/nD)^2}$ and select values of K from figure 4.

2. The effect of the thrust on the airplane lift is

$$\Delta C_{L_p} = T_c \left(\frac{2D^2}{S_w}\right) \sin \alpha_T$$

3. The effect of the propeller forces on the airplane pitching moment is

$$\Delta C_{m_P} = \left(\frac{2D^2}{S_W}\right) \frac{1}{(V/nD)^2} \left(C_T \frac{z}{\bar{c}_W} + K \sin \alpha_T \frac{l_1}{\bar{c}_W}\right)$$

C. Wing lift increment due to the slipstream

1. The location of the wing with respect to the slipstream center line is

$$h_W = l_1 (\alpha_T - \epsilon_p) - d_W \quad \text{(angles in radians)}$$

where ϵ_p is determined from figure 31.

2. The slipstream-velocity increment will be assumed to have reached its full value at the wing, so that

$$s = 2a = -1 + \sqrt{1 + \frac{8}{\pi} T_c}$$

3. The portion of the span of the wing immersed in the slipstream is

$$b_{W_i} = \sqrt{D_1^2 - 4h_W^2}, \quad \text{where} \quad D_1 = D \sqrt{\frac{1 + a}{1 + s}}$$

4. The aspect ratio of the immersed portion is $b_{W_i}/\bar{c}_{W_i}$, so that λ may now be determined from figure 37; it is usually equal to 1.0.

5. The wing-lift increment is

$$\Delta C_{L_W} = \frac{b_{W_i} \bar{c}_{W_i}}{S_W} s \left(\lambda C_{L_o} - 0.6 a_o \Delta\epsilon\right)$$

where C_{L_o} is the power-off lift coefficient, a_o is the infinite aspect ratio lift-curve slope (0.11), and $\Delta\epsilon = \epsilon_p$ is the change in angle of attack between propeller-operating and propeller-removed conditions.

The propeller-operating characteristics as determined in step A are calculated for a velocity based on the power-

off lift coefficient. Although the approximation is fairly close, a second approximation with the use of the power-on lift coefficient may be made at this point if further refinement is desired. The results of the illustrative example presented in a later section indicate that this second approximation is usually unnecessary. The change in tail lift may be assumed to be negligible.

D. Location of the tail relative to the slipstream center line and the immersed span of the tail

1. The location is

$$h_t = l_1 (\alpha_T - \epsilon_p) + l_2 (\alpha_T - \epsilon_{w_p} - \epsilon_p) - d_t$$

(angles in radians) where ϵ_p is determined from figure 31. The value of ϵ_{w_p} is calculated by the use of references 12 and 13 or from $\epsilon_{w_p} = (C_{L_o} + \Delta C_{L_w})\,\phi$, where ϕ is given in table I.

2. The portion of the span of the tail immersed in the slipstream is

$$b_{t_i} = 2\sqrt{R^2 - h_t^2}$$

and the aspect ratio of the immersed portion is $b_{t_i}/\bar{c}_{t_i}$.

E. Velocity increments at the tail

It is assumed that the tail area outside the slipstream is acted on by the free-stream dynamic pressure.

1. The velocity-increment factor due to the slipstream is

$$s_s = \sqrt{1 + \frac{8}{\pi} T_c} - 1$$

2. The velocity-increment factor in the fuselage boundary layer will be taken, for all cases, as

$$s_f = -0.07$$

3. The velocity-increment factor in the wing wake is

$$s_w = \sqrt{1 + \left(\frac{\Delta q}{q_o}\right)_w} - 1$$

where (from reference 12)

$$\left(\frac{\Delta q}{q_o}\right)_w = \frac{2.42\ c_{d_o}^{1/2}}{\frac{l_3}{c_r} + 0.3} \cos^2 \left[\frac{\frac{\pi}{2} \frac{m}{c_r}}{0.68\ c_{d_o}^{1/2} \left(\frac{l_3}{c_r} + 0.15\right)^{1/2}} \right]$$

for $$\frac{\frac{m}{c_r}}{0.68\ c_{d_o}^{1/2} \left(\frac{l_3}{c_r} + 0.15\right)^{1/2}} < 1$$

If the expression is greater than 1, $\left(\frac{\Delta q}{q_o}\right)_w = 0$;

$$m = l_3\ (\gamma - \alpha_T + \epsilon_{w_p}) \quad \text{(angles in radians)}$$

and c_{d_o} is the section profile-drag coefficient in the vicinity of the root chord.

F. Effect of slipstream on the tail pitching moment

Either of two procedures may be followed to obtain the effect of the slipstream on the tail pitching moment, depending on the manner in which the isolated tail lift is determined. Figure 44 illustrates the situation. Note that all coefficients are based on wing area.

1. The value of $C_{L_{t_{is}}}$ may be determined from propeller-removed tail-on and tail-removed tests and is

$$C_{L_{t_{is}}} = \frac{C_{L_{t_o}}}{1 + \frac{2(R_f + \delta)}{S_t} \bar{c}_{t_i} (s_f + s_w)\lambda}$$

where

$$C_{L_{t_o}} = -\frac{\bar{c}_w}{l_a}\left(C_{m_A} - C_{m_{(f+w)}}\right)$$

The value of δ is given by equation (10), a value for C_{D_f} being assumed; c_{t_i} is the mean geometric chord of the tail immersed in the fuselage boundary layer; λ is determined from figure 37 and corresponds to

$$\frac{2(R_f + \delta}{\bar{c}_{t_i}}$$

Substitution of this value of $C_{L_{t_{is}}}$ in the following equation for ΔC_{m_t} gives the effect of the slipstream on the tail pitching moment.

2. The value of $C_{L_{t_{is}}}$ may also be directly determined from the isolated tail characteristics by the use of the effective angle of attack at the tail. The isolated tail characteristics may be estimated from reference 18 or reference 19 or from wind-tunnel tests of the tail. The effective angle of attack of the tail (power off) is $\alpha = \alpha_T - \epsilon_{w_o} + i_t$, where ϵ_{w_o} may be found from references 12 and 13. The effect of the slipstream on the tail pitching moment is

$$\Delta C_{m_t} = -\frac{l_a}{\bar{c}_w}\frac{b_{t_i}\,\bar{c}_{t_i}}{S_t} s_s \left(C_{L_{t_{is}}} \lambda_t - \frac{S_t}{S_w}\lambda' a_o \Delta\epsilon\right)$$

where

$$\Delta\epsilon = \epsilon_{w_p} + \epsilon_p - \epsilon_{w_o}$$

The value of Δ_t is determined from figure 41, $\lambda' = 0.6$, $a_o = 0.11$, and the other factors have been previously evaluated.

G. Calculated effects of propeller operation

1. The power-on lift is

$$C_{L_p} = C_{L_o} + \Delta C_{L_p} + \Delta C_{L_w} + \Delta C_{L_t}$$

where ΔC_{L_t} may usually be neglected.

2. The power-on pitching moment is

$$C_{m_p} = C_{m_o} + \Delta C_{m_p} + \Delta C_{m_t}$$

3. From the plot of C_{m_p} against α_T or C_{L_p} the effect of propeller operation on pitching moments may be determined.

H. Determination of elevator angle required from trim

The problem is to calculate the power-on elevator effectiveness for each angle of attack. The procedure is very similar to that used to determine the tail-lift increment with propeller operation.

1. If it is assumed that $\left(\frac{dC_m}{d\delta_e}\right)_o$ is given,

$$\left(\frac{dC_m}{d\delta_e}\right)_{is} = \frac{\left(\frac{dC_m}{d\delta_e}\right)_o}{1 + \frac{2(R_f + \delta)}{S_t} \bar{c}_{t_i} (s_f + s_w) \lambda}$$

2. The power-on elevator effectiveness is given by

$$\left(\frac{dC_m}{d\delta_e}\right)_p = \left[1 + \frac{b_{t_i} \bar{c}_{t_i}}{S_t} \lambda_t s_s + \frac{2(R_f+\delta)\bar{c}_{t_i}}{S_t} \lambda (-0.07 + s_w)\right] \left(\frac{dC_m}{d\delta_e}\right)_{is}$$

or may also be expressed as

$$\left(\frac{dC_m}{d\delta_e}\right)_p = \left(\frac{dC_m}{d\delta_e}\right)_o + \frac{b_{t_i}\bar{c}_{t_i}}{S_t}\,\lambda_t\, s_s \left(\frac{dC_m}{d\delta_e}\right)_{is}$$

3. The elevator angle required to trim is

$$\delta_e = \frac{C_{m_p}}{\left(\frac{dC_m}{d\delta_e}\right)_p}$$

Illustrative Example

The detailed procedure of the preceding sections has been applied to a typical case. The given data are presented below and the steps in the calculation are given in table VI.

Airplane:

Wing area S_w, square feet	250
Wing span b_w, feet	40
Gross weight, pounds	6000
Ratio of distance from propeller disk to center of gravity to mean wing chord $l_1/\bar{c}_w$	1.44
Ratio of distance from center of gravity to thrust line to mean wing chord $z/\bar{c}_w$	.08
Distance from center of gravity to elevator hinge line l_2, feet	18
Aspect ratio of wing	6.4
Taper ratio of wing	2:1
Wing chord at root c_r, feet	8.34
Distance from trailing edge of root chord to elevator hinge line l_3, feet	12
Span of tail b_t, feet	12.27

L-761

Airplane (cont.):

Aspect ratio of tail	3
Taper ratio of tail	2.83:1
Ratio of tail span to wing span b_t/b_w	.506

Engine:

Ungeared engine developing 1000 horsepower at 2100 rpm

Propeller:

Constant-speed operation

Diameter of propeller, three-blade Bureau of Aeronautics drawing No. 5868-9 (reference 17), feet	9
Section profile-drag coefficient in vicinity of root chord c_{d_o}	.01

Lift and pitching-moment curves; tail on and tail off:

Data given in table VI.

The results of the illustrative example, summarized in figure 45, are of the same general nature as those obtained from the tests of the two airplanes in the full-scale wind tunnel. In general, the effects of the increased velocity and the downwash on the horizontal tail tend to cancel, although the difference may still affect the pitching moments. The results also indicate that the direct effect of the propeller is probably the most important single parameter influencing the longitudinal stability.

Figure 45, in addition, presents the pitching-moment curves for various elevator deflections and it should be noted that the longitudinal stability changes with elevator deflection.

CONCLUSIONS

The following conclusions probably apply more or less generally to single-engine monoplanes without flaps:

1. The location of the thrust line relative to the center of gravity is the most important single factor determining the effect of propeller operation on pitching moments.

2. The direct effect of the propeller forces on the pitching moment of the airplane can be calculated with satisfactory accuracy by the methods given.

3. The effect of the slipstream on the pitching moment of the wing-fuselage combination may be neglected.

4. The slipstream increases the velocity of the air at the tail but also increases the downwash, thus usually affecting the pitching moment in opposite ways.

5. The wing downwash and the downwash in the slipstream of an inclined propeller are approximately additive at the tail.

6. The velocity distribution in the fuselage boundary layer at the tail approximately obeys the 1/7-power law, and the thickness of the boundary layer corresponds to the entire fuselage drag.

7. The location of the wing wake and the velocity distribution in the wake correspond satisfactorily to equations derived in NACA Reports Nos. 651 and 648.

8. The change in the lift of the wing due to the passage of a slipstream over it may be computed with reasonable precision by the method of R. & M. No. 1788. The method has been modified, however, for application to the tail.

9. The methods of analysis used in this paper lead to a procedure that is sufficiently accurate for engineering design.

Langley Memorial Aeronautical Laboratory,
National Advisory Committee for Aeronautics,
Langley Field, Va.

REFERENCES

1. DeFrance, Smith J.: The N.A.C.A. Full-Scale Wind Tunnel. Rep. No. 459, NACA, 1933.

2. Theodorsen, Theodore, and Silverstein, Abe: Experimental Verification of the Theory of Wind-Tunnel Boundary Interference. Rep. No. 478, NACA, 1934.

3. Silverstein, Abe, and Katzoff, S.: Experimental Investigation of Wind-Tunnel Interference on the Downwash behind an Airfoil. Rep. No. 609, NACA, 1937.

4. Lesley, E. P., Worley, George F., and Moy, Stanley: Air Propellers in Yaw. Rep. No. 597, NACA, 1937.

5. Glauert, H.: Airplane Propellers. Vol. IV, div. L of Aerodynamic Theory, W. F. Durand, ed., Julius Springer (Berlin), 1935, pp. 351-359.

6. Glauert, H.: The Stability Derivatives of an Airscrew. R. & M. No. 642, British A.C.A., 1919.

7. Millikan, Clark B.: The Influence of Running Propellers on Airplane Characteristics. Jour. Aero. Sci., vol. 7, no. 3, Jan. 1940, pp. 85-103.

8. Biermann, David, and Hartman, Edwin P.: Tests of Two Full-Scale Propellers with Different Pitch Distributions, at Blade Angles up to 60°. Rep. No. 658, NACA, 1939.

9. Theodorsen, Theodore, Stickle, George W., and Brevoort, M. J.: Characteristics of Six Propellers Including the High-Speed Range. Rep. No. 594, NACA, 1937.

10. Silverstein, Abe: Toward a Rational Method of Tail-Plane Design. Jour. Aero. Sci., vol. 6, no. 9, July 1939, pp. 361-369.

11. Freemen, Hugh B.: Measurements of Flow in the Boundary Layer of a 1/40-Scale Model of the U.S. Airship "Akron." Rep. No. 430, NACA, 1932.

12. Silverstein, Abe, Katzoff, S., and Bullivant, W. Kenneth: Downwash and Wake behind Plain and Flapped Airfoils. Rep. No. 651, NACA, 1939.

13. Silverstein, Abe, and Katzoff, S.: Design Charts for Predicting Downwash Angles and Wake Characteristics behind Plain and Flapped Wings. Rep. No. 648, NACA, 1939.

14. Katzoff, S.: Longitudinal Stability and Control with Special Reference to Slipstream Effects. Rep. No. 690, NACA, 1940.

15. Koning, C.: Influence of the Propeller on the Other Parts of the Airplane Structure. Vol. IV, div. M of Aerodynamic Theory, W. F. Durand, ed., Julius Springer (Berlin), 1935, pp. 362-430.

16. Smelt, R., and Davies, H.: Estimation of Increase in Lift Due to Slipstream. R. & M. No. 1788, British A.R.C., 1937.

17. Hartman, Edwin P., and Biermann, David: The Aerodynamic Characteristics of Full-Scale Propellers Having 2, 3, and 4 Blades of Clark Y and R.A.F. 6 Airfoil Sections. Rep. No. 640, NACA, 1938.

18. Silverstein, Abe, and Katzoff, S.: Aerodynamic Characteristics of Horizontal Tail Surfaces. Rep. No. 688, NACA, 1940.

19. Martinov, A., and Kolosov, E.: Some Data on the Static Longitudinal Stability and Control of Airplanes (Design of Control Surfaces). T.M. No. 941, NACA, 1940.

TABLE I

Values of Angle of Inclination of Wing Wake ϕ for Various Wings

Aspect ratio	Taper ratio	ϕ (radian)
6	1	0.10
	2	.13
	3	.13
	5	.14
9	1	0.08
	2	.10
	3	.11
	5	.12
12	1	0.05
	2	.08
	3	.09
	5	.10

TABLE II

Experimental and Calculated Elevator Effectiveness for XSBA-1 and BT-9B Airplanes, Propeller Removed

(The λ-curve of reference 16 used for computations)

Airplane	α_T (deg)	$s_o = -0.07 + s_w$	Elevator effectiveness, $dC_n/d\delta_e$	
			Experimental	Calculated (a)
XSBA-1	1.3	-0.11	-0.014	-0.015
	3.7	-.13	-.013	-.015
	7.7	-.09	-.015	-.015
	12.7	-.07	-.016	-.015
BT-9B	0.2	-0.07	-0.014	-0.014
	3.7	-.07	-.013	-.013
	7.7	-.07	-.013	-.013
	11.9	-.07	-.013	-.013

[a]The calculated values were obtained from the following equation:

$$\left(\frac{dC_m}{d\delta_e}\right)_o = \left[1 + \frac{2(R_f + \delta)\bar{c}_{t_i}}{S_t}\lambda\ (-0.07 + s_w)\right]\left(\frac{dC_m}{d\delta_e}\right)_{is}$$

TABLE III

Experimental and Calculated Elevator Effectiveness for XSBA-1 and BT-9B Airplanes, Propeller Operating

Airplane	α_T (deg)	$\frac{8}{\pi} T_c$	s_s	Elevator effectiveness, $dC_m/d\delta_e$		
				Experimental	Calculated from λ-curve of reference 16 (a)	Calculated from λ_t-curve of reference 15 (b)
XSBA-1	3.7	0.39	0.18	-0.020	-0.017	-0.017
	7.7	.54	.24	-.020	-.018	-.019
	7.7	.71	.31	-.023	-.019	-.020
	12.7	1.30	.52	-.028	-.021	-.024
	12.7	1.60	.61	-.030	-.022	-.026
BT-9B	0.2	0.14	0.07	-0.015	-0.014	-0.014
	3.7	.21	.10	-.014	-.014	-.014
	3.7	.42	.19	-.016	-.015	-.016
	7.7	.42	.19	-.015	-.015	-.016

[a]The calculated values were obtained from the following equation:

$$\left(\frac{dC_m}{d\delta_e}\right)_p = \left[1 + \frac{b_{t_i}\bar{c}_{t_i}}{S_t}\lambda s_s + \frac{2(R_f+\delta)\bar{c}_{t_i}}{S_t}\lambda(-0.07+s_w)\right]\left(\frac{dC_m}{d\delta_e}\right)_{is}$$

For XSBA-1 airplane: $\left(\frac{dC_m}{d\delta_e}\right)_{is} = -0.016$

For BT-9B airplane: $\left(\frac{dC_m}{d\delta_e}\right)_{is} = -0.014$

[b]The calculated values were obtained from the following equation:

$$\left(\frac{dC_m}{d\delta_e}\right)_p = 1 + \left[\frac{b_{t_i}\bar{c}_{t_i}}{S_t}\lambda_t s_s + \frac{2(R_f+\delta)\bar{c}_{t_i}}{S_t}\lambda(-0.07+s_w)\right]\left(\frac{dC_m}{d\delta_e}\right)_{is}$$

TABLE IV

The Effect of Propeller Operation on the Longitudinal Stability of the XSBA-1 Airplane

$\frac{8}{\pi} T_c$	Longitudinal stability, $-dC_m/d\alpha_T$					
	$\alpha_T = 7^\circ$		$\alpha_T = 10^\circ$		$\alpha_T = 13^\circ$	
	Experimental	Calculated	Experimental	Calculated	Experimental	Calculated
(a)	0.0090	---	0.015	---	0.026	---
0.7	.013	0.011	.017	0.016	.026	0.027
.9	---	---	.018	.016	.025	.027
1.0	---	---	.018	.016	.024	.027
1.2	---	---	.018	.016	.025	.027
1.3	---	---	.018	.016	.025	.027
1.5	---	---	---	---	.025	.027
1.6	---	---	---	---	.025	.027

[a]Propeller removed.

TABLE V

The Effect of Propeller Operation on the Longitudinal Stability of the BT-9B Airplane

$\frac{8}{\pi} T_c$	Longitudinal stability, $-dC_m/d\alpha_T$					
	$\alpha_T = 5^\circ$		$\alpha_T = 7^\circ$		$\alpha_T = 11^\circ$	
	Experimental	Calculated	Experimental	Calculated	Experimental	Calculated
(a)	0.011	---	0.011	---	0.012	---
0.2	.010	0.011	.011	0.011	.012	0.013
.3	.010	.011	.011	.011	.012	.013
.5	.008	.008	.009	.011	.012	.013
.7	.007	.007	.008	.009	.012	.014
1.0	---	---	---	---	.012	.014
1.3	---	---	---	---	.012	.014

[a]Propeller removed.

TABLE VI

ILLUSTRATIVE EXAMPLE

A. Determination of propeller-operating characteristics B. Direct effect of the propeller C. Wing lift increment due to slipstream

α_T (deg)	C_{L_o}	$\sqrt{C_{L_o}}$	V (mph)	V/nD	β (deg)	C_T	T_c	K	sin α_T	ΔC_{L_p}	ΔC_{m_p}	$\frac{K}{\left(\frac{V}{nD}\right)^2}$	ϵ_p/α_T	ϵ_p (deg)	h_w (ft)	b_{w_i} (ft)	s	ΔC_{L_w}
1	0.251	0.501	283.5	0.900	25.5	0.084	0.104	0.0535	0.0175	0.001	0.006	0.066	0.170	0.2	0.13	8.8	0.14	0.009
4	.474	.689	206.5	.655	22.5	.107	.249	.0280	.0698	.011	.017	.065	.260	1.0	.47	8.5	.28	.037
8	.772	.880	161.4	.513	21.5	.120	.456	.0195	.1392	.041	.034	.074	.356	2.8	.81	8.2	.47	.075
12	1.062	1.032	137.8	.437	21.0	.129	.678	.0145	.2079	.091	.050	.076	.426	5.1	1.09	7.8	.65	.124
14	1.195	1.093	130.0	.413	20.8	.133	.780	.0135	.2419	.122	.058	.079	.451	6.3	1.21	7.7	.73	.146

A'. Determination of propeller-operating characteristics (2d approx.) D. Tail immersion in slipstream E. Velocity increments at the tail over immersed area

α_T (deg)	C_{L_p}	$\sqrt{C_{L_p}}$	V (mph)	V/nD	β (deg)	C_T	$C_{L_{w_p}}$	ϵ_{w_p} (deg)	h_t (ft)	b_{t_i} (ft)	s_s	s_f	s_w	Estimated C_{D_f}
1	0.261	0.511	278.5	0.884	25.0	0.085	0.260	1.9	-0.25	9.0	0.14	-0.07	-0.06	0.021
4	.522	.723	197.0	.629	22.0	.110	.511	3.4	.35	9.0	.28	-.07	-.07	.023
8	.888	.943	151.2	.480	21.0	.125	.847	5.2	.85	9.0	.47	-.07	-.04	.027
12	1.277	1.130	126.0	.400	20.6	.135	1.186	6.6	1.22	8.9	.65	-.07	0	.033
14	1.463	1.210	117.7	.374	20.5	.137	1.341	7.2	1.44	8.9	.73	-.07	0	.036

F. Effect of slipstream on pitching moment ($\lambda_t = 1.55$) G. Summation H. Elevator angle required for trim

α_T (deg)	$C_{L_{t_o}}$	$C_{L_{t_{is}}}$	$\Delta\epsilon$ (deg)	ΔC_{L_t}	ΔC_{m_t}	C_{L_p}	C_{m_p}	$\left(\frac{dC_m}{d\delta_e}\right)_o$	δ_{e_o} (deg)	$\left(\frac{dC_m}{d\delta_e}\right)_{is}$	$\left(\frac{dC_m}{d\delta_e}\right)_p$	δ_{e_p} (deg)
1	-0.012	-0.014	0.3	-0.002	0.006	0.259	0.037	-0.013	2.0	-0.016	-0.016	2.3
4	.003	.004	1.2	0	0	.522	.019	-.012	.2	-.015	-.018	1.1
8	.024	.028	3.2	.005	-.014	.893	-.017	-.013	-2.8	-.015	-.022	-.8
12	.048	.055	5.7	.012	-.035	1.282	-.077	-.013	-7.1	-.015	-.026	-3.0
14	.067	.078	7.0	.027	-.078	1.490	-.164	-.013	-11.1	-.015	-.028	-5.9

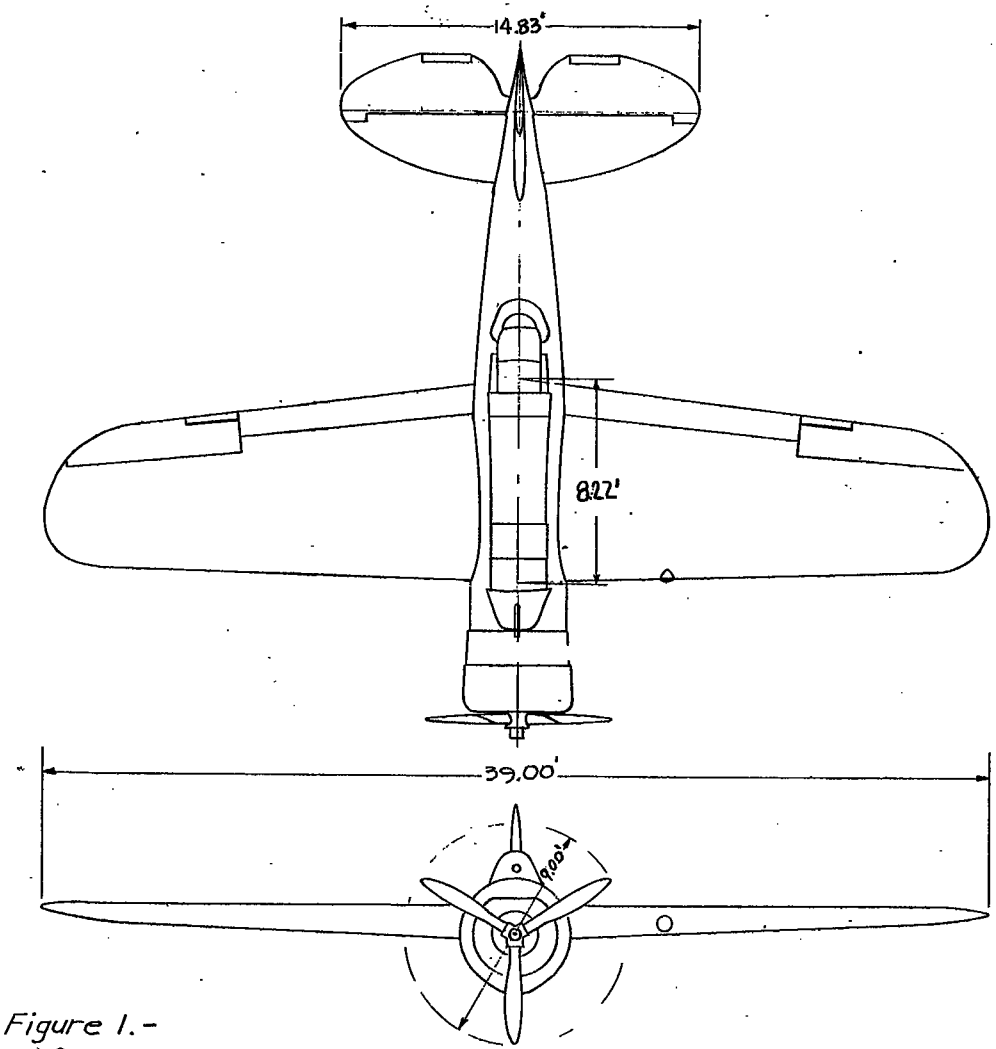

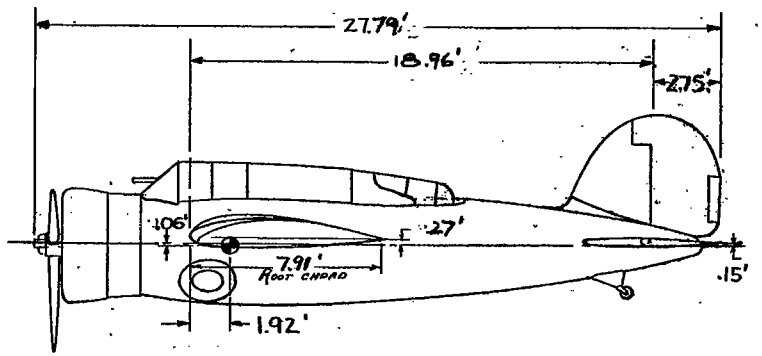

Figure 1.-

Principal dimensions of XSBA-1 airplane. Gross weight, 5921 pounds; wing area, 258 square feet. Horizontal tail area: 62.2 square feet; stabilizer (with 5.8 sq ft of fuselage), 34.5 square feet; elevator (back of hinge line), 27.7 square feet.

Fig. 1

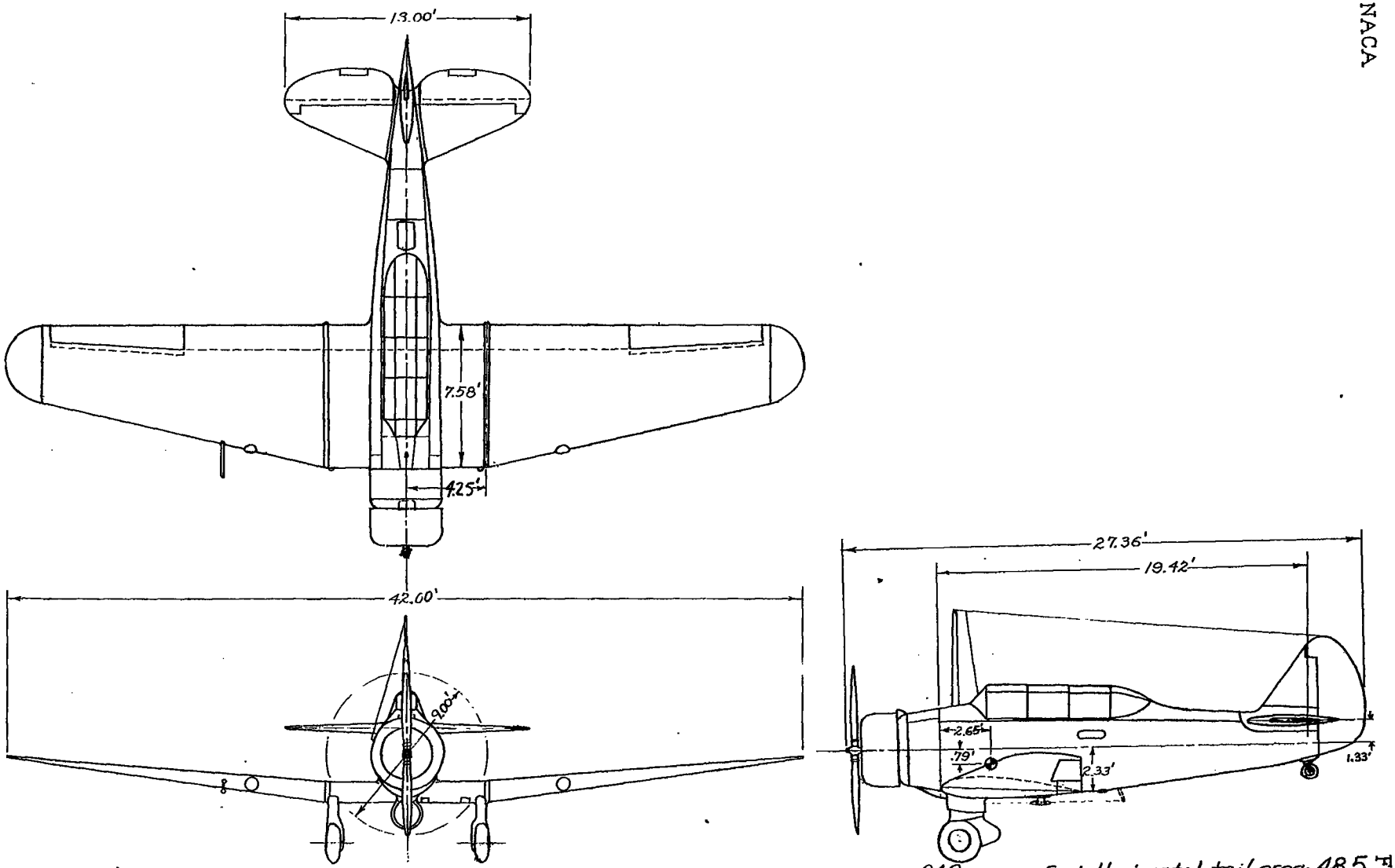

Figure 2.- Principal dimensions of BT-9B airplane. Gross weight, 4420 pounds; wing area, 248 square feet. Horizontal tail area: 48.5 square feet; stabilizer (with 4.4 sq ft of fuselage), 28.3 square feet; elevator (back of hinge line), 19.2 square feet.

Fig. 2

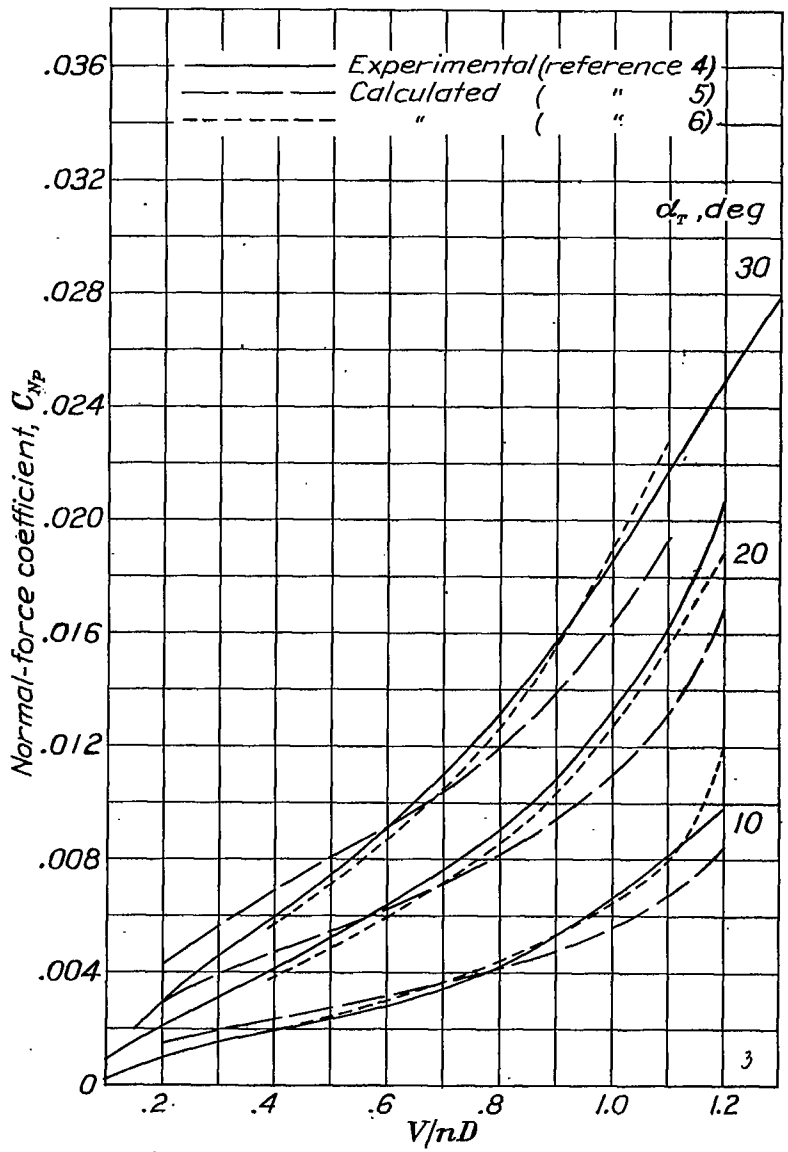

Figure 3.- Comparison of calculated and experimental normal-force coefficients. β, 24.6°.

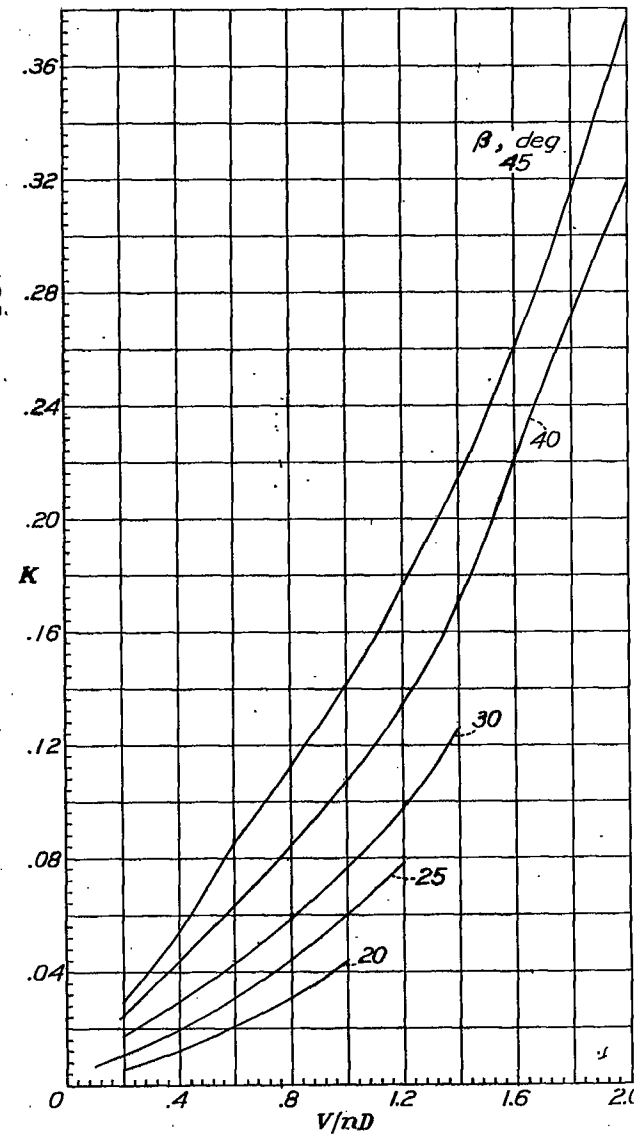

Figure 4.- Variation of K with β and V/nD for three-blade propellers. (Propeller data from references 8 and 9).

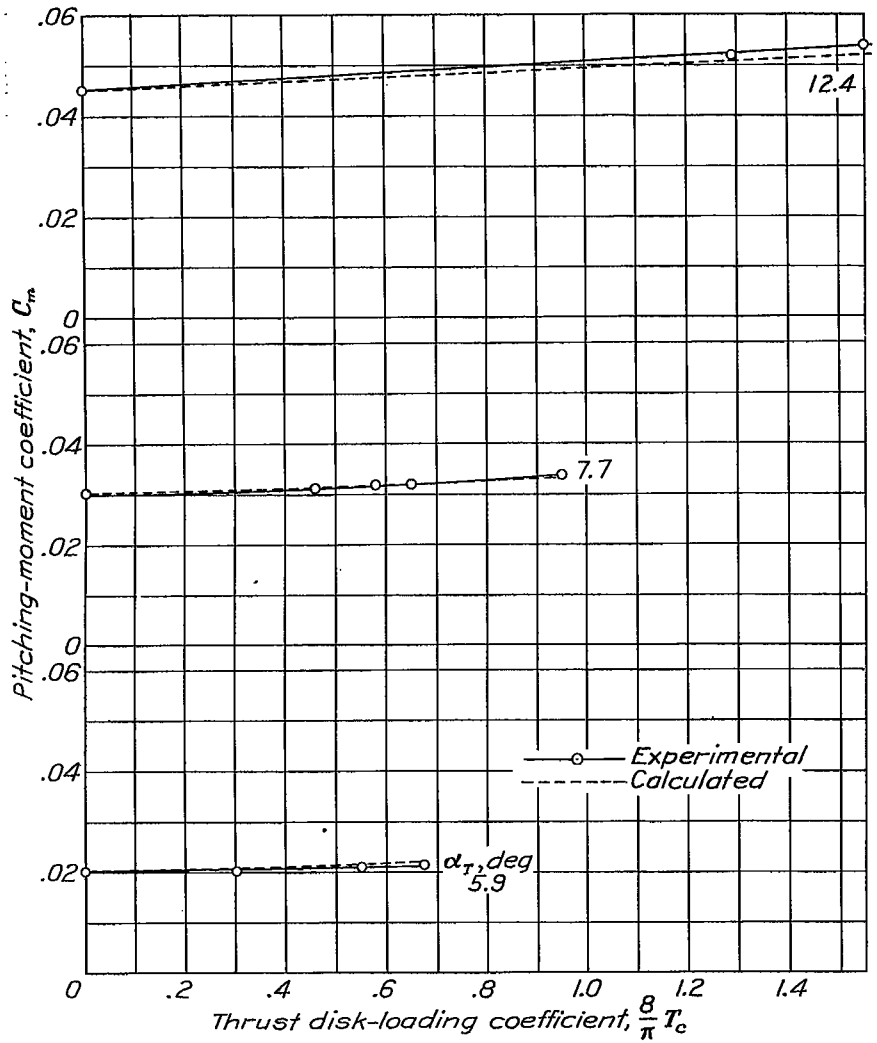

Figure 5.- Comparison of calculated and experimental effect of propeller operation on pitching moment of XSBA-1 airplane with horizontal tail removed.

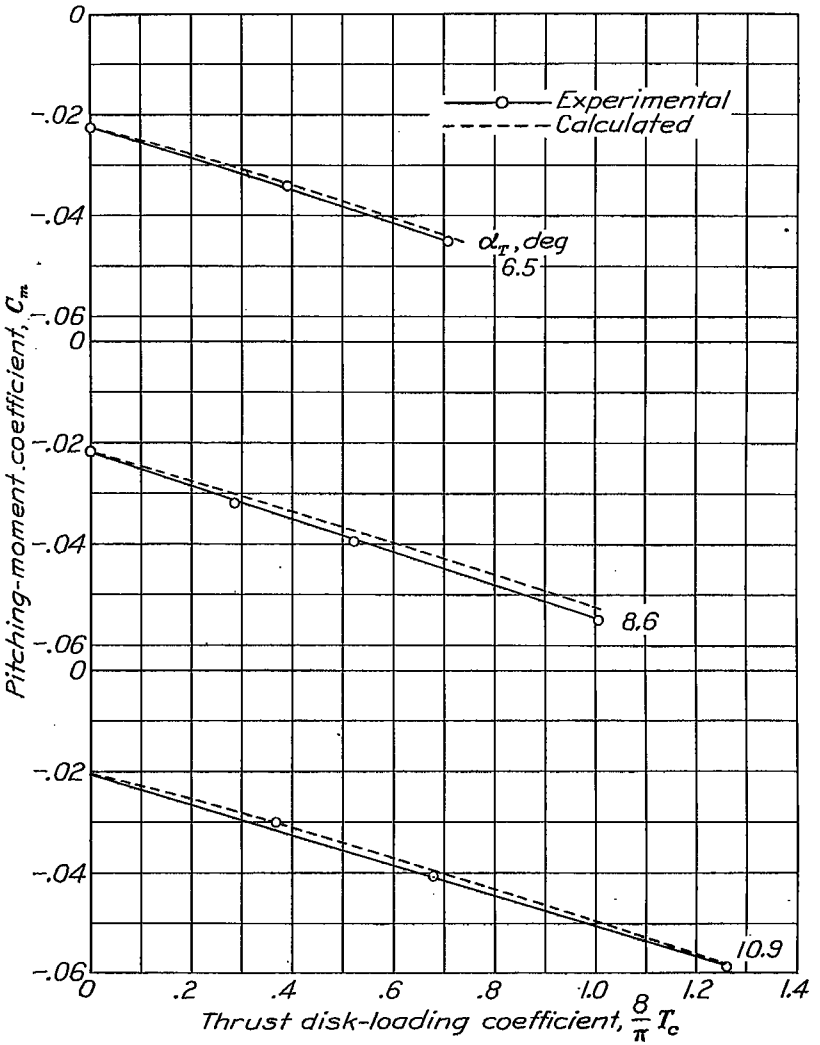

Figure 6.- Comparison of calculated and experimental effect of propeller operation on pitching moment of BT-9B airplane with horizontal tail removed.

L-761

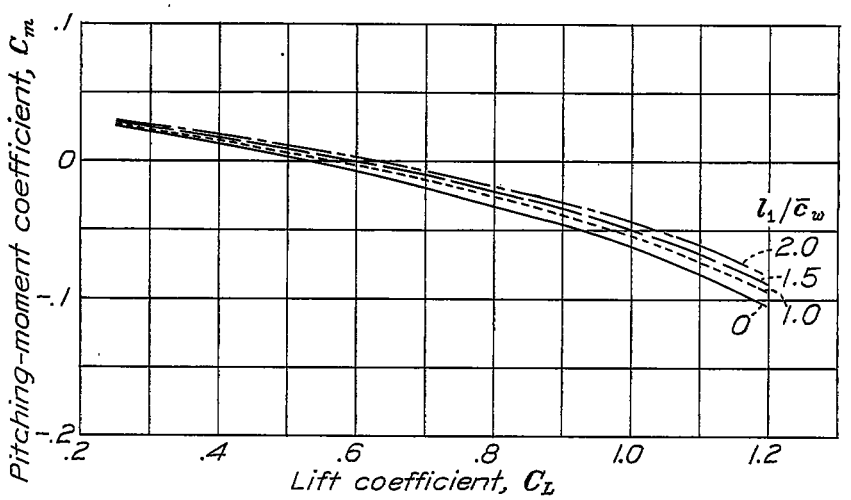

Figure 7.- Calculated effect of normal force on pitching moment for a range of $l_1/\bar{c}_w$ for a 1000-horsepower, single-engine monoplane.

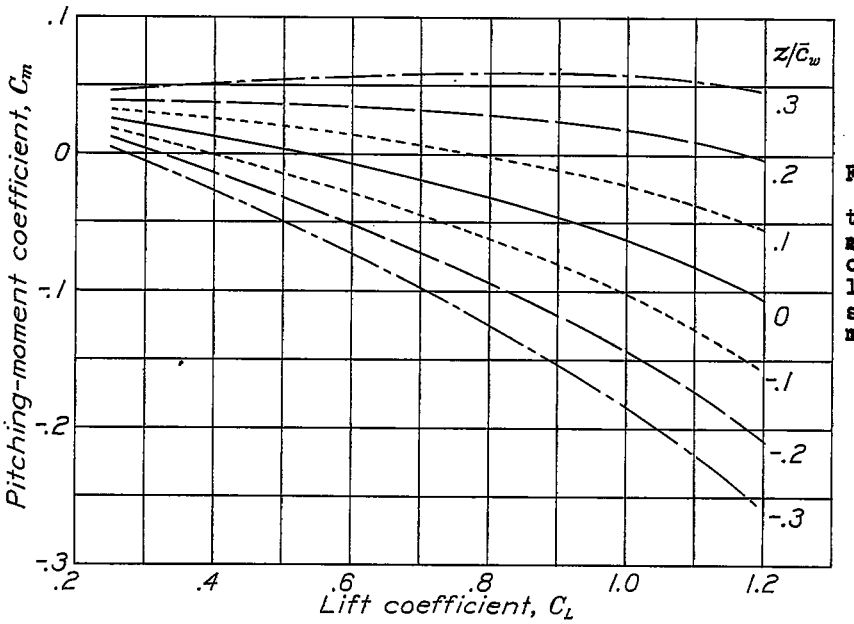

Figure 8.- Calculated effect of thrust on pitching moment for a range of $z/\bar{c}_w$ for a 1000-horsepower, single-engine monoplane.

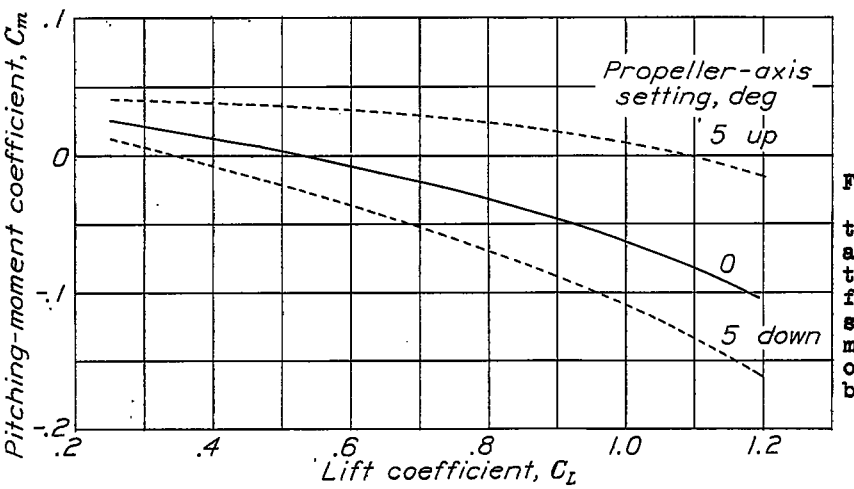

Figure 9.- Calculated effect of tilting propeller axis about propeller hub on the pitching moment for a 1000-horsepower, single-engine monoplane. Center of gravity, 1.5 $\bar{c}_w$ back of propeller.

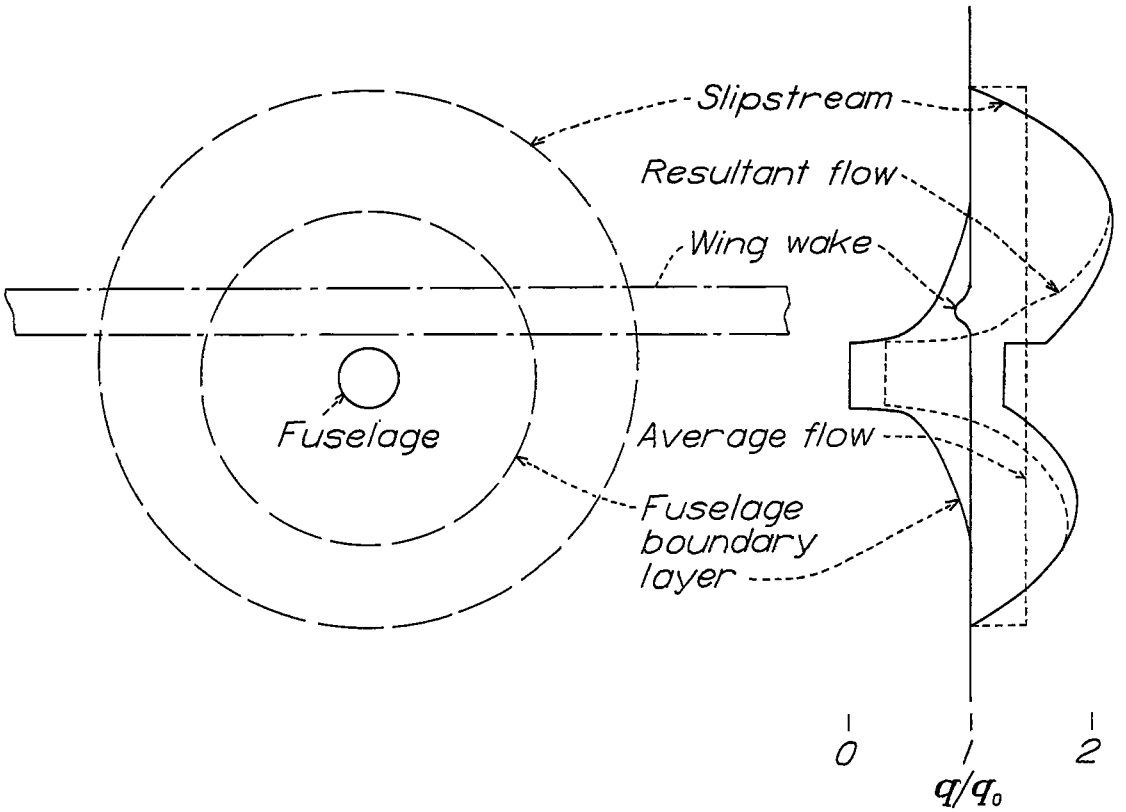

Figure 10.- Idealized cross section of field of flow at the tail of a single-engine monoplane. Dynamic-pressure distribution in a vertical plane through center of fuselage.

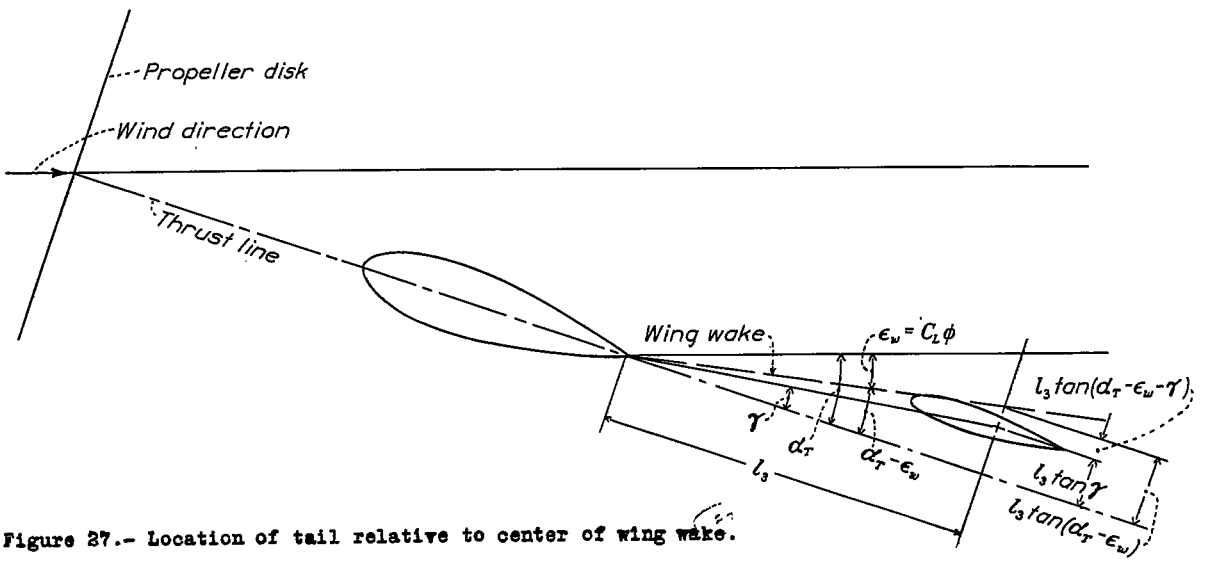

Figure 27.- Location of tail relative to center of wing wake.

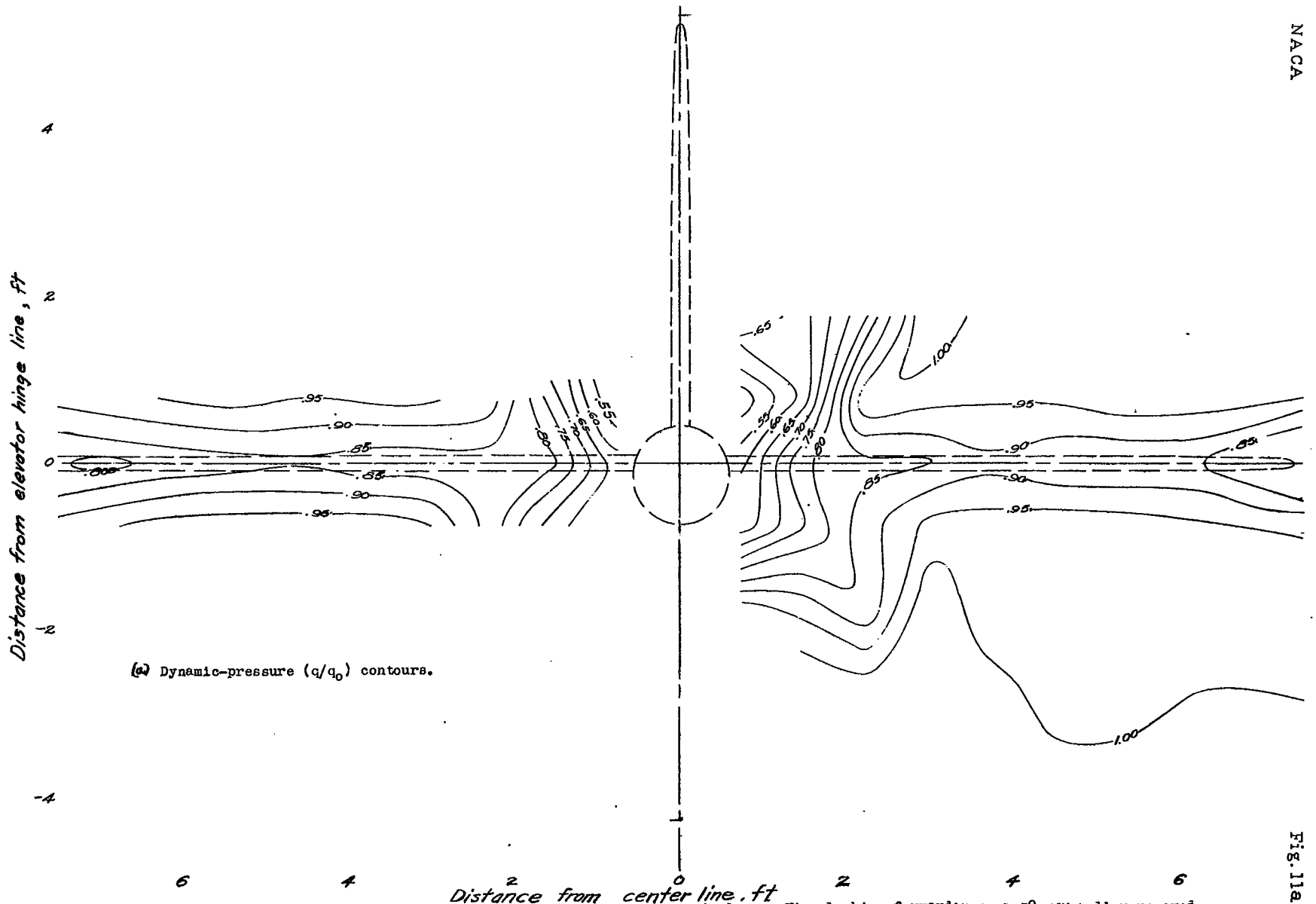

(a) Dynamic-pressure (q/q_0) contours.

Figure 11.- Air flow in the plane of the elevator hinge line of the XSBA-1 airplane. View looking forward; α_{T_c}, 1.3°; propeller removed.

NACA

Fig. 11a

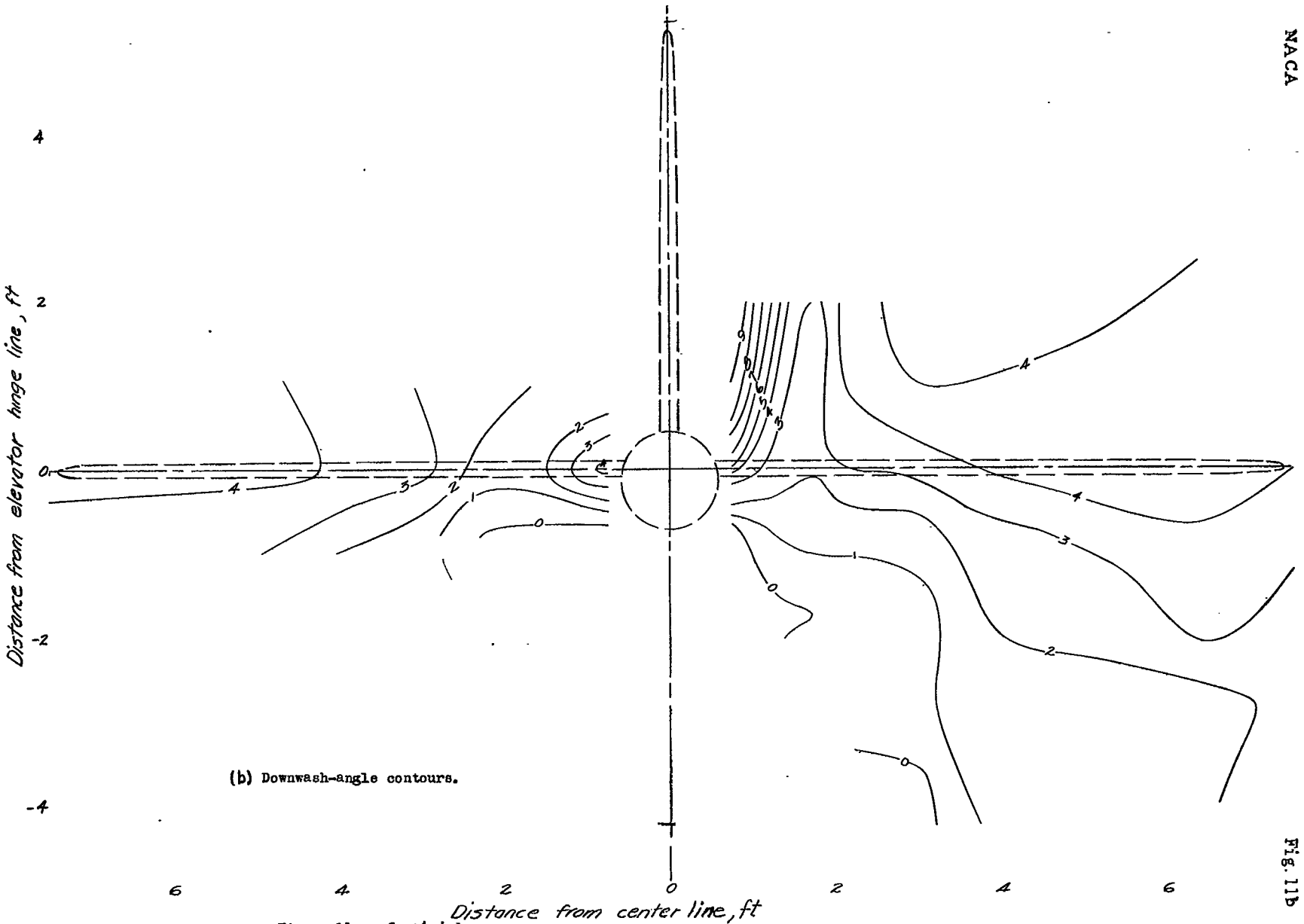

(b) Downwash-angle contours.

Figure 11. - Concluded.

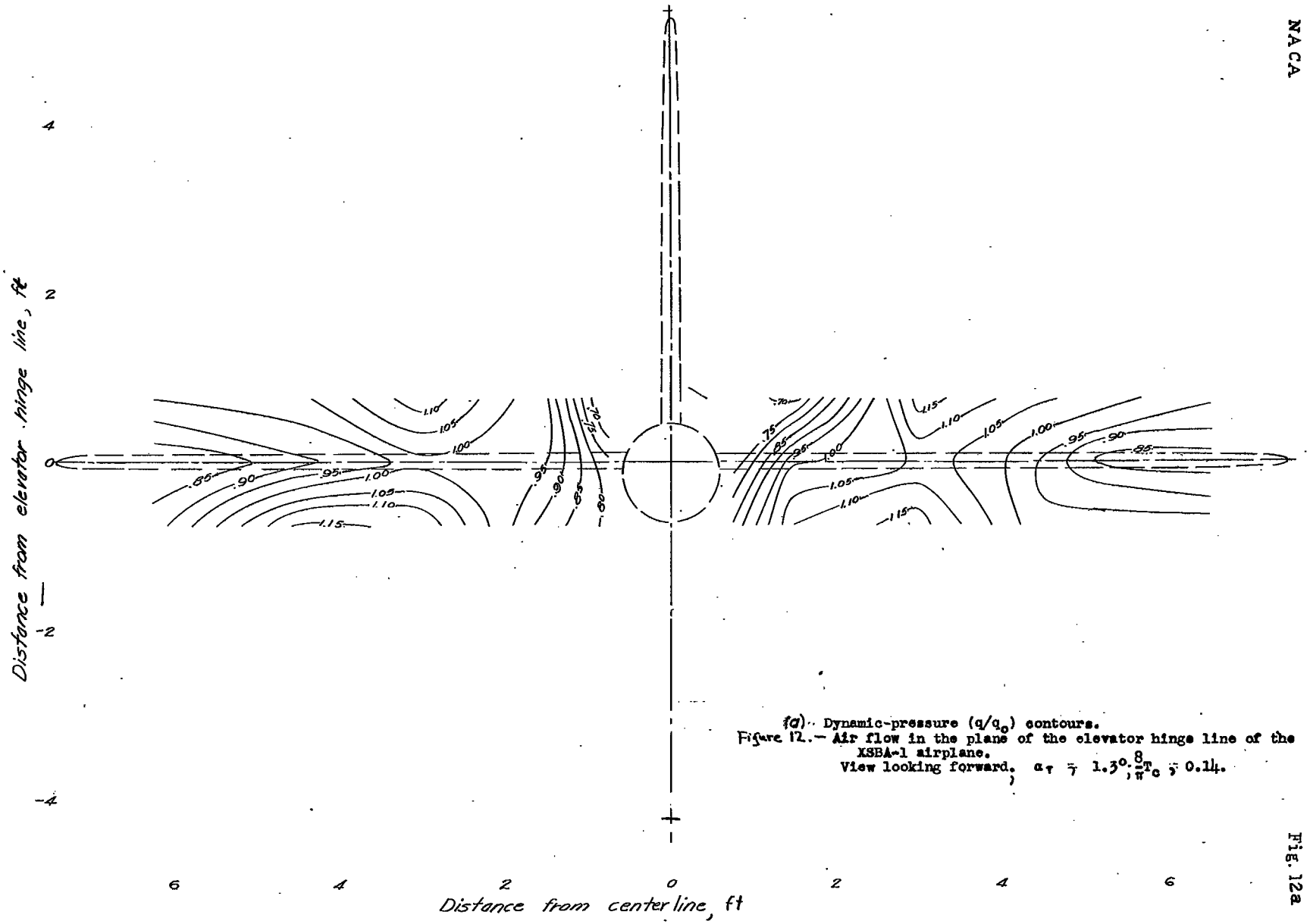

(a) Dynamic-pressure (q/q_o) contours.

Figure 12.— Air flow in the plane of the elevator hinge line of the XSBA-1 airplane.
View looking forward. $\alpha_T = 1.3°$; $\frac{8}{\pi}T_c = 0.14$.

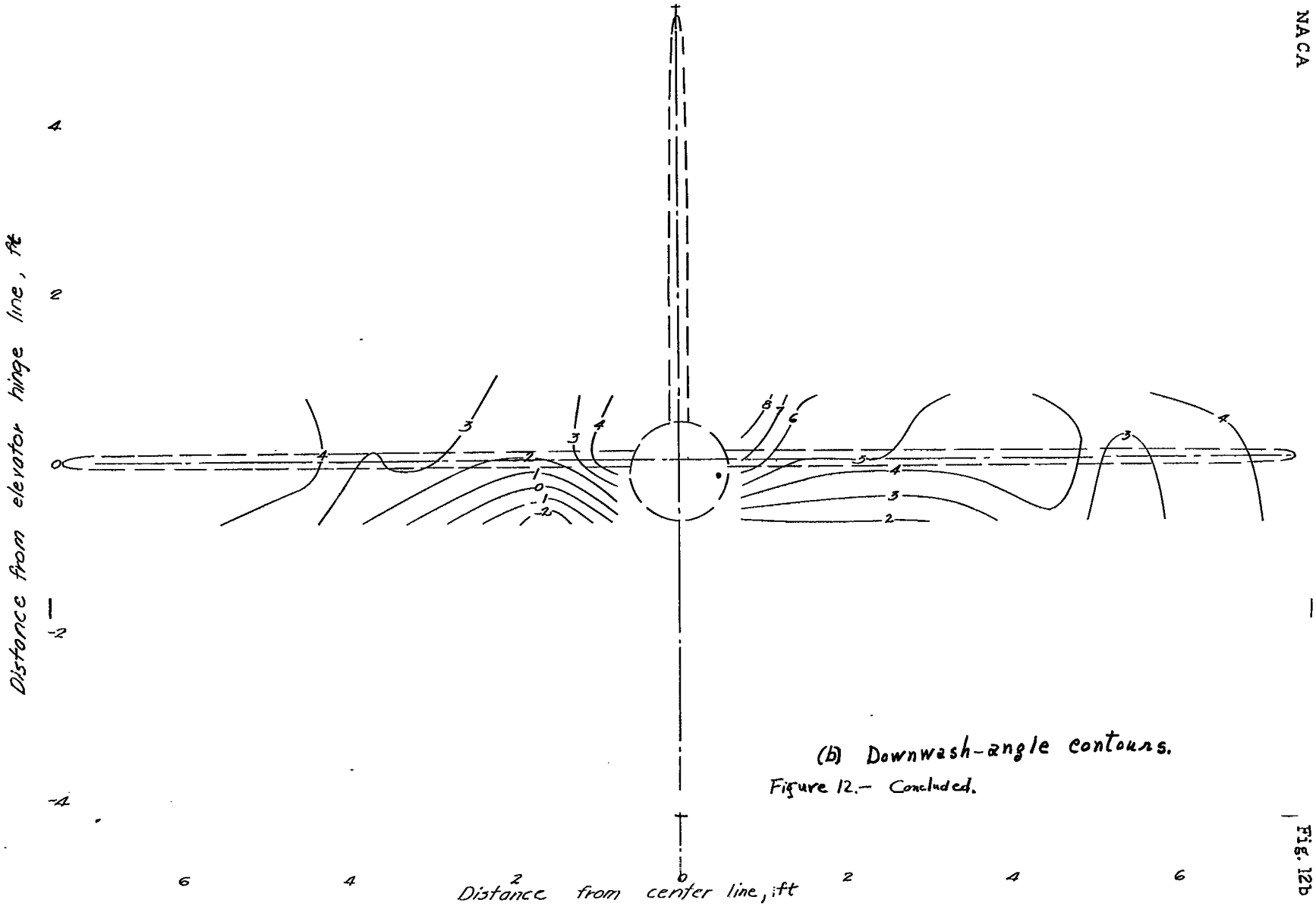

(b) Downwash-angle contours.

Figure 12.- Concluded.

NACA

Fig. 12b

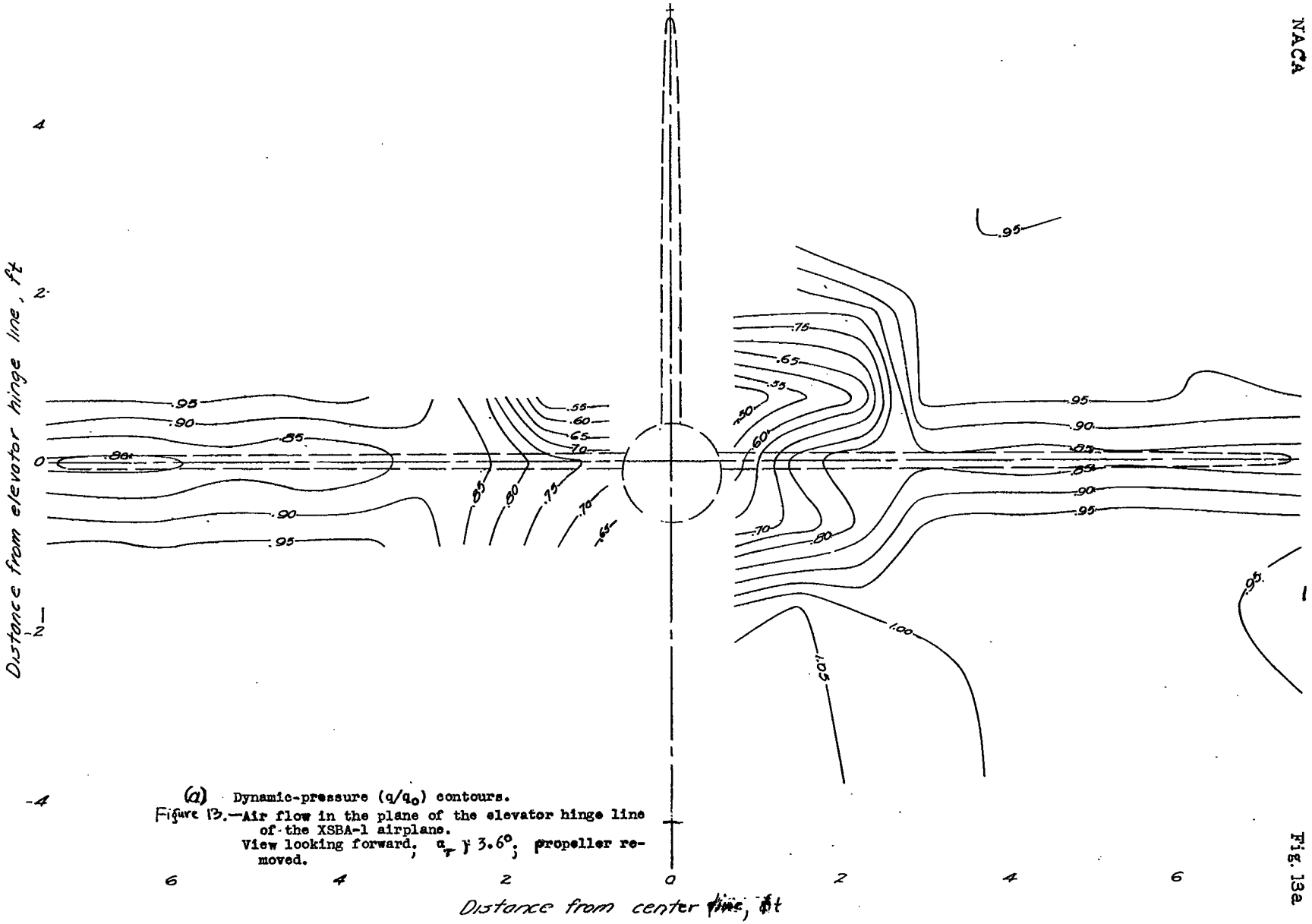

(a) Dynamic-pressure (q/q_0) contours.

Figure 13.—Air flow in the plane of the elevator hinge line of the XSBA-1 airplane. View looking forward, α_T 3.6°; propeller removed.

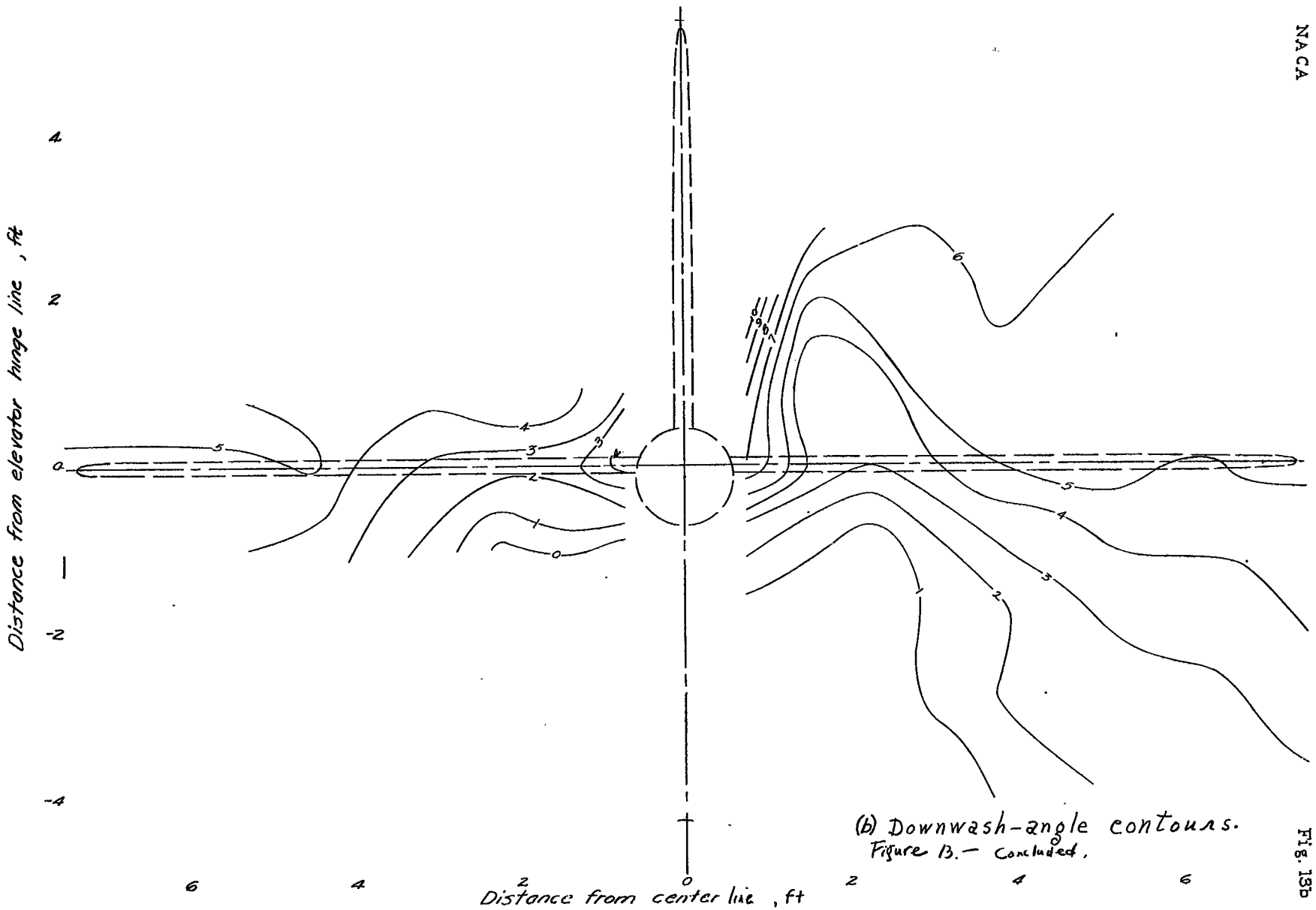

(b) Downwash-angle contours.

Figure 13.— Concluded.

NACA

Fig. 13b

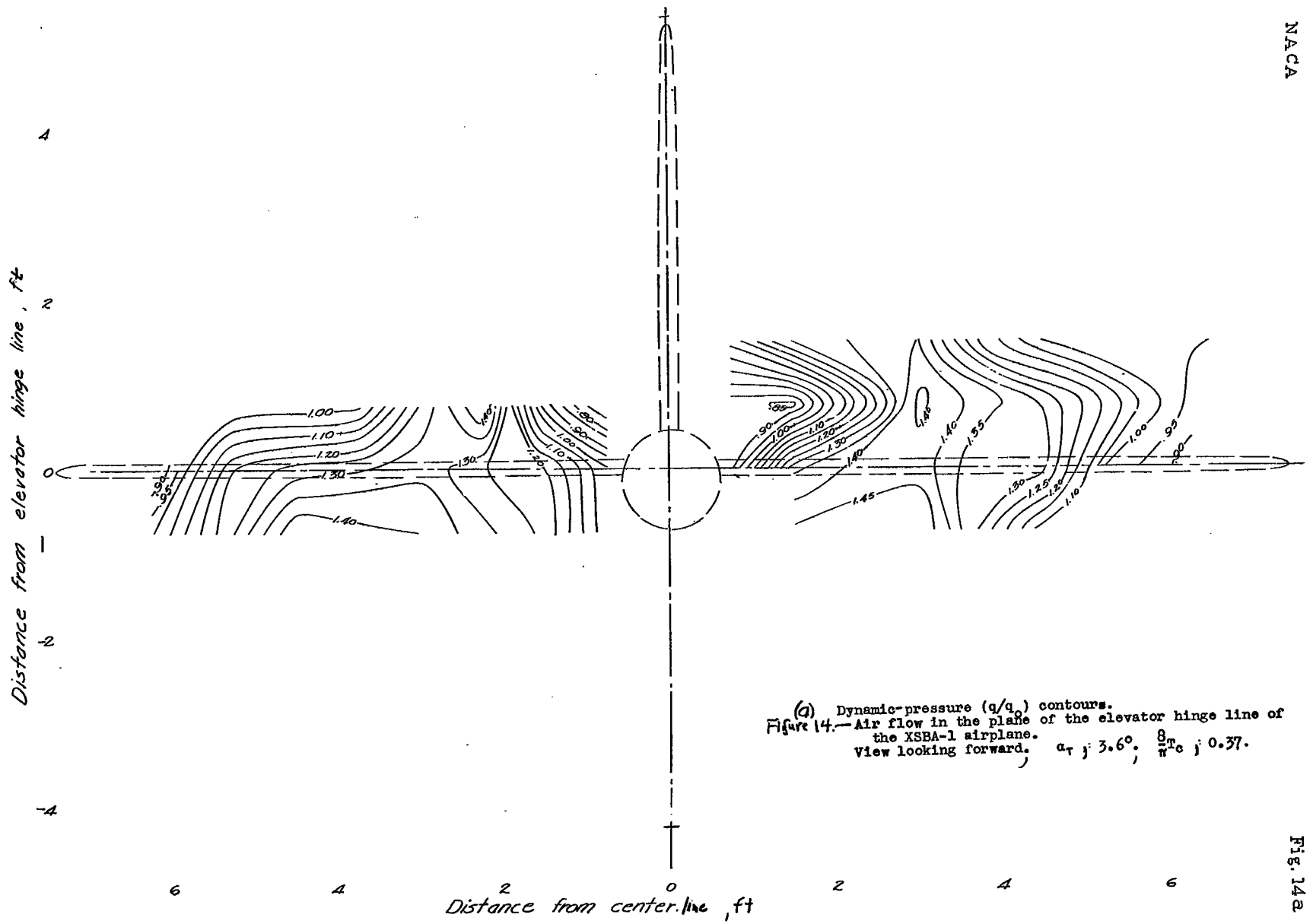

(a) Dynamic-pressure (q/q_o) contours.

Figure 14.— Air flow in the plane of the elevator hinge line of the XSBA-1 airplane. View looking forward. $\alpha_T = 3.6°$; $\frac{\delta}{\pi} T_c = 0.37$.

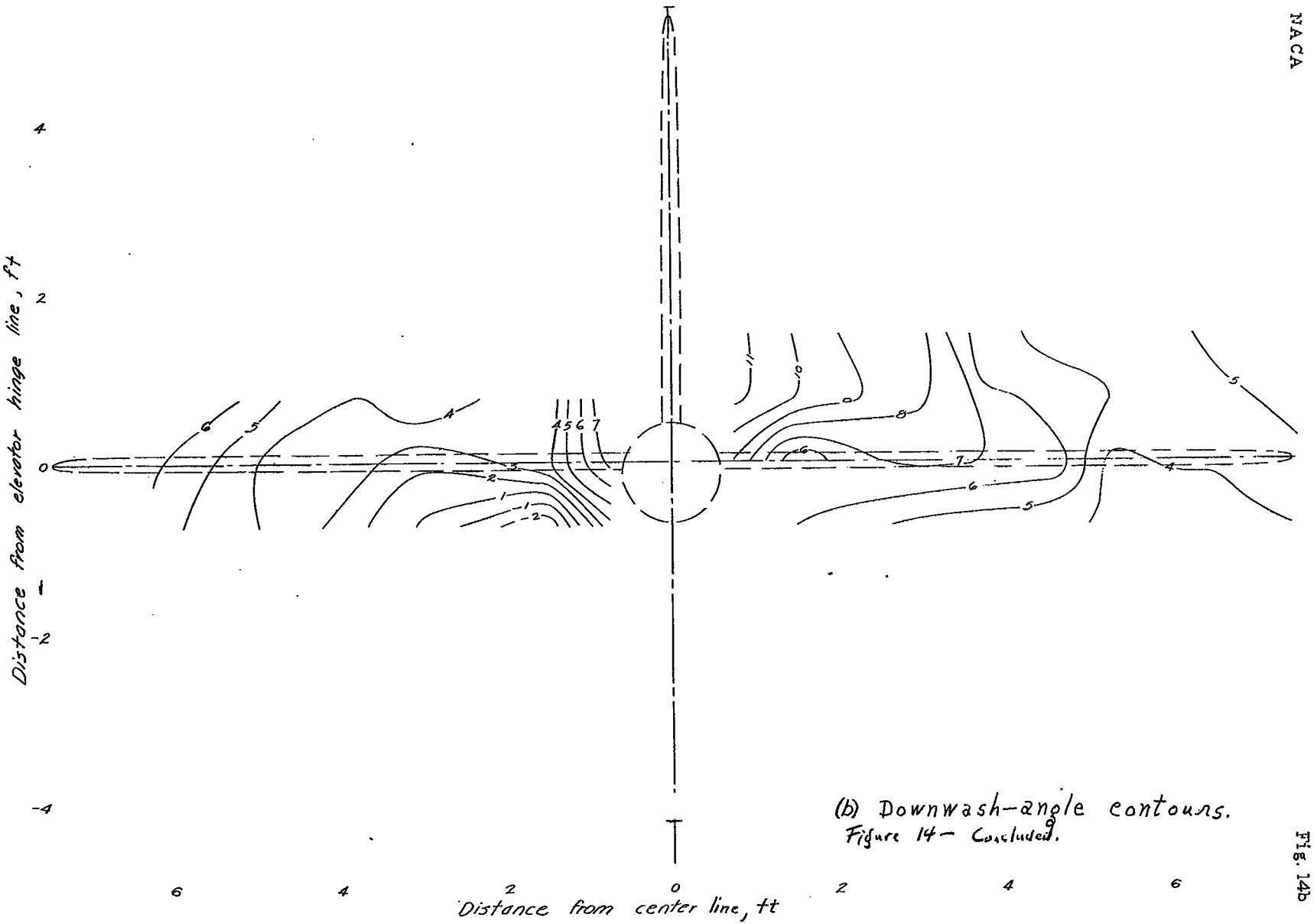

(b) Downwash-angle contours.

Figure 14 - Concluded.

NACA

Fig. 14b

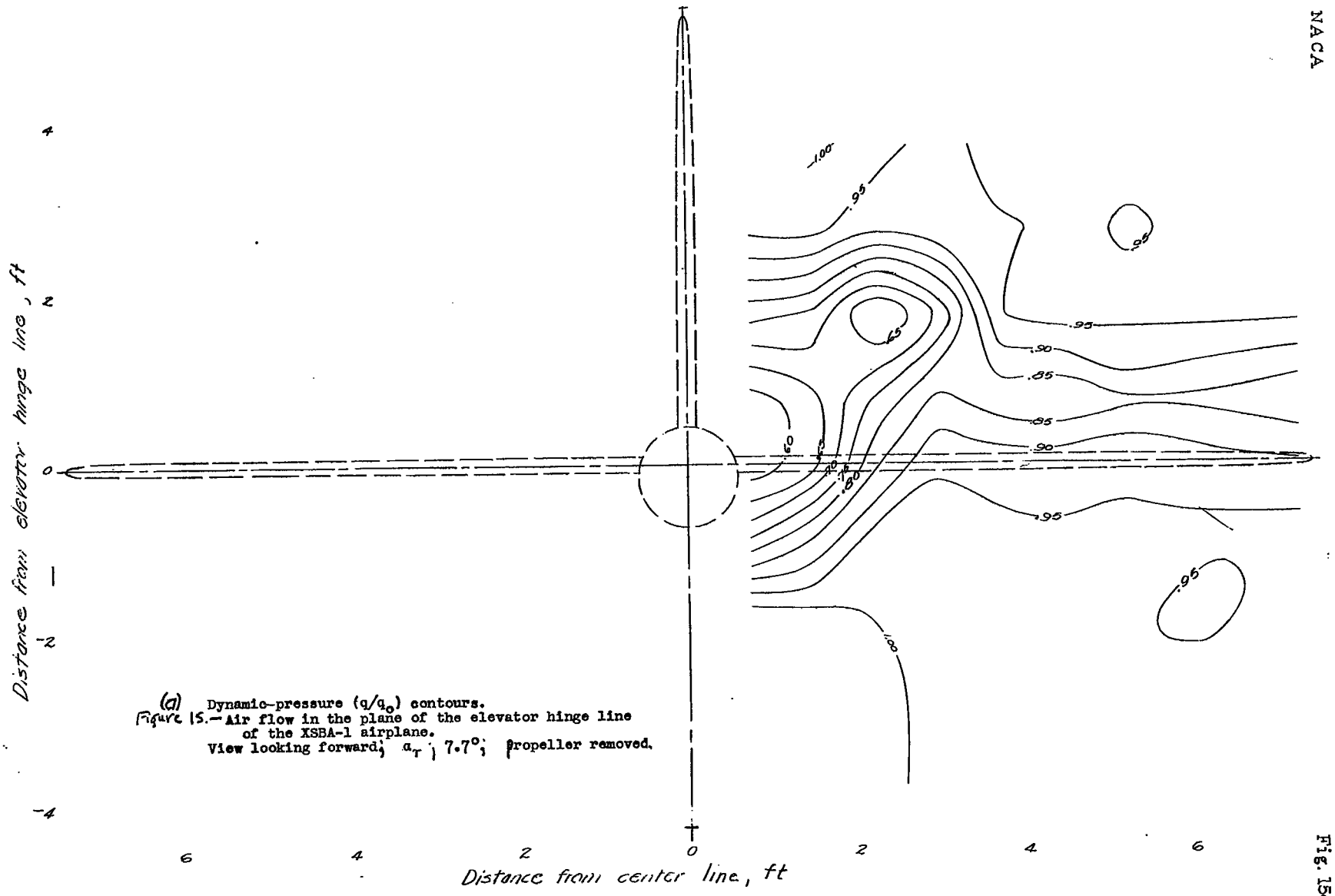

(a) Dynamic-pressure (q/q_o) contours.

Figure 15.— Air flow in the plane of the elevator hinge line of the XSBA-1 airplane. View looking forward; α_T | 7.7°; propeller removed.

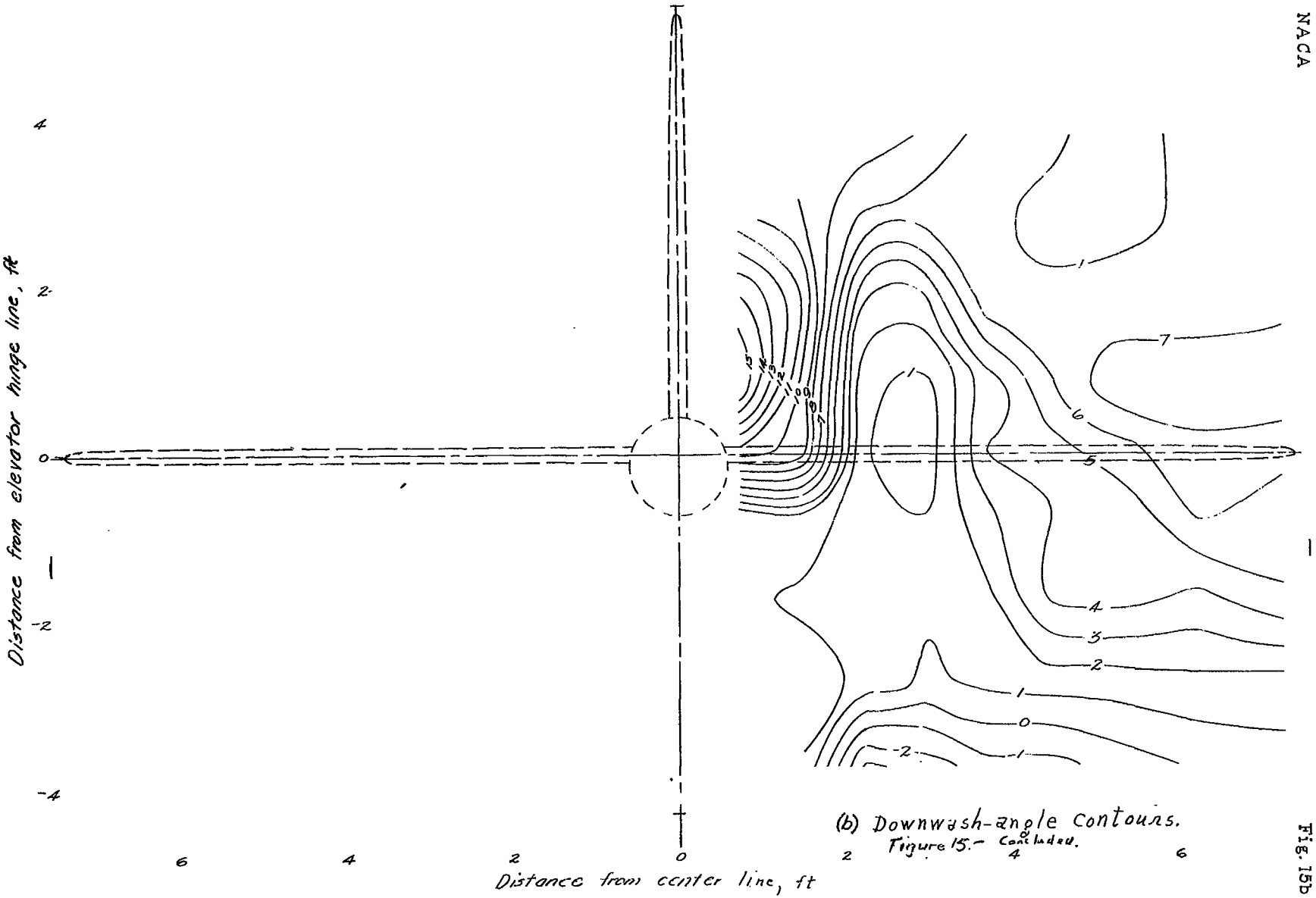

(b) Downwash-angle contours.

Figure 15.- Concluded.

NACA

Fig. 15b

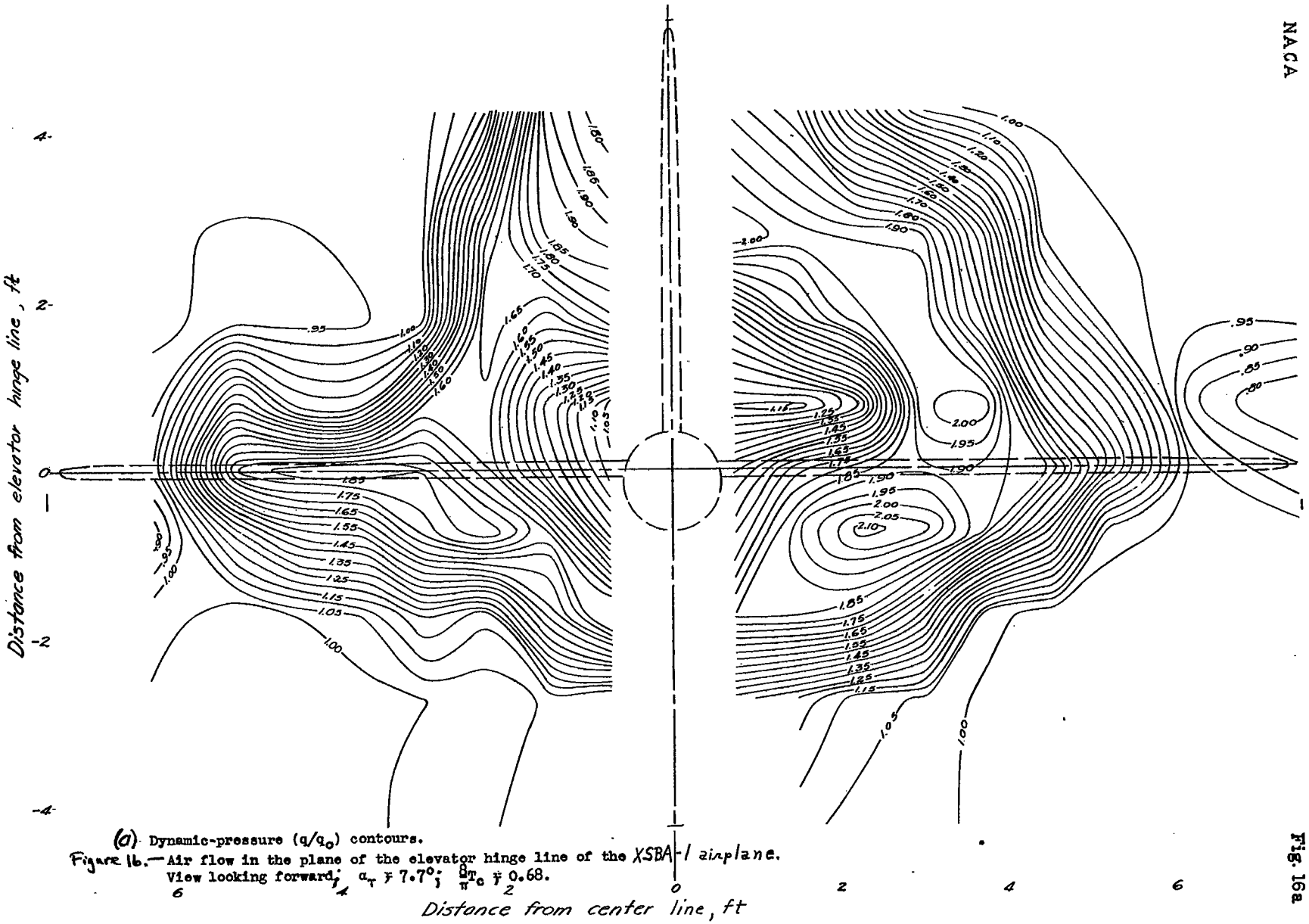

(a) Dynamic-pressure (q/q_o) contours.

Figure 16.— Air flow in the plane of the elevator hinge line of the XSBA-1 airplane. View looking forward; $\alpha_T \approx 7.7°$; $\frac{a_T}{\pi r_c} \approx 0.68$.

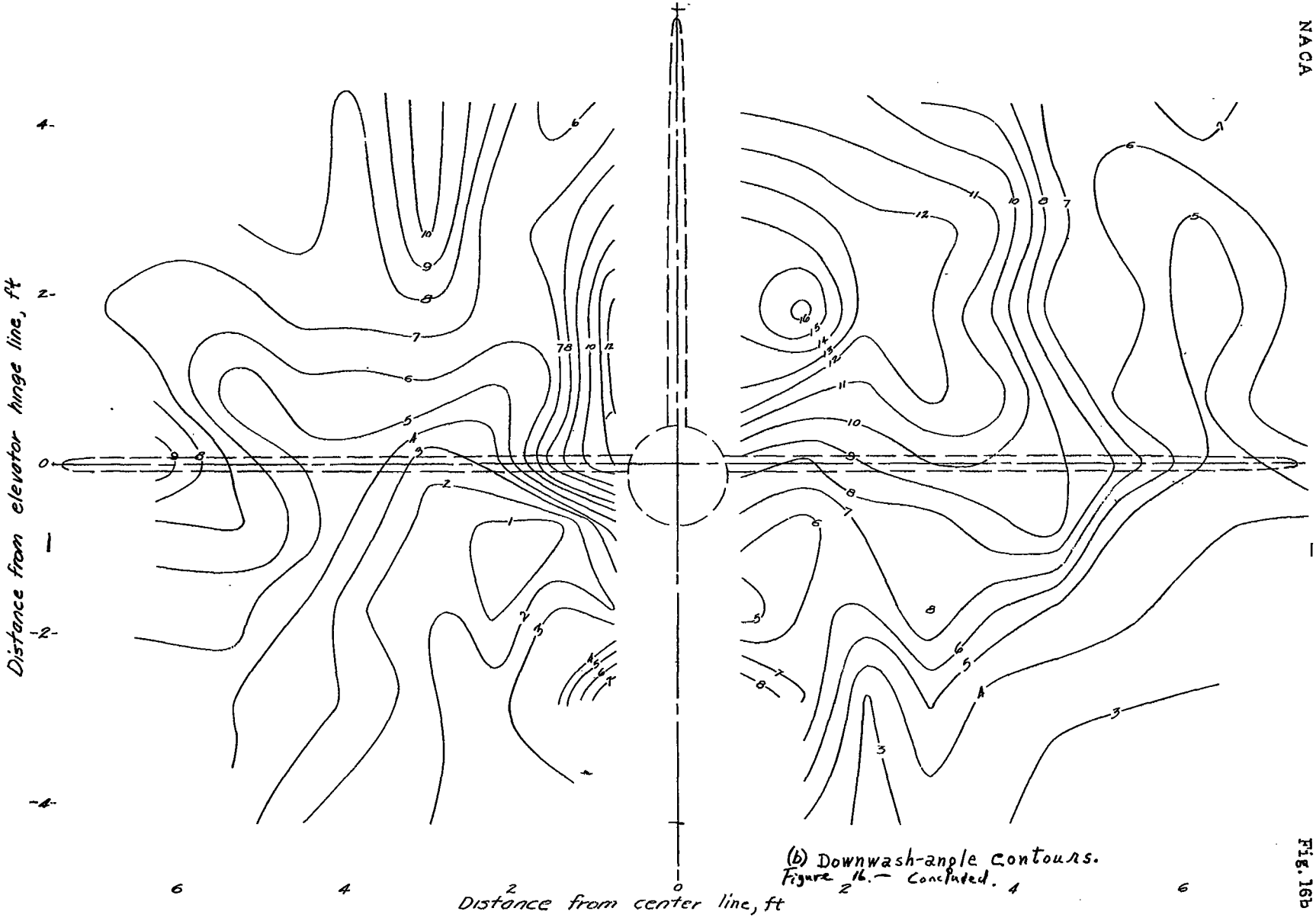

(b) Downwash-angle contours.

Figure 16.— Concluded.

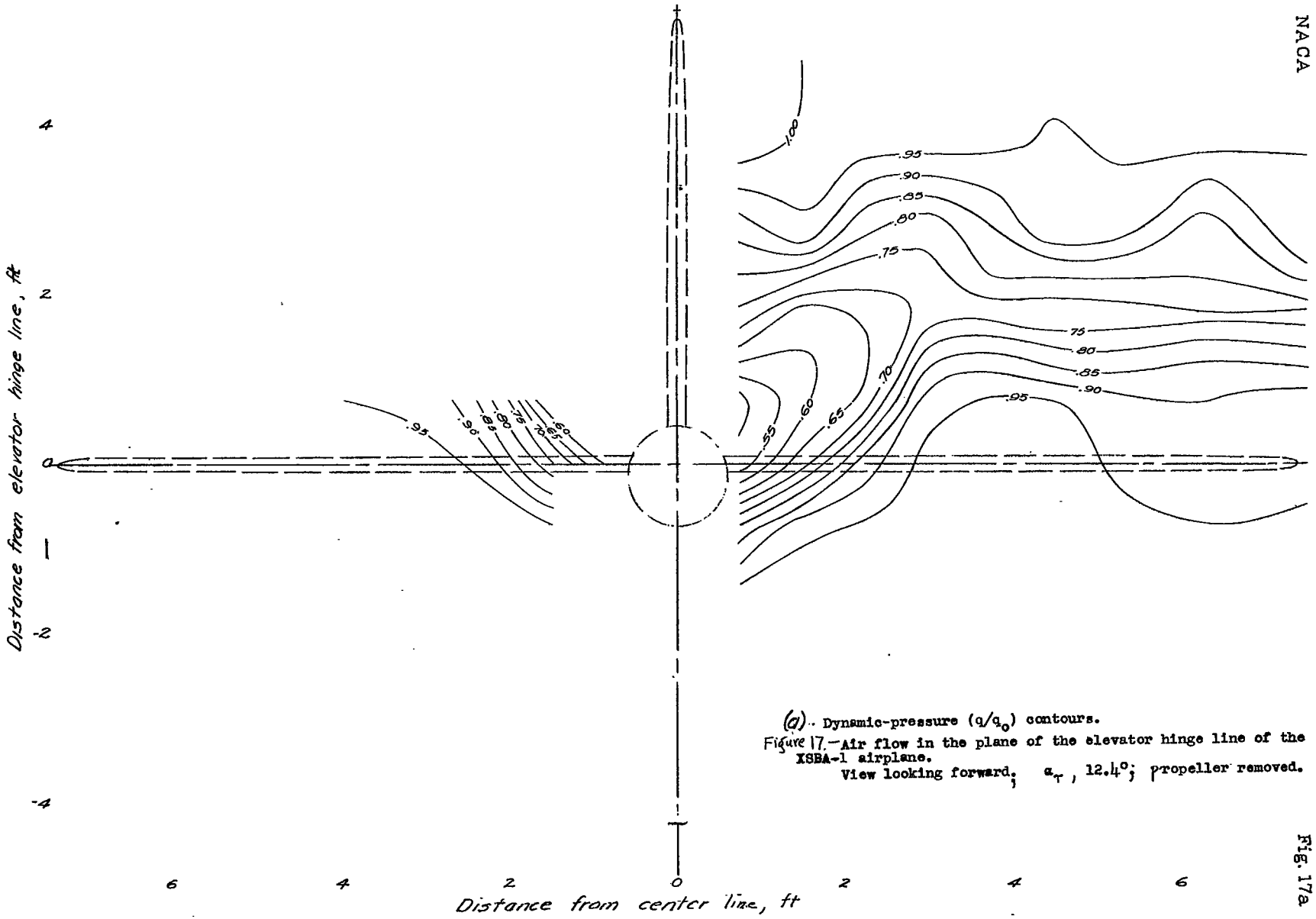

(a) Dynamic-pressure (q/q_0) contours.

Figure 17.—Air flow in the plane of the elevator hinge line of the XSBA-1 airplane.
View looking forward; α_T, 12.4°; propeller removed.

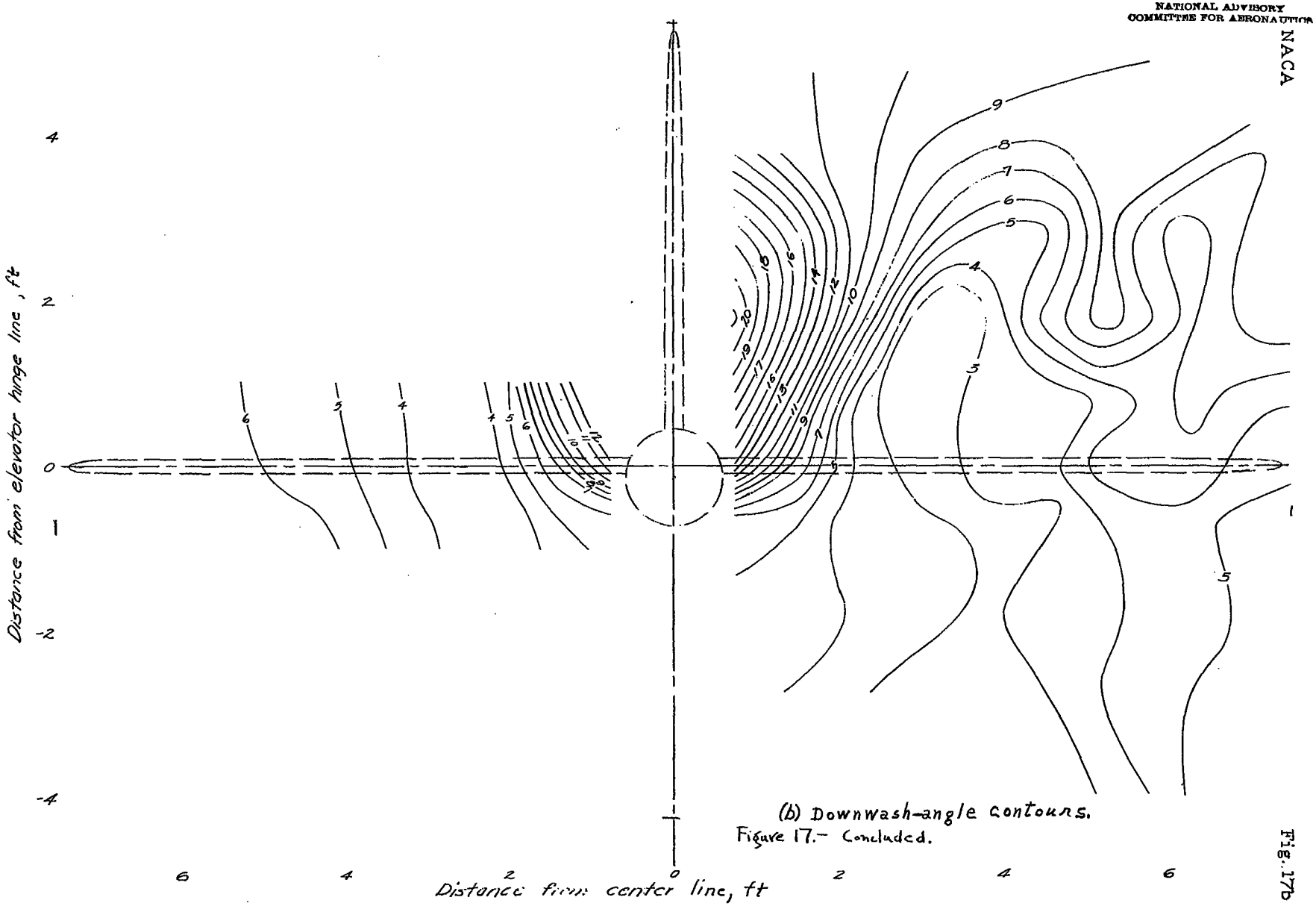

(b) Downwash-angle contours.

Figure 17.- Concluded.

Fig. 17b

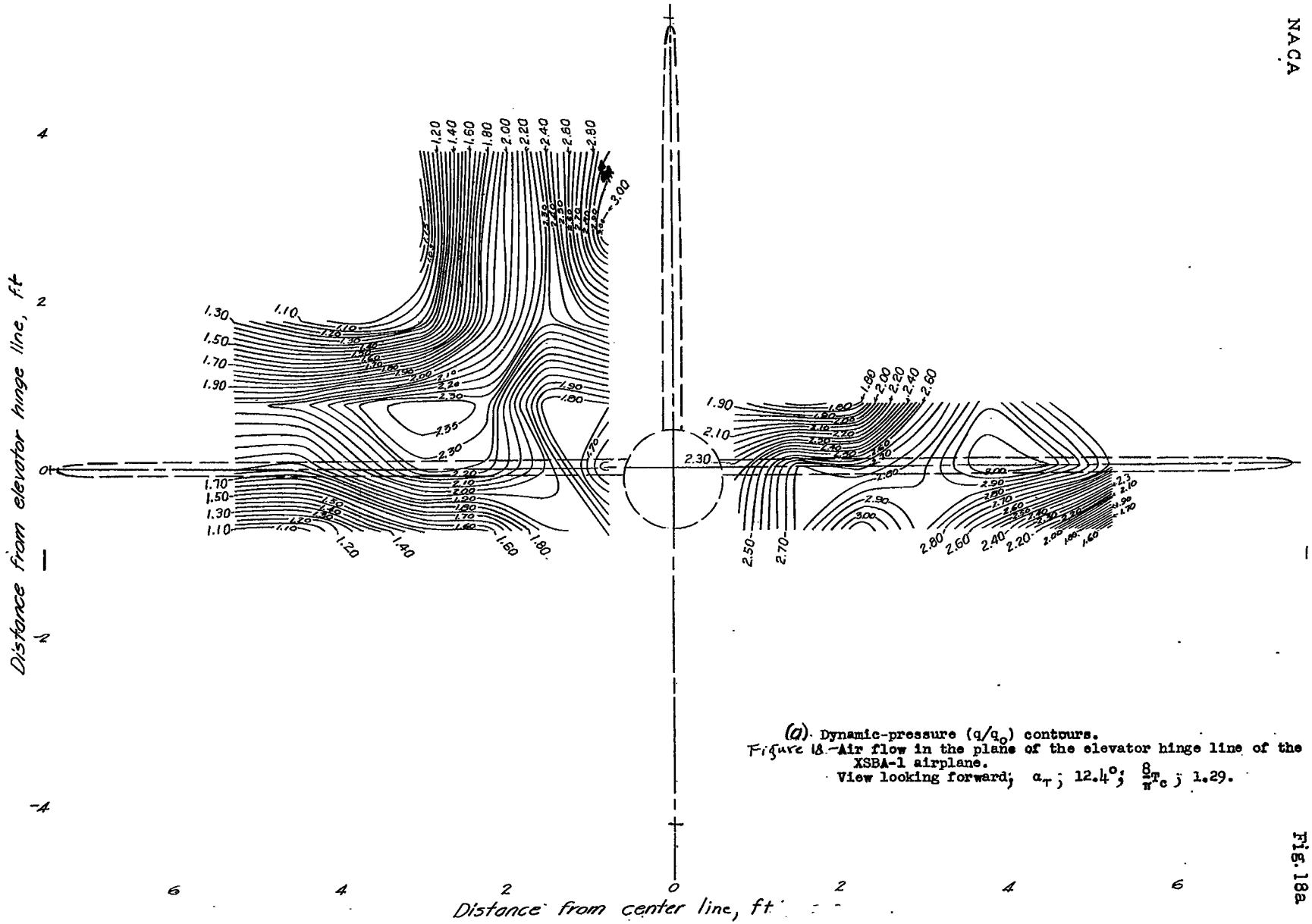

(a) Dynamic-pressure (q/q_o) contours.

Figure 18.—Air flow in the plane of the elevator hinge line of the XSBA-1 airplane.
View looking forward; α_T, 12.4°; $\frac{\delta}{\pi} T_c$, 1.29.

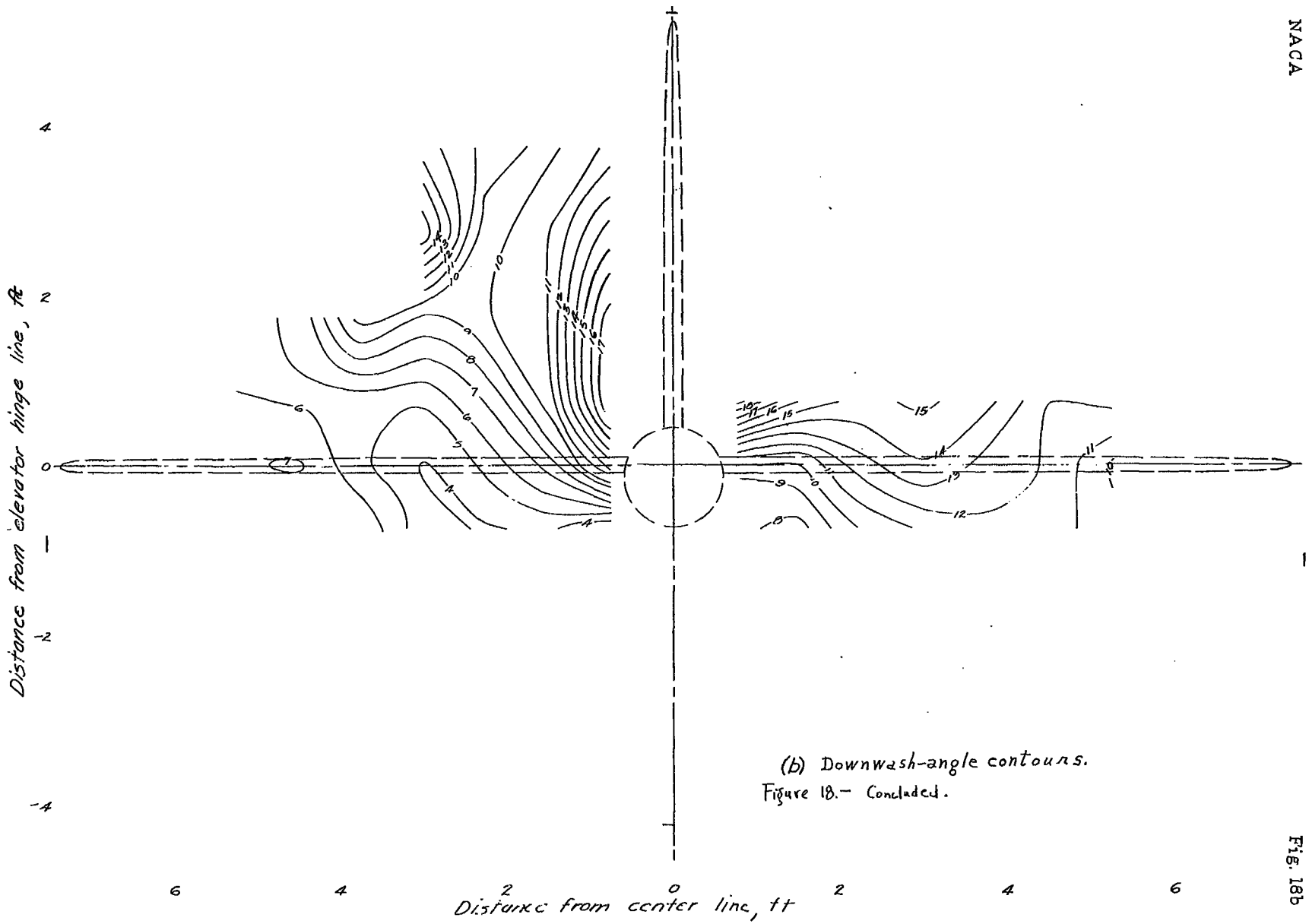

(b) Downwash-angle contours.

Figure 18.- Concluded.

NACA

Fig. 18b

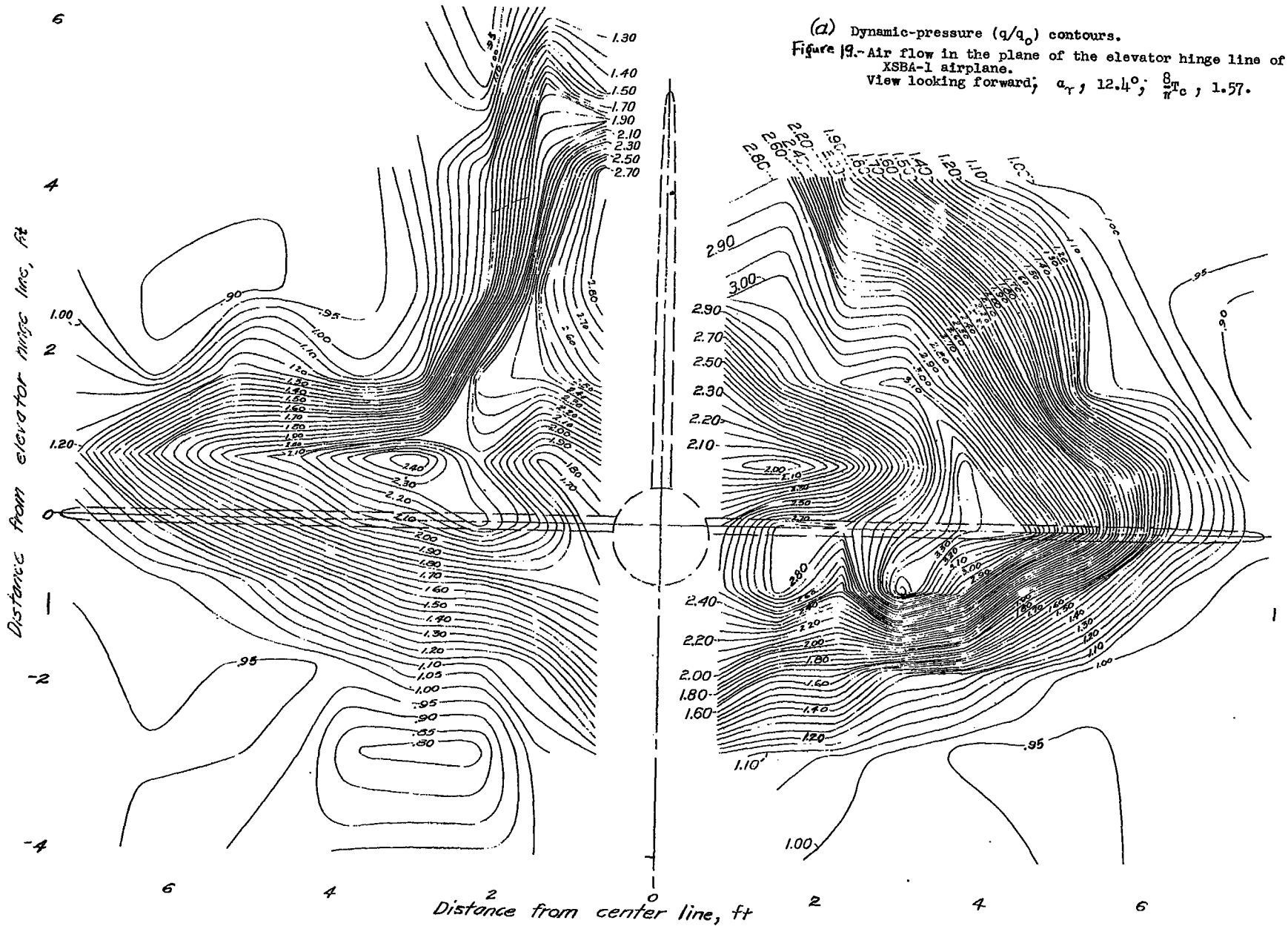

(a) Dynamic-pressure (q/q_o) contours.

Figure 19.- Air flow in the plane of the elevator hinge line of the XSBA-1 airplane.
View looking forward; α_T, 12.4°; $\frac{\delta_T}{\pi}c$, 1.57.

Fig. 19a

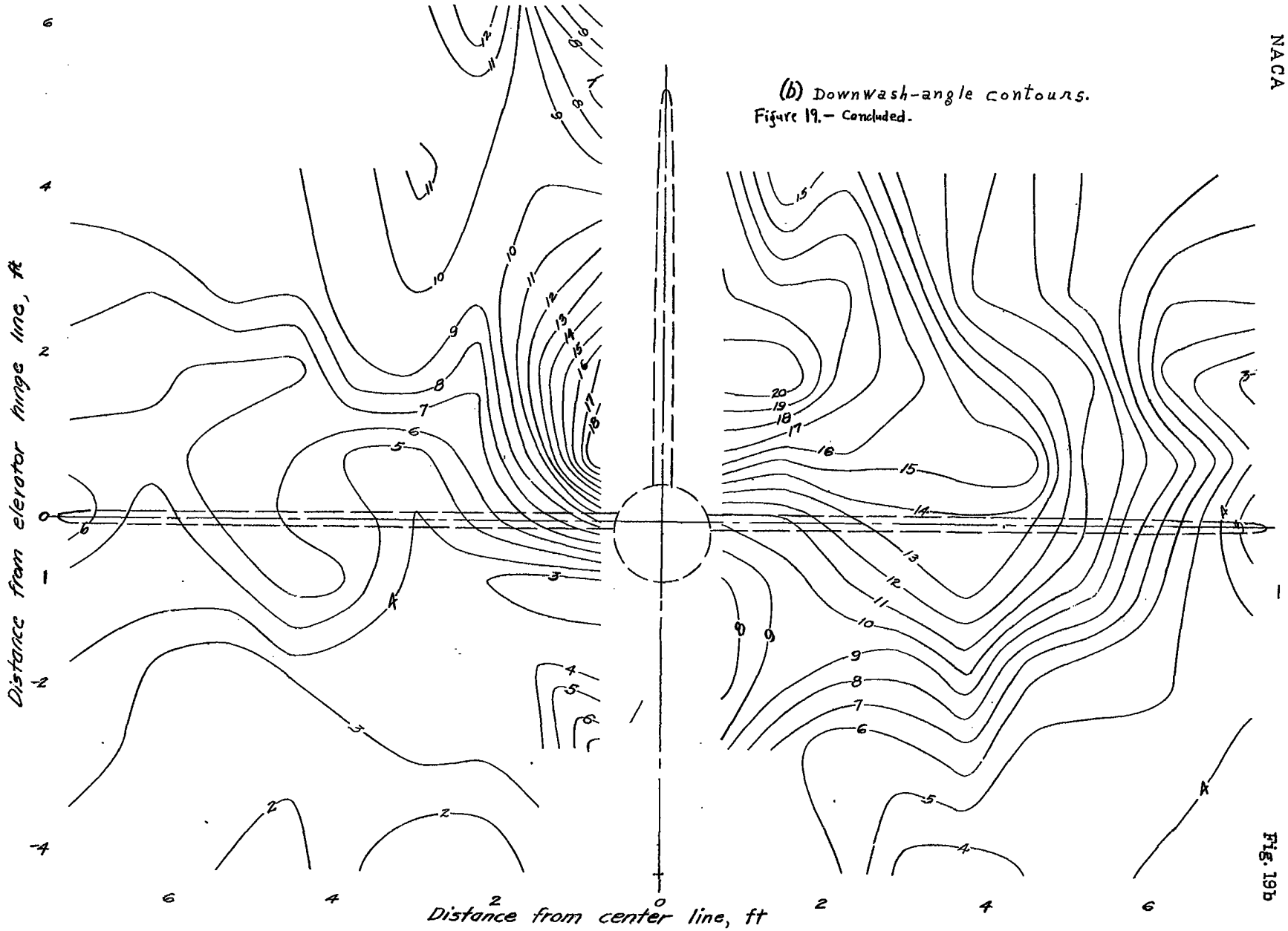

(b) Downwash-angle contours.

Figure 19.- Concluded.

NACA

Fig. 19b

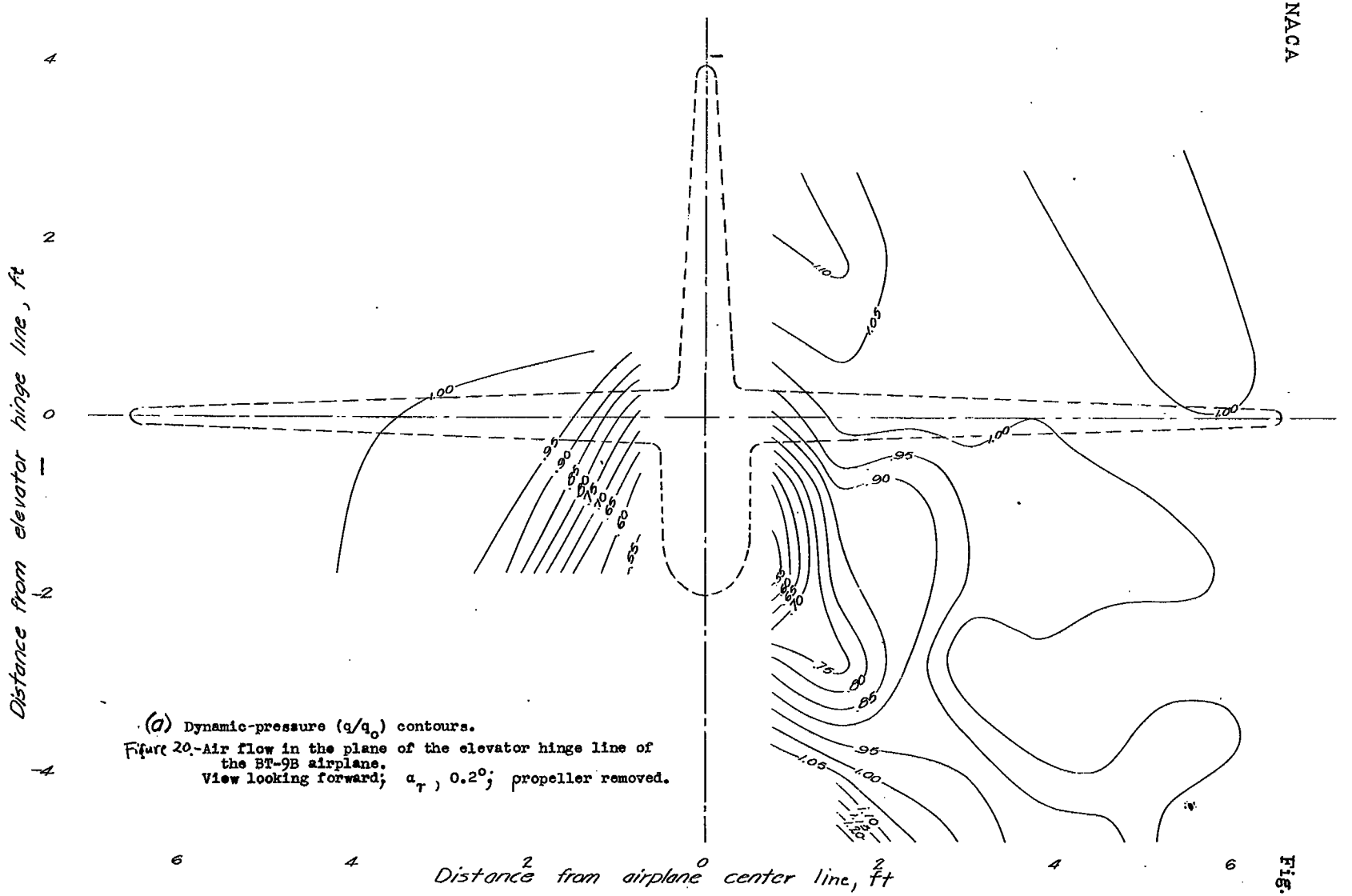

(a) Dynamic-pressure (q/q_o) contours.

Figure 20.-Air flow in the plane of the elevator hinge line of the BT-9B airplane. View looking forward; α_T, 0.2°; propeller removed.

NACA

Fig. 20a

L-761

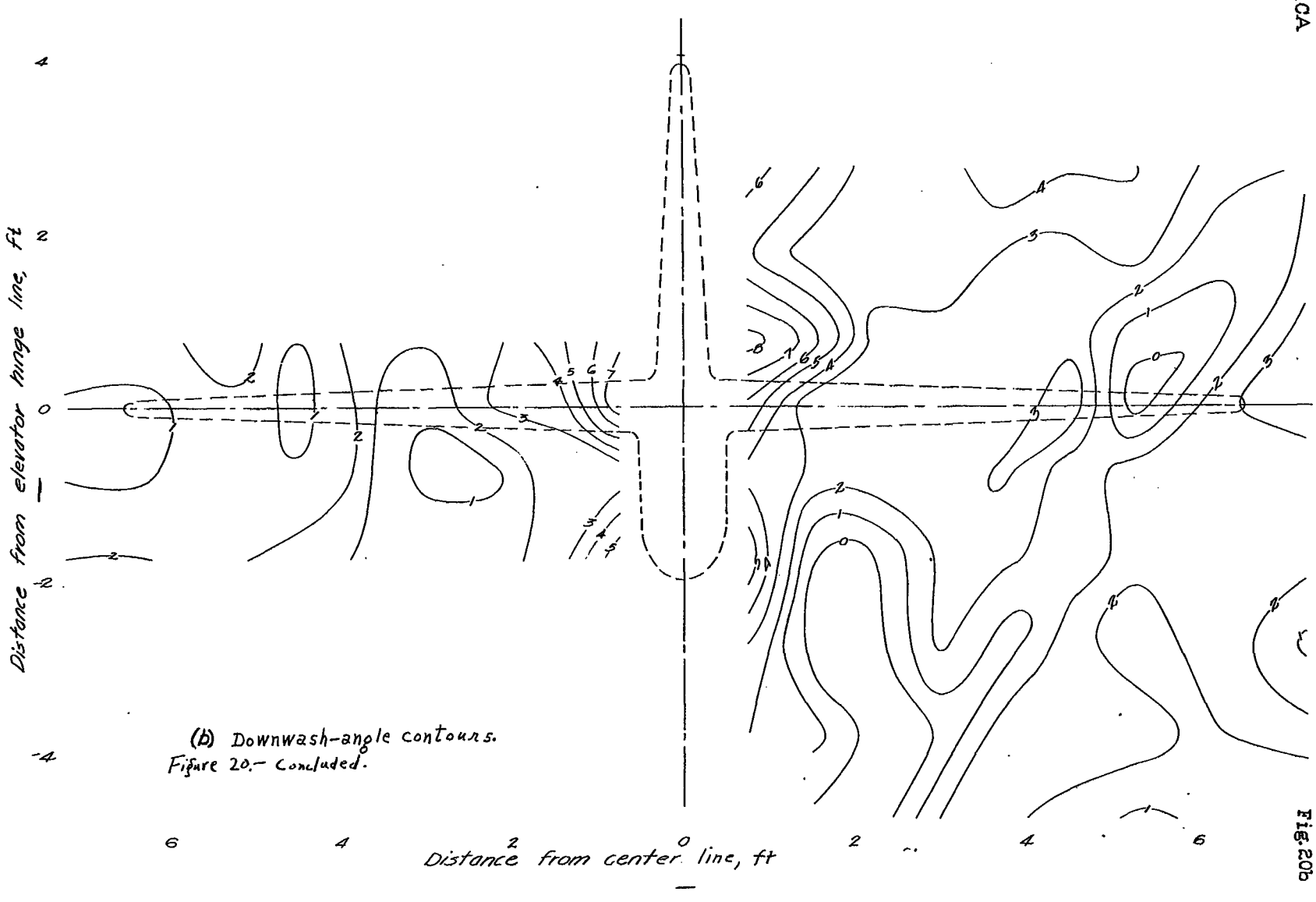

(b) Downwash-angle contours.

Figure 20.- Concluded.

NACA

Fig. 20b

(a) Dynamic-pressure (q/q_o) contours.

Figure 21.—Air flow in the plane of the elevator hinge line of the BT-9B airplane.
View looking forward; α_T, 0.2°; $\frac{\delta}{\pi}T_c$, 0.15.

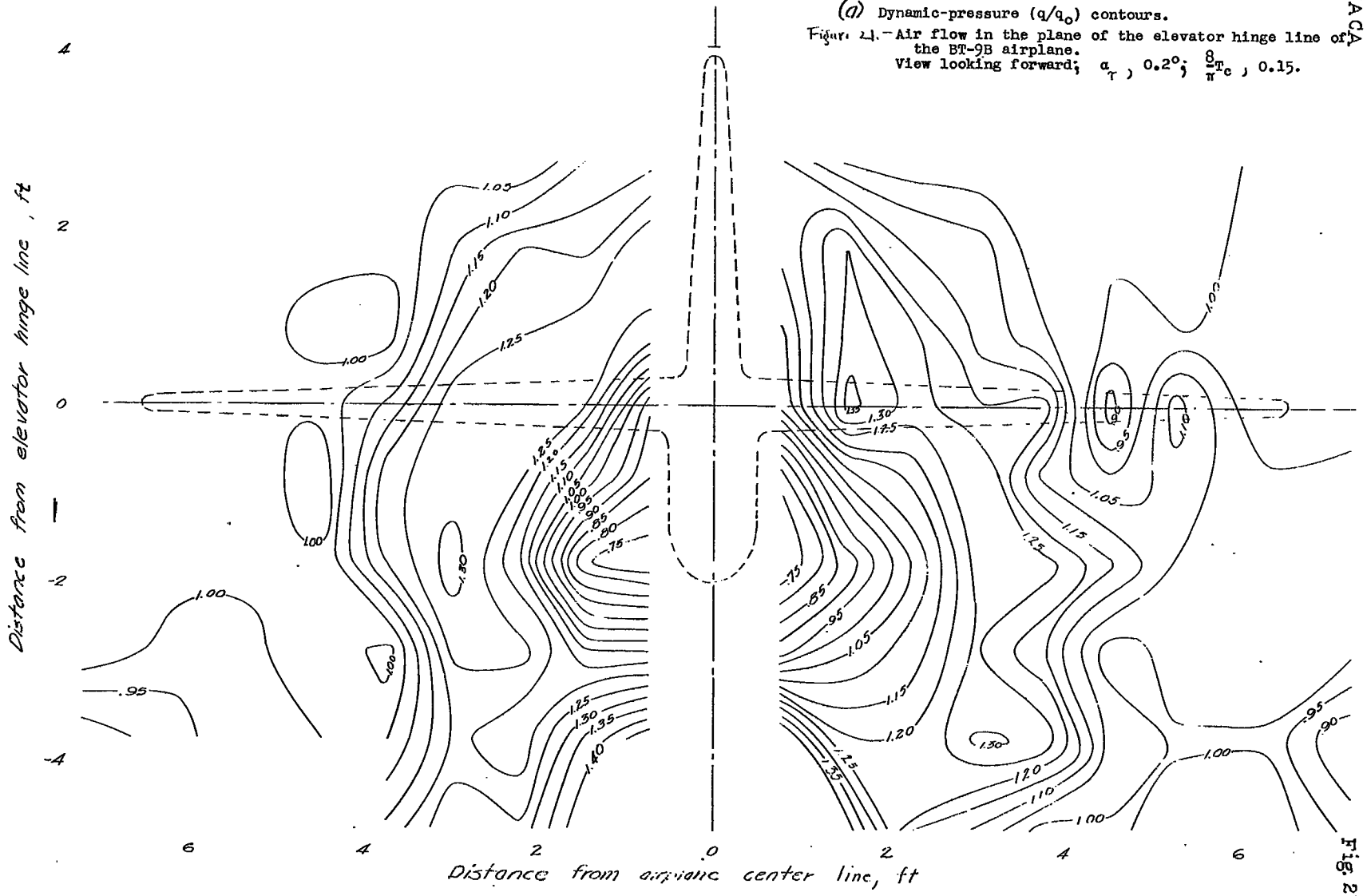

NACA

Fig. 21a

(b) Downwash-angle contours.

Figure 21.- Concluded.

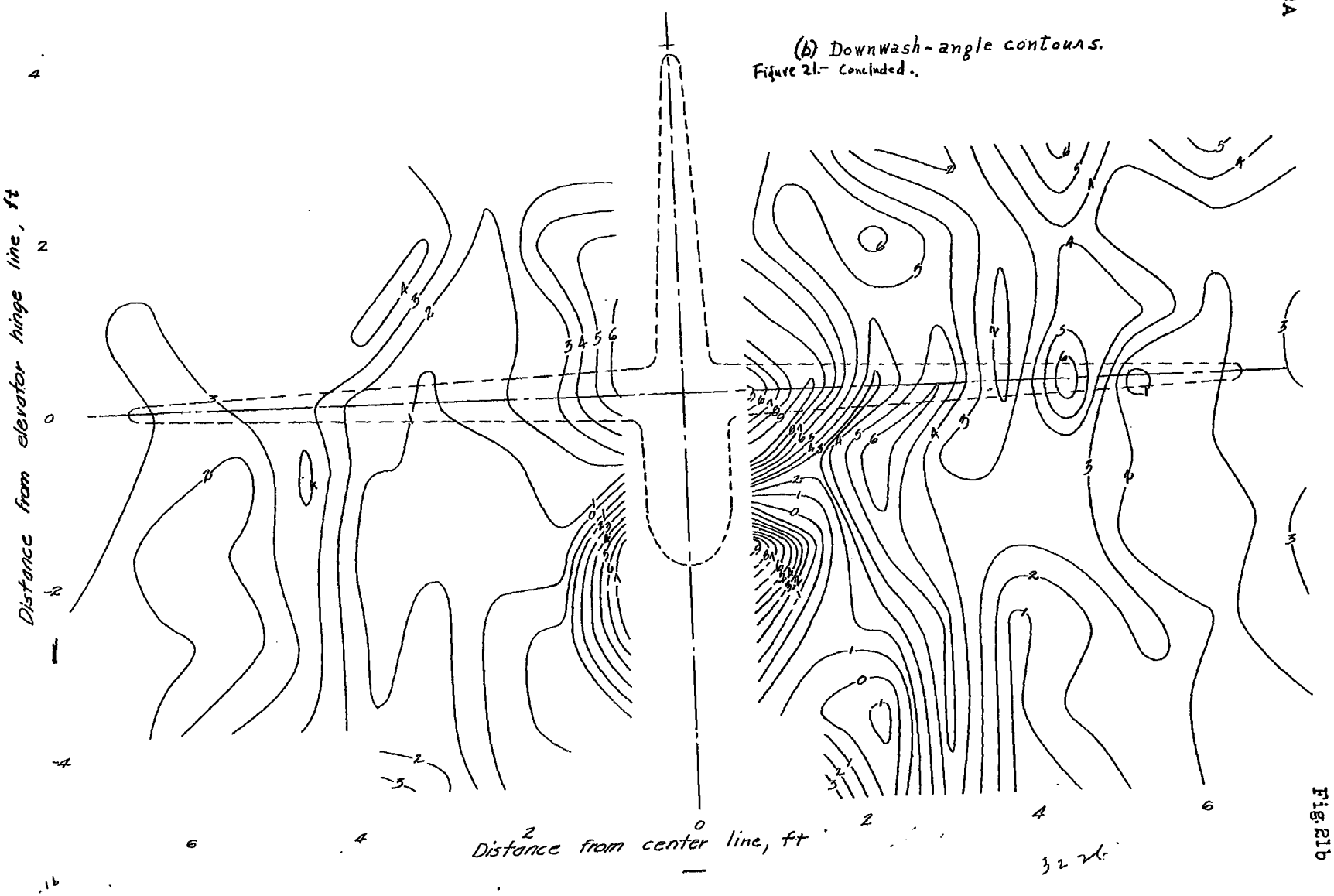

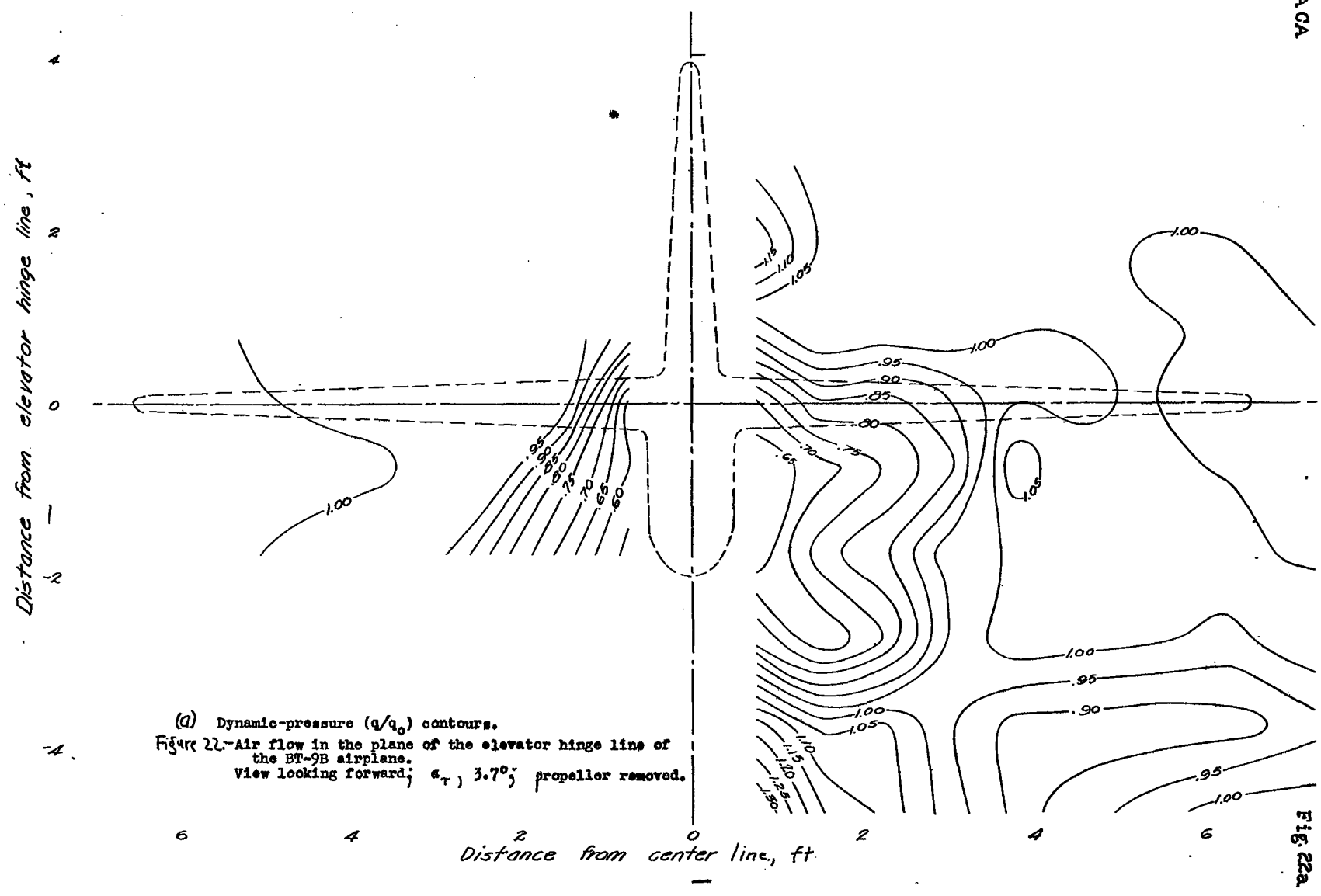

(a) Dynamic-pressure (q/q_0) contours.

Figure 22.- Air flow in the plane of the elevator hinge line of the BT-9B airplane. View looking forward; (α_T 3.7°; propeller removed.

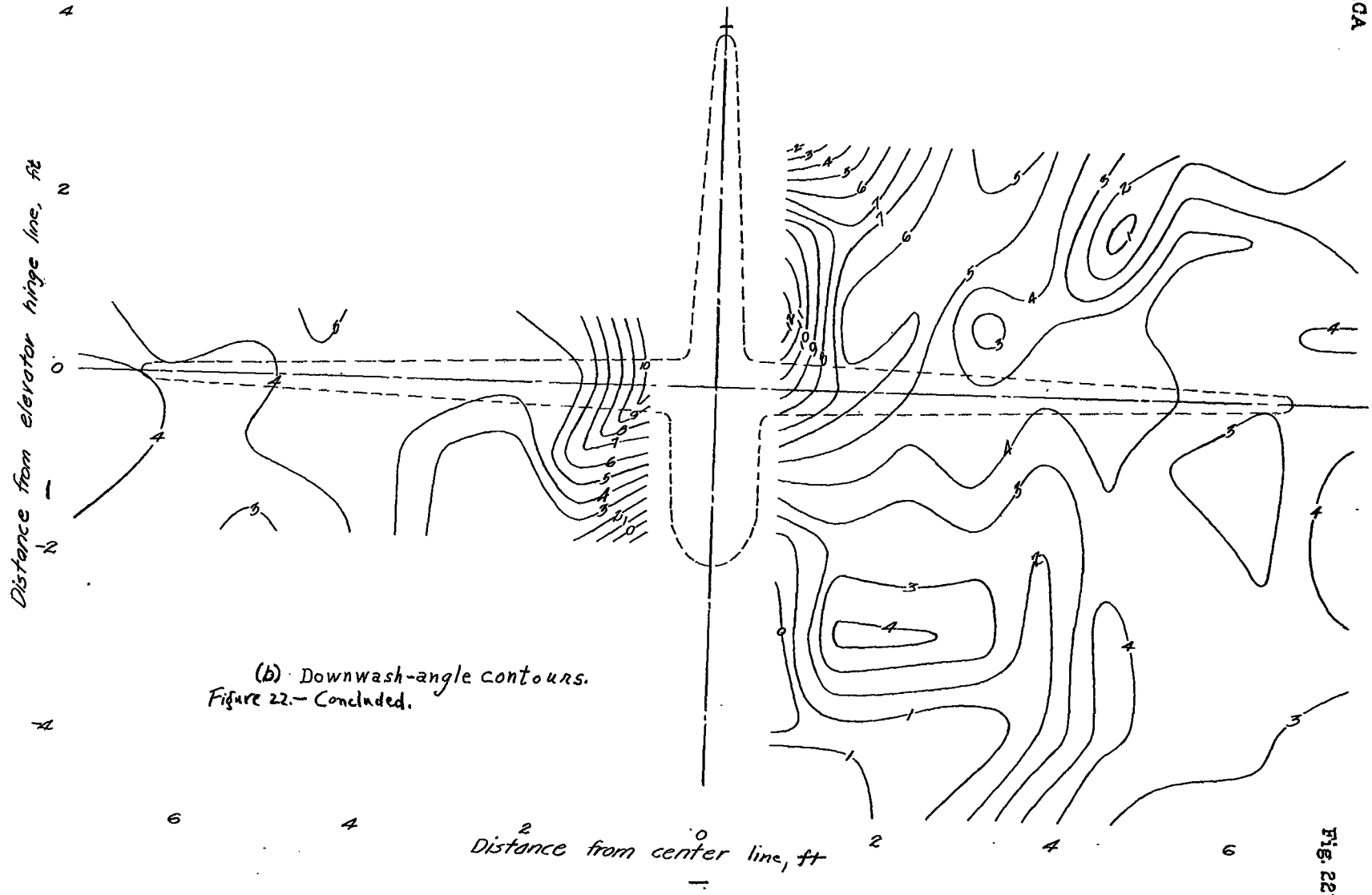

(b) Downwash-angle contours.

Figure 22.- Concluded.

Fig. 22b

(a) Dynamic-pressure (q/q_0) contours.

Figure 23.-Air flow in the plane of the elevator hinge line of the BT-9B airplane. View looking forward; α_T, 3.7°; $\frac{\delta}{\pi}T_c$, 0.44.

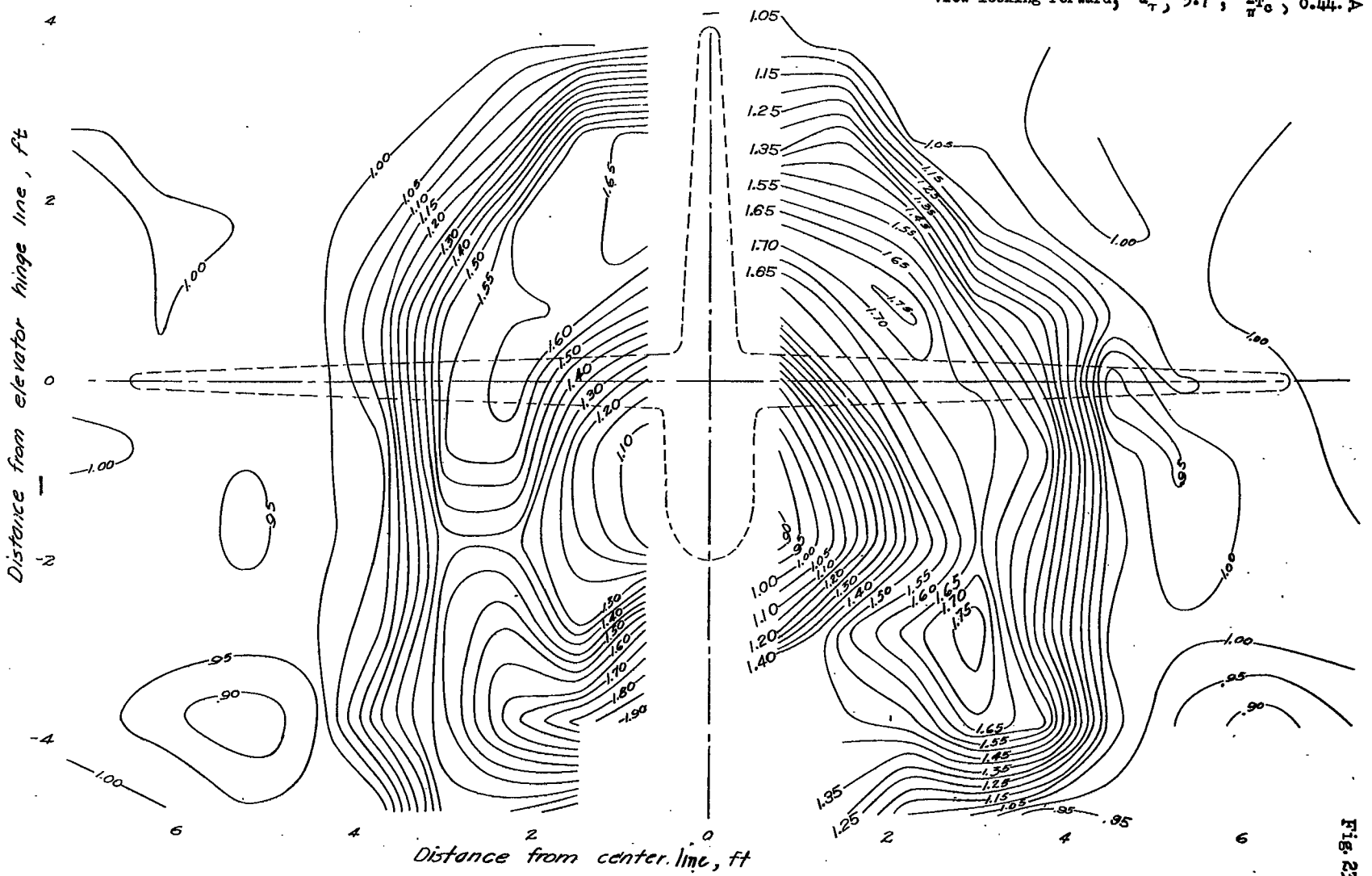

NACA

Fig. 23a

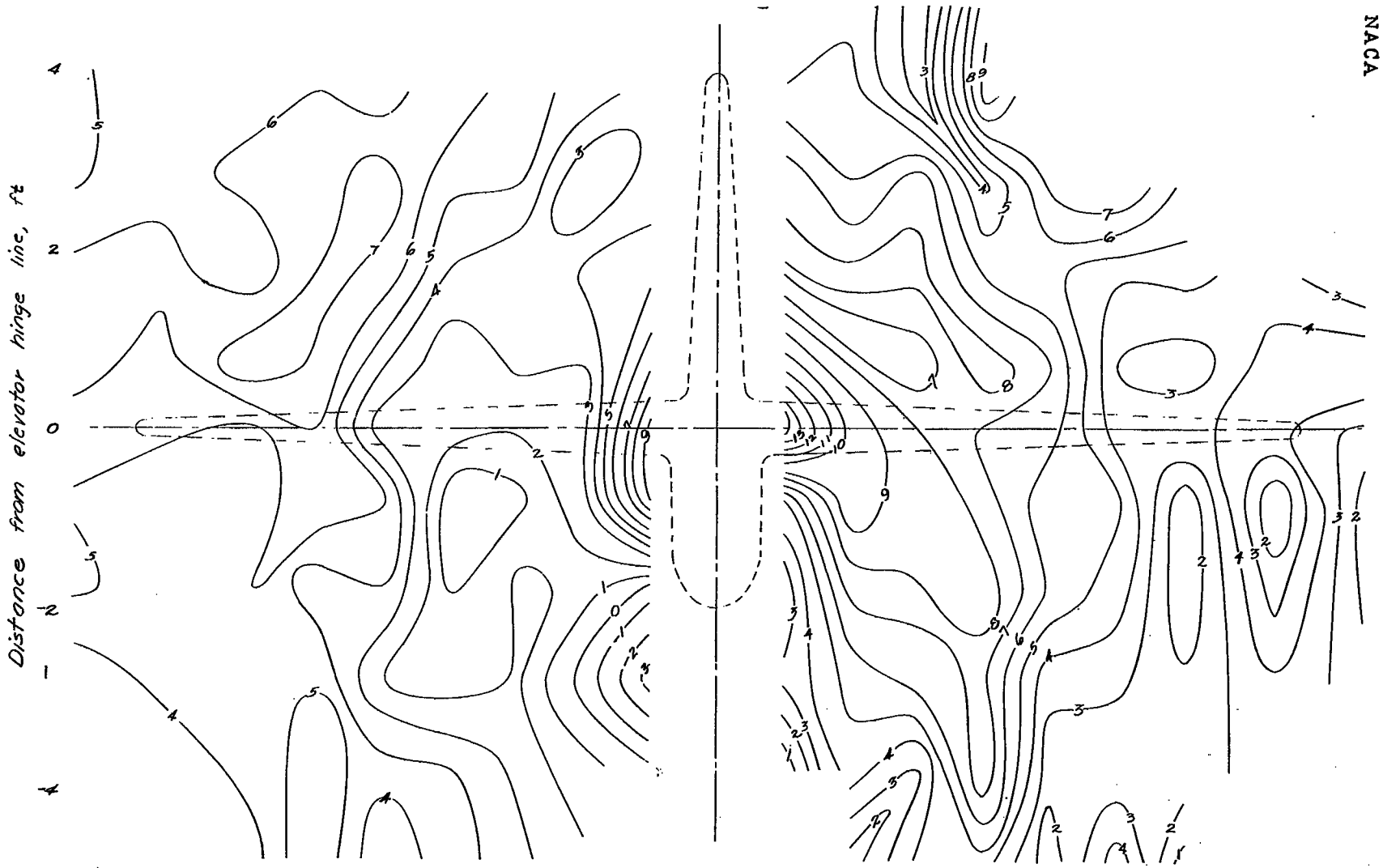

(b) Downwash-angle contours.

Figure 23.- Concluded.

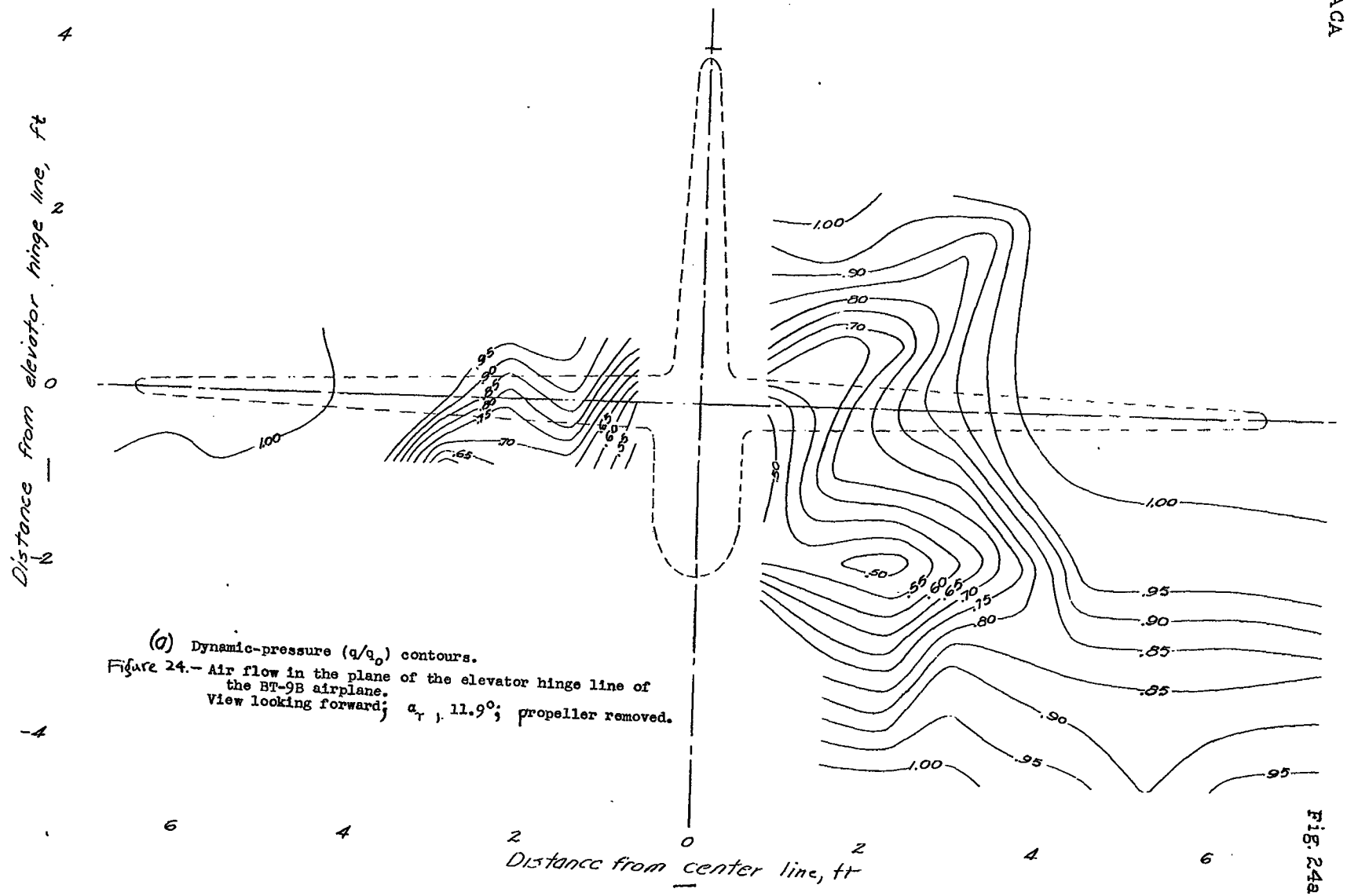

(a) Dynamic-pressure (q/q_0) contours.

Figure 24.— Air flow in the plane of the elevator hinge line of the BT-9B airplane. View looking forward; α_r, 11.9°; propeller removed.

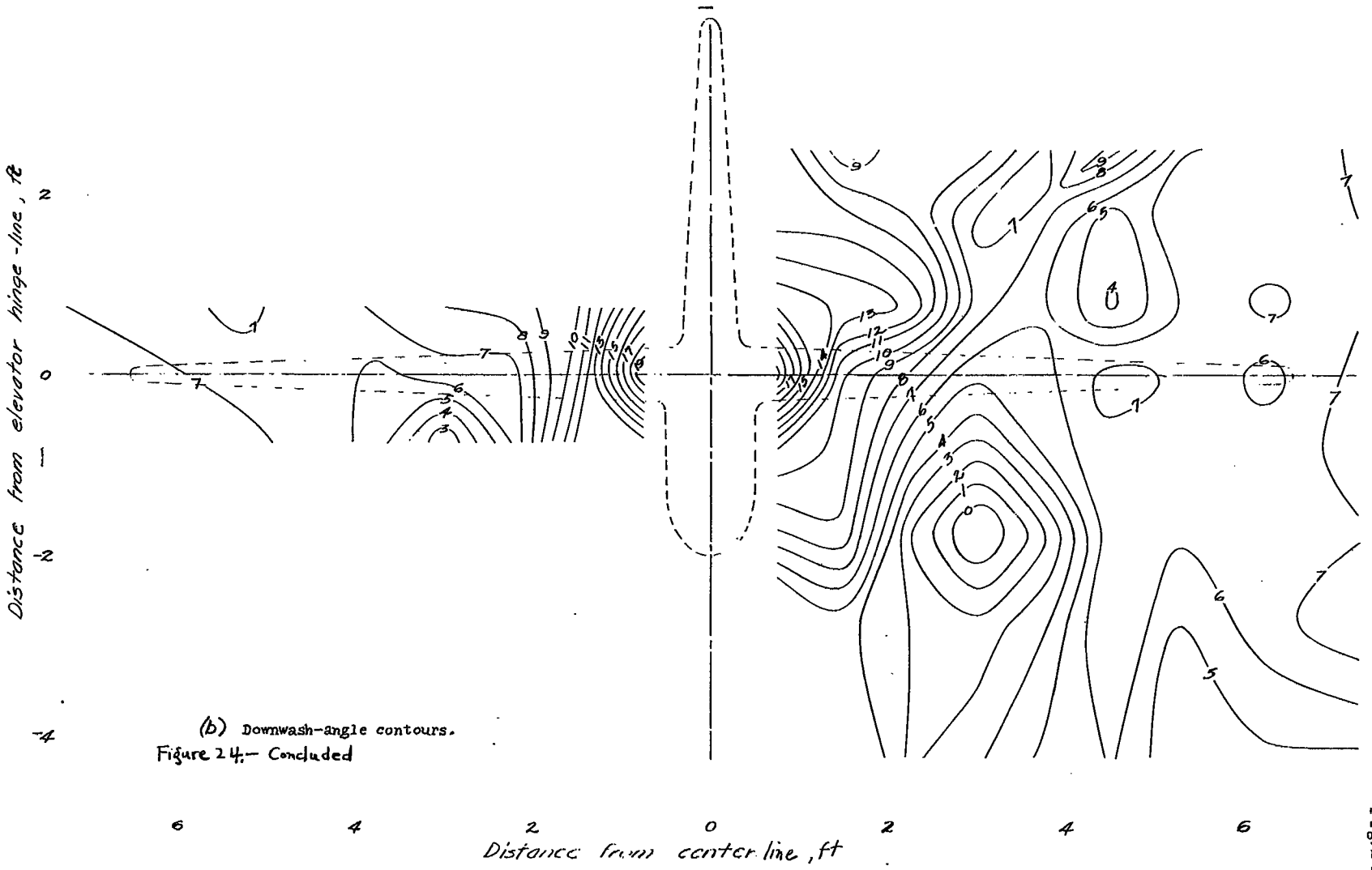

(b) Downwash-angle contours.

Figure 24.- Concluded

(a) Dynamic-pressure (q/q_o) contours.

Figure 25.- Air flow in the plane of the elevator hinge line of the BT-9B airplane. View looking forward; α_T, 11.9°; $\frac{\delta_T}{\pi}c$, 0.74.

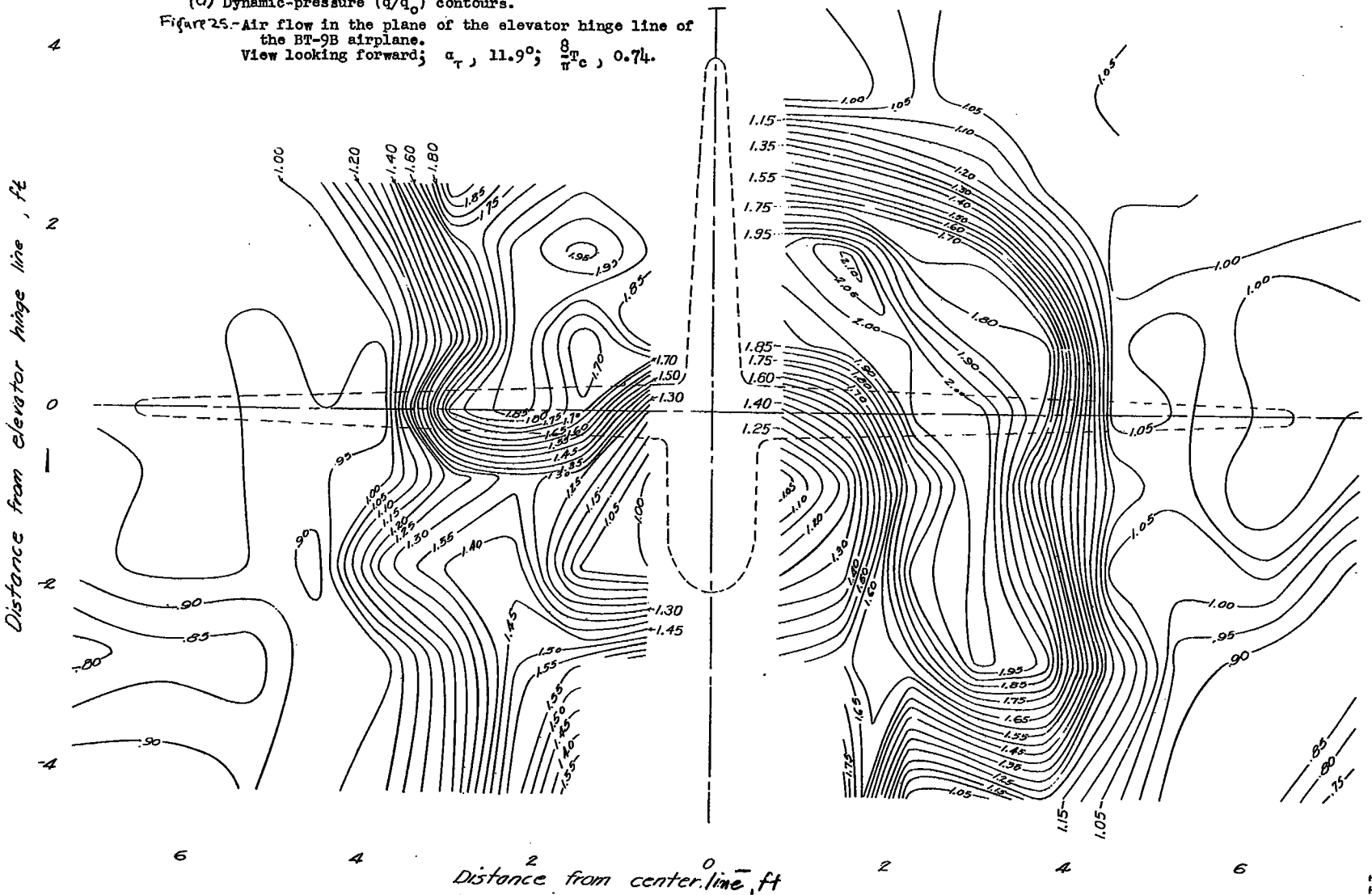

NACA

Fig. 25a

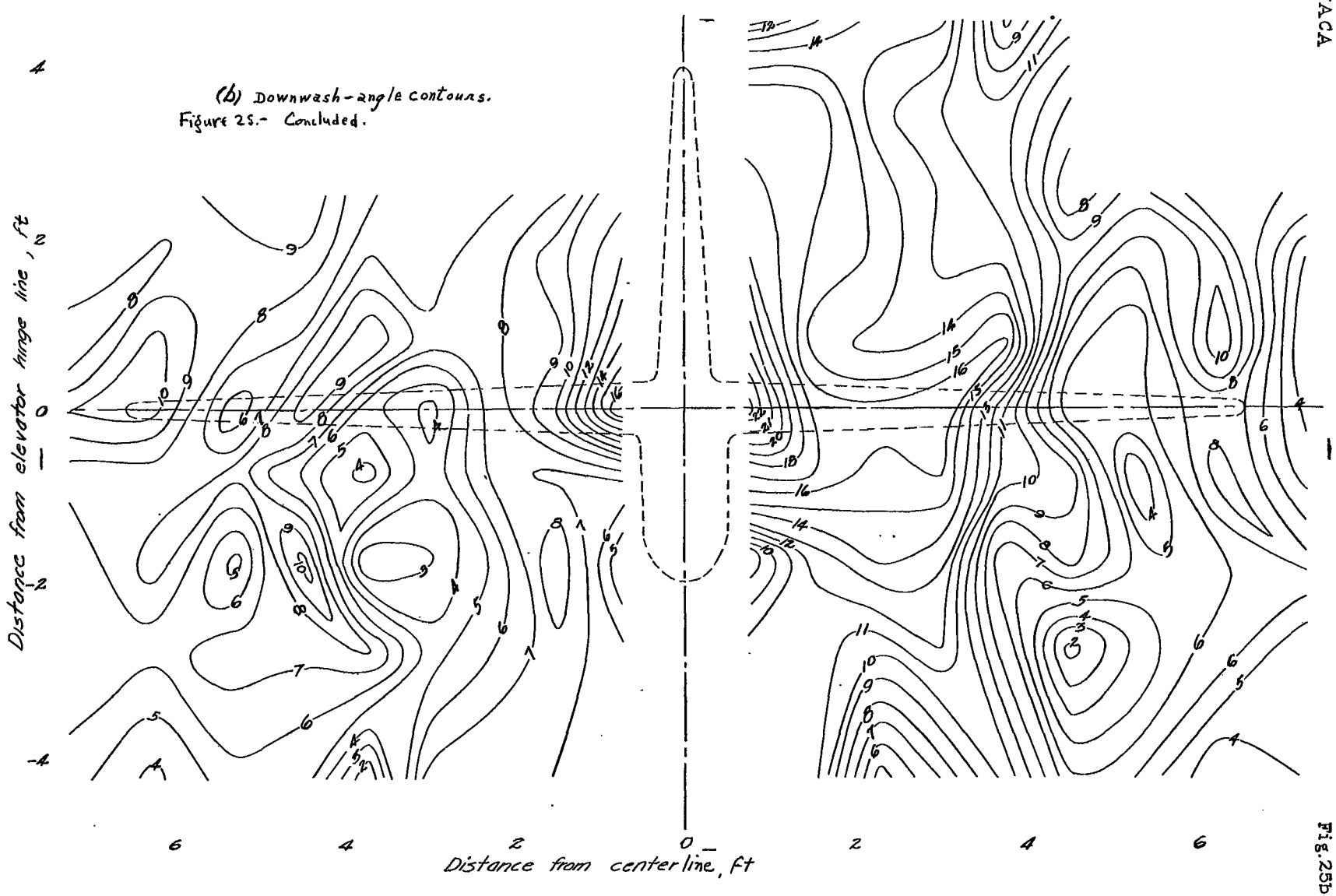
(b) Downwash-angle contours.
Figure 25.- Concluded.
Distance from elevator hinge line, ft
4
2
0
-2
-4
6
4
2
0
2
4
6
Distance from centerline, ft

NACA

Fig. 25b

(a) Dynamic-pressure (q/q_0) contours.

Figure 26.- Air flow in the plane of the elevator hinge line of the BT-9B airplane. View looking forward; α_T, 11.9°; $\frac{8}{\pi}T_c$, 0.74.

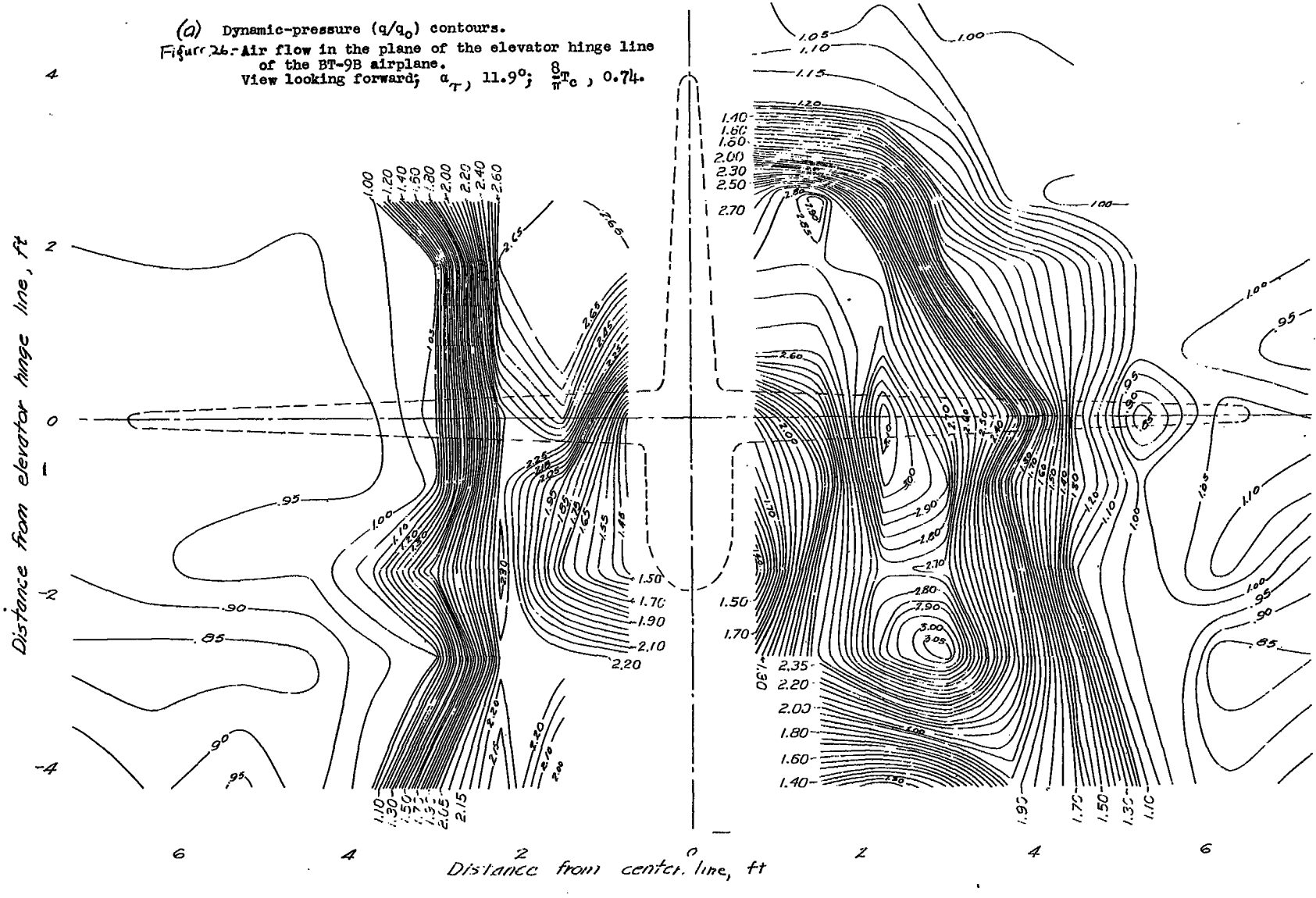

NACA

Fig. 26a

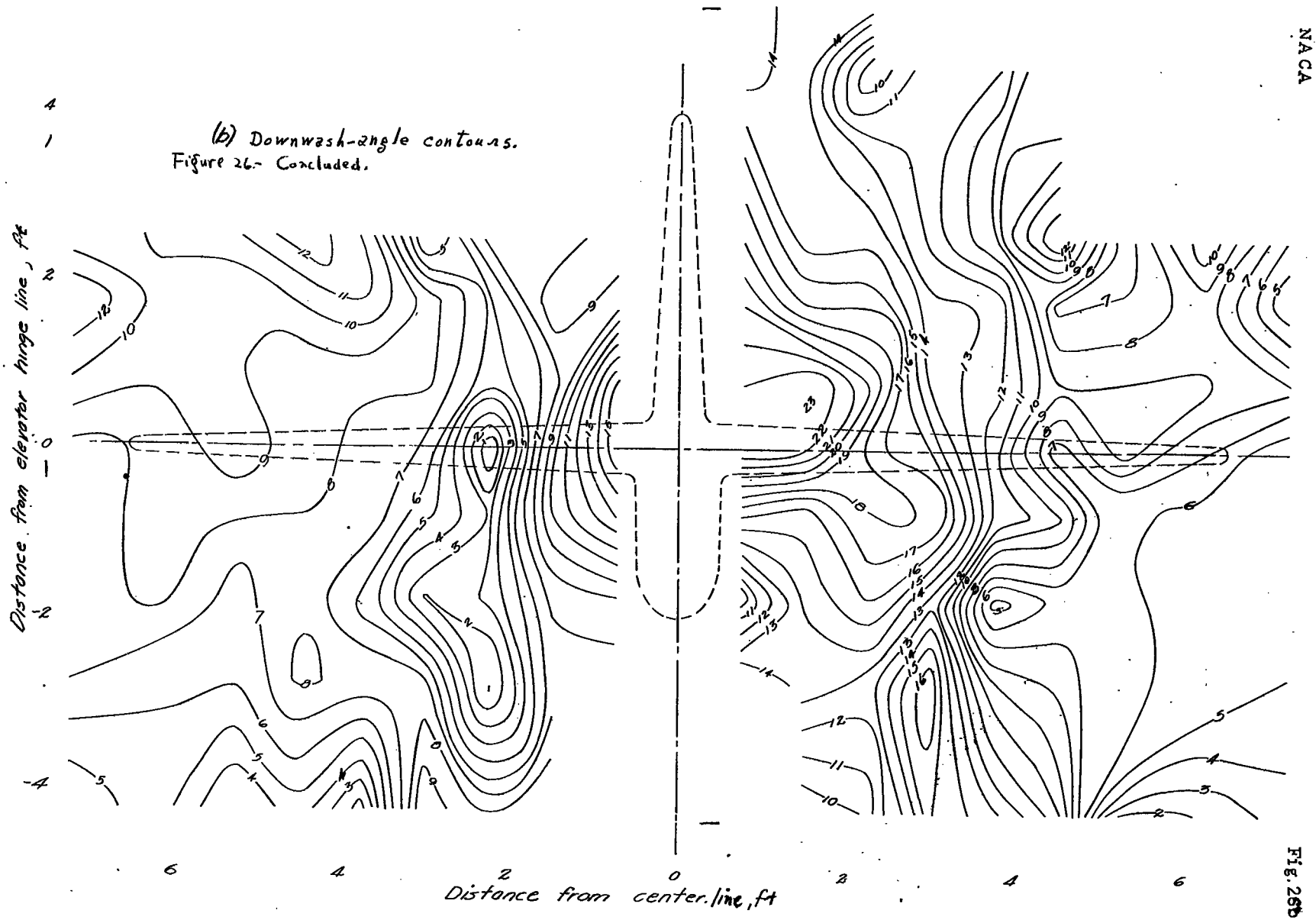

(b) Downwash-angle contours.

Figure 26.- Concluded.

L-761

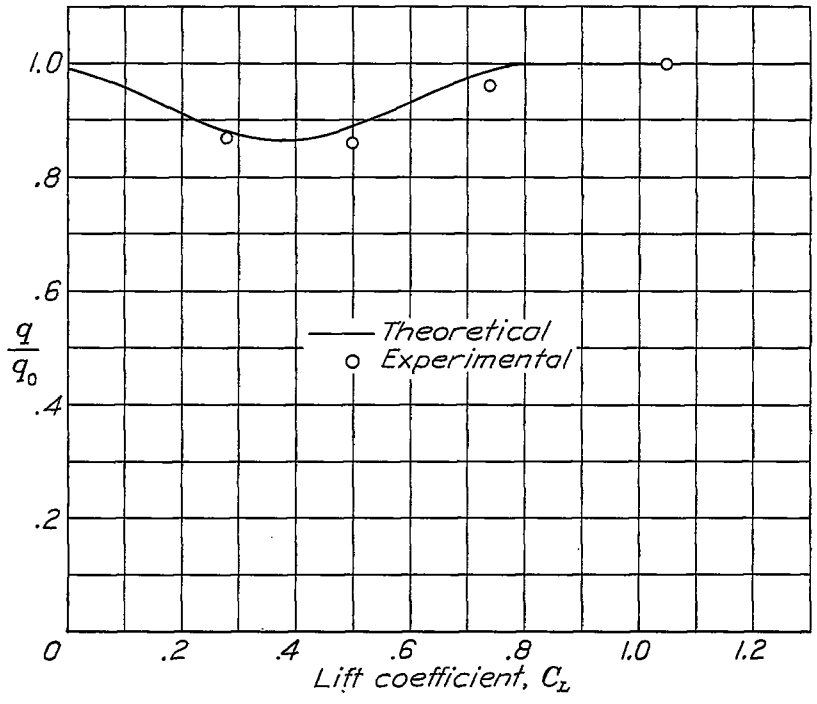

Figure 28.- Comparison of theoretical and experimental values of q/q_0 at tail location of XSBA-1 airplane due to wing wake.

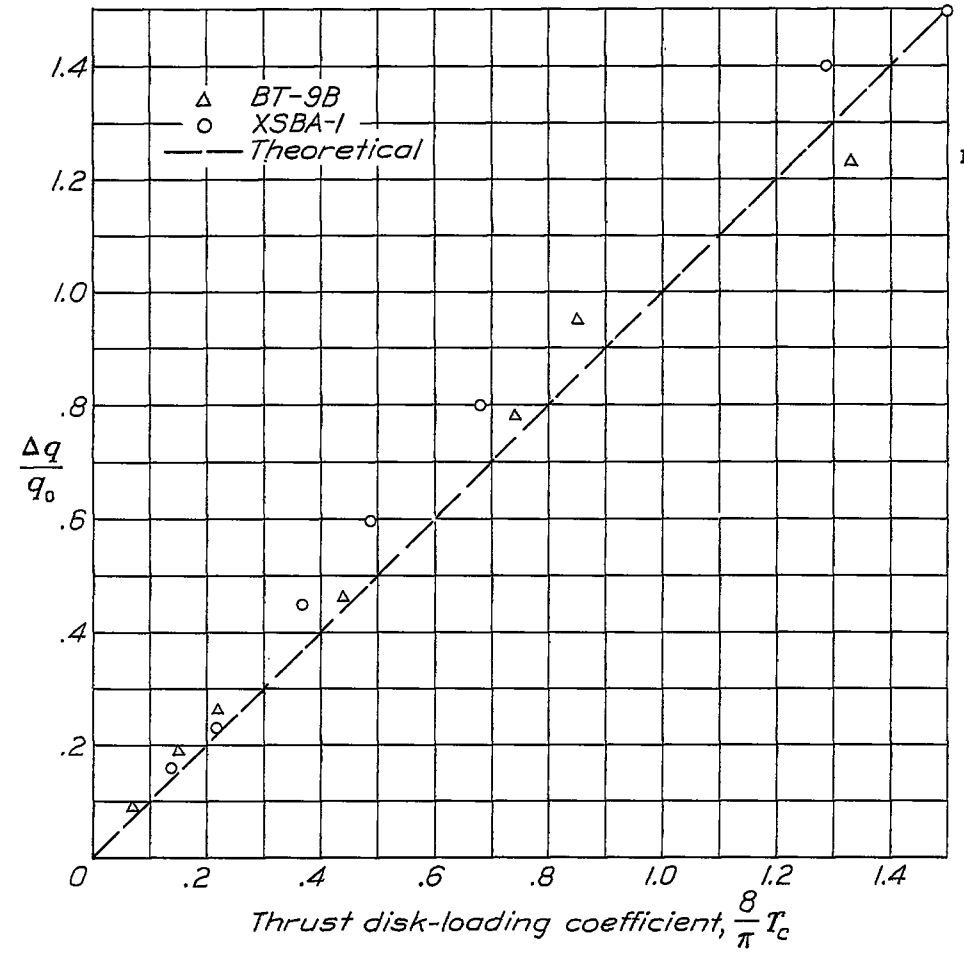

Figure 29.- Comparison of experimental and theoretical values of $\Delta q/q_0$ at the slipstream center line of the XSBA-1 and BT-9B airplanes. Points given represent average increment over a span of 4.5 feet(propeller radius).

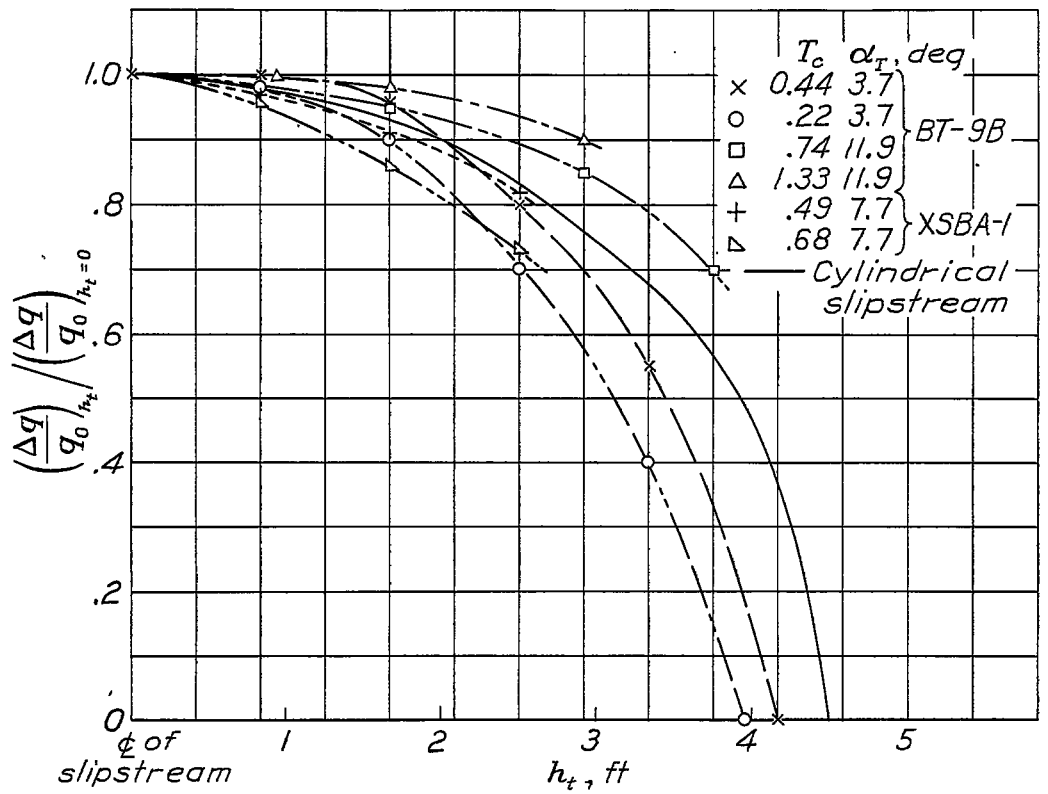

Figure 30.- Comparison of variation of actual average slipstream velocity with that expected from an idealized (cylindrical) slipstream for different distances from the slipstream center. (Results based on a constant propeller diameter of 9 ft.)

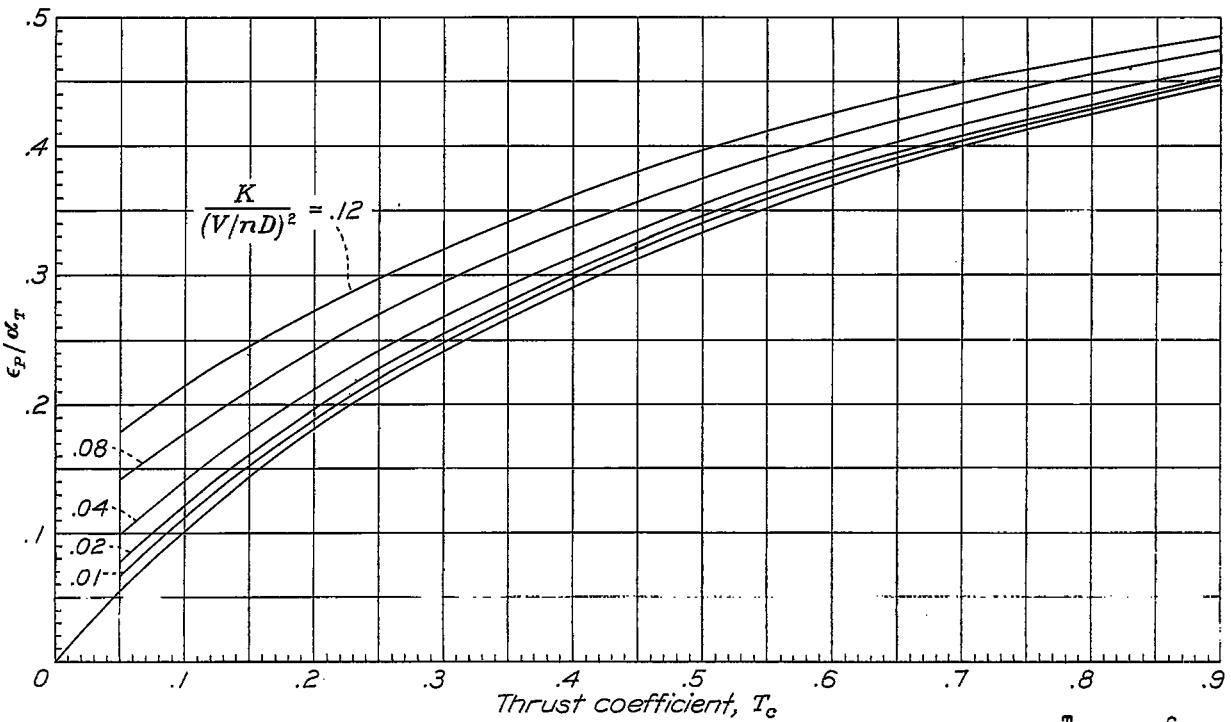

Figure 31.- Effect of propeller operating characteristics on downwash. $T_c = \frac{T}{\rho V^2 D^2} = \frac{C_T}{(V/nD)^2}$

L-761

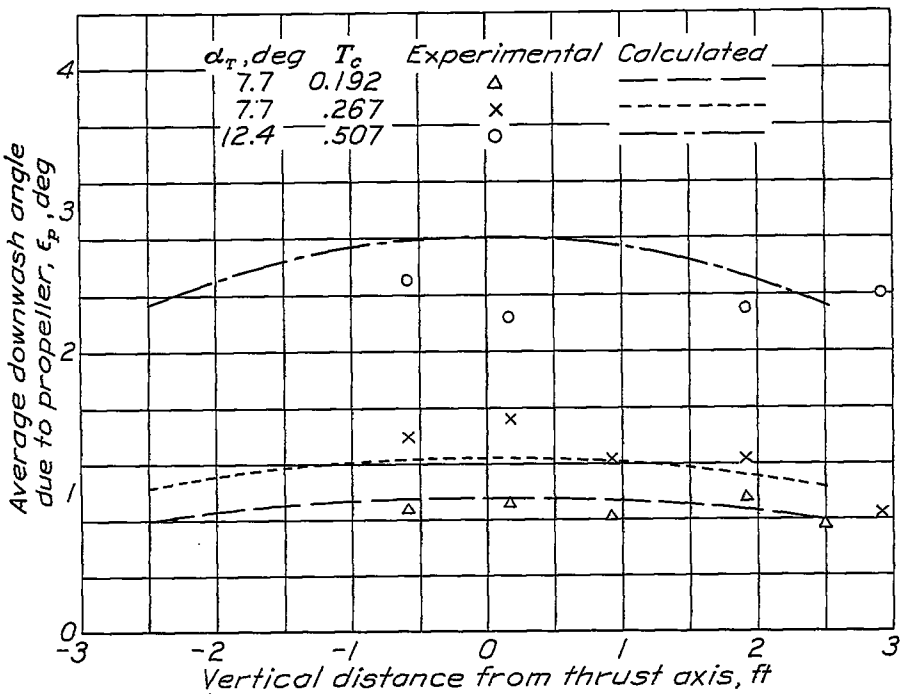

Figure 32.- Comparison of calculated and experimental average downwash angle due to propeller across tail span of XSBA-1 airplane.

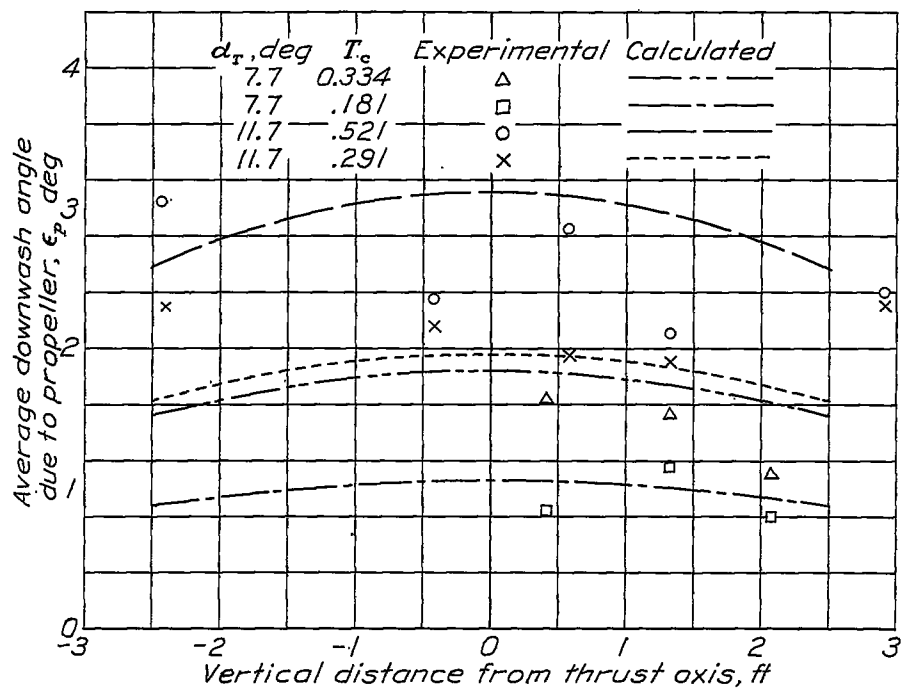

Figure 33.- Comparison of calculated and experimental average downwash angle due to propeller across tail span of BT-9B airplane.

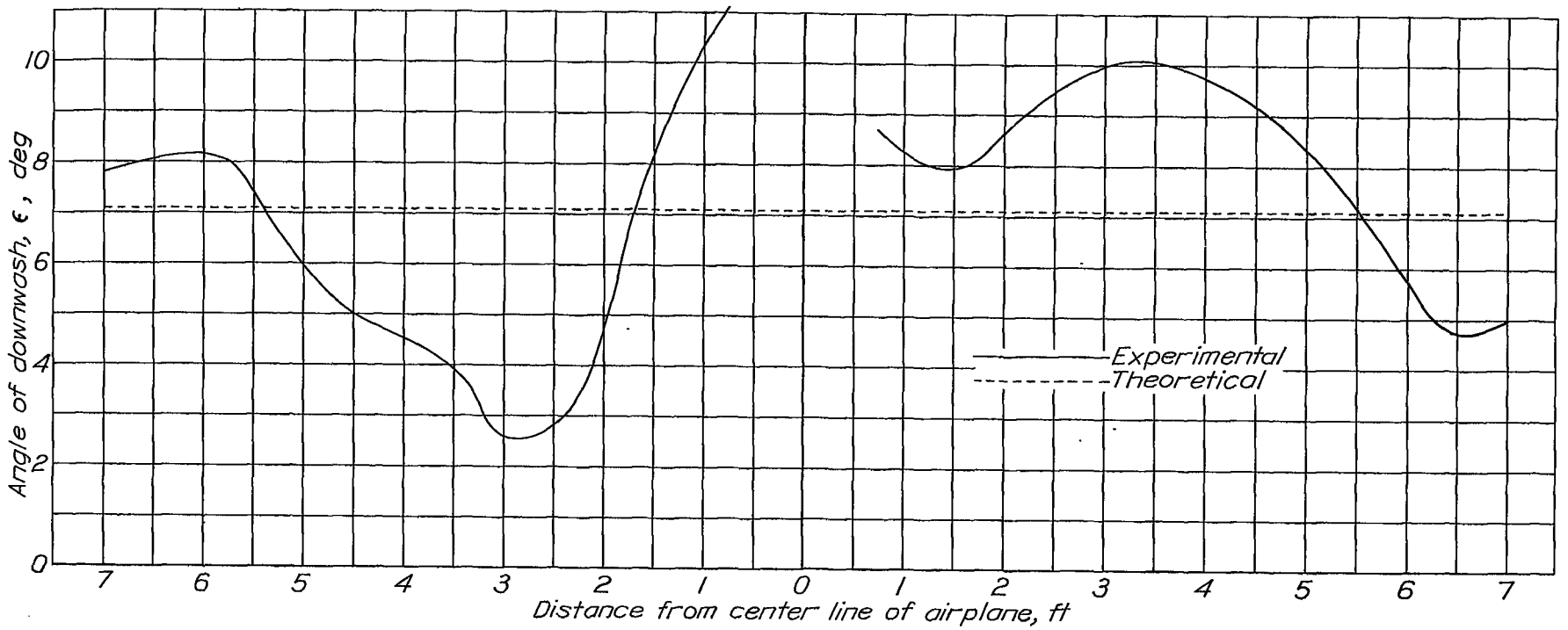

Figure 34.- Comparison of theoretical and experimental downwash-angle distribution in propeller slipstream. Across the hinge line of the XSBA-1 airplane ; α_T , 7.7° ; $8/\pi\ T_c$, 0.27 .

L-761

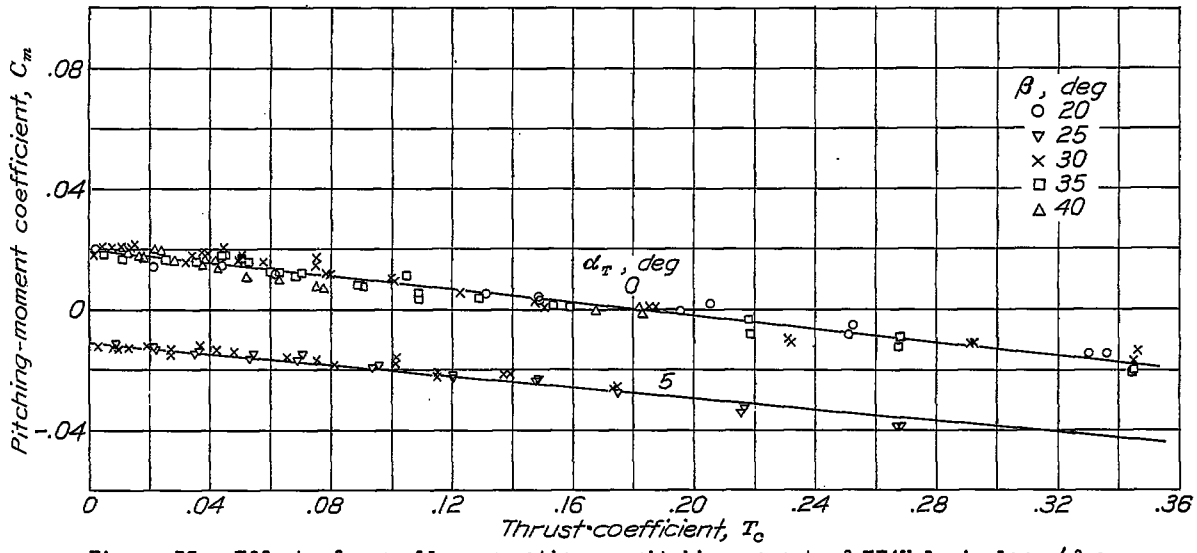

Figure 35.- Effect of propeller operation on pitching moment of XF4U-1 airplane (from unpublished data of 20-ft wind tunnel).

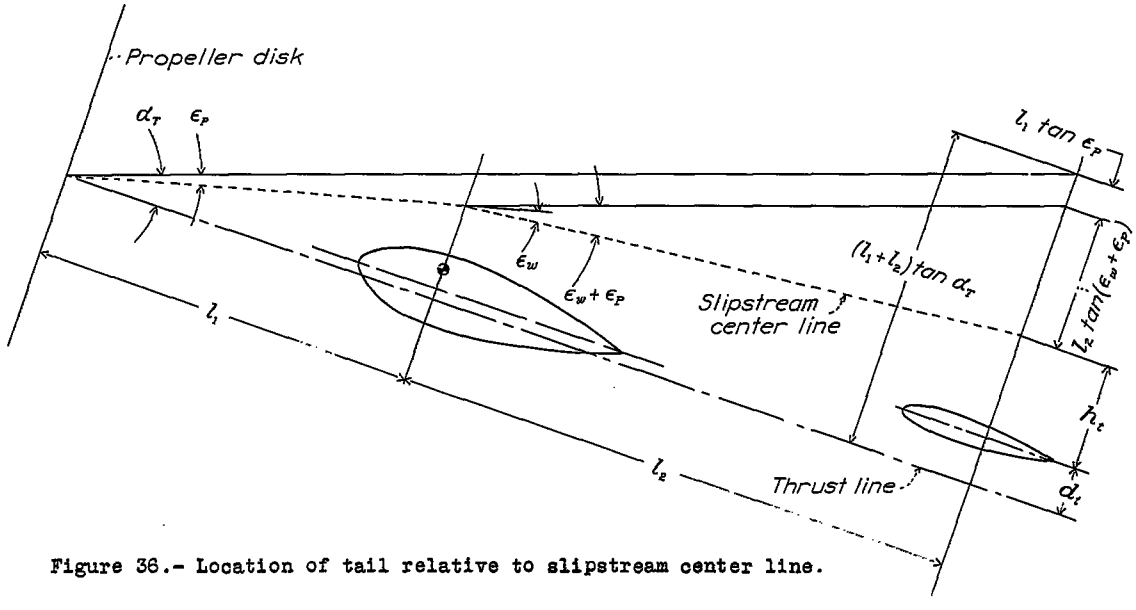

Figure 36.- Location of tail relative to slipstream center line.

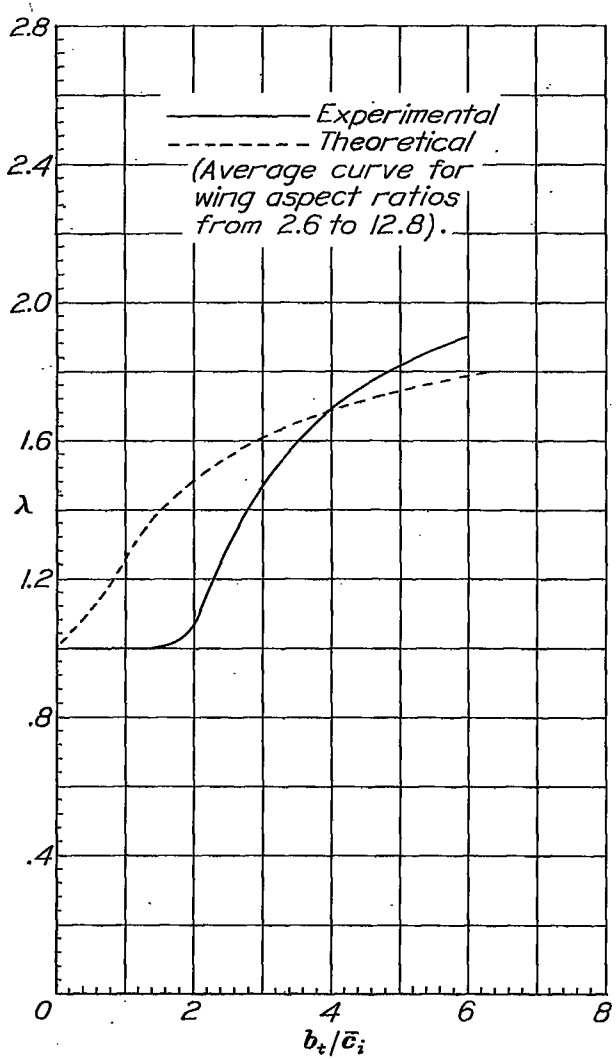

Figure 37.- Comparison of λ - curves from references 15 and 16.

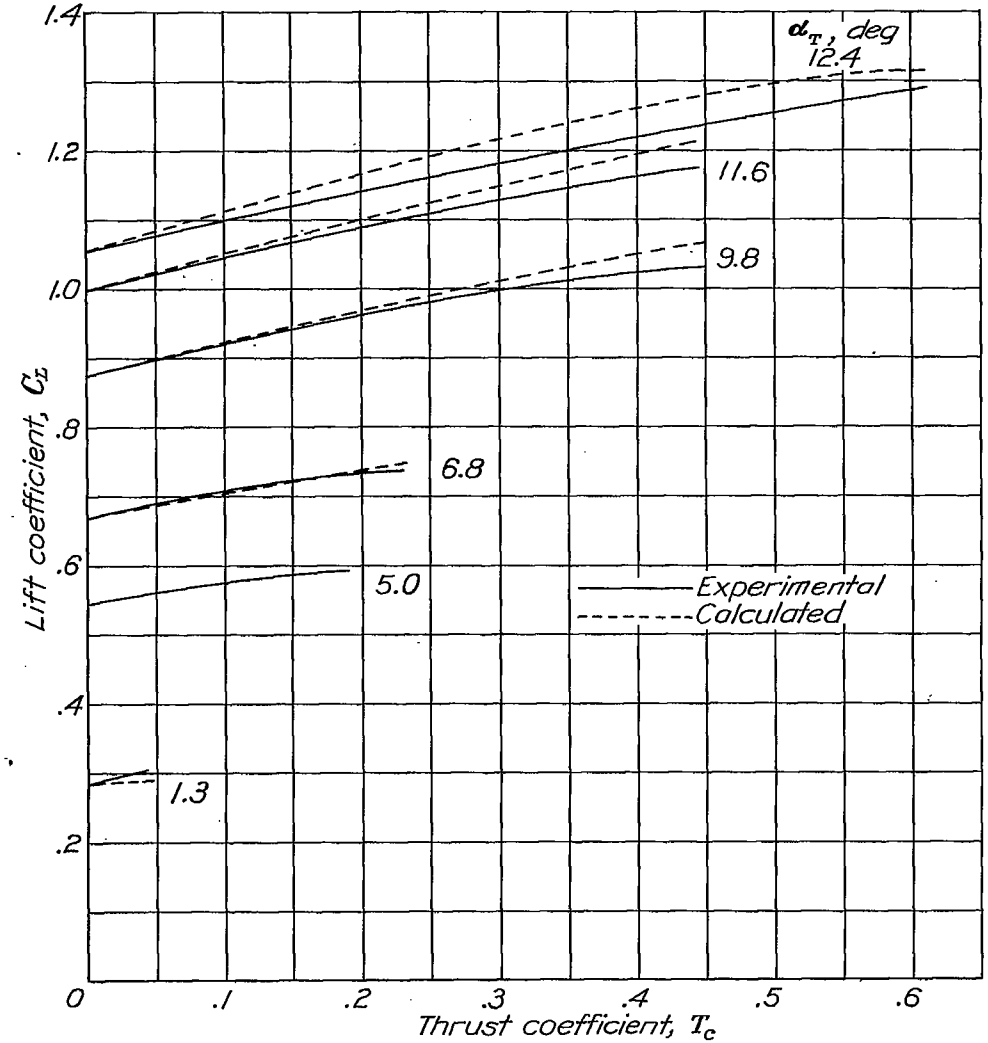

Figure 38.- Comparison of calculated and experimental effect of propeller operation on lift of XSBA-1 airplane with tail removed.

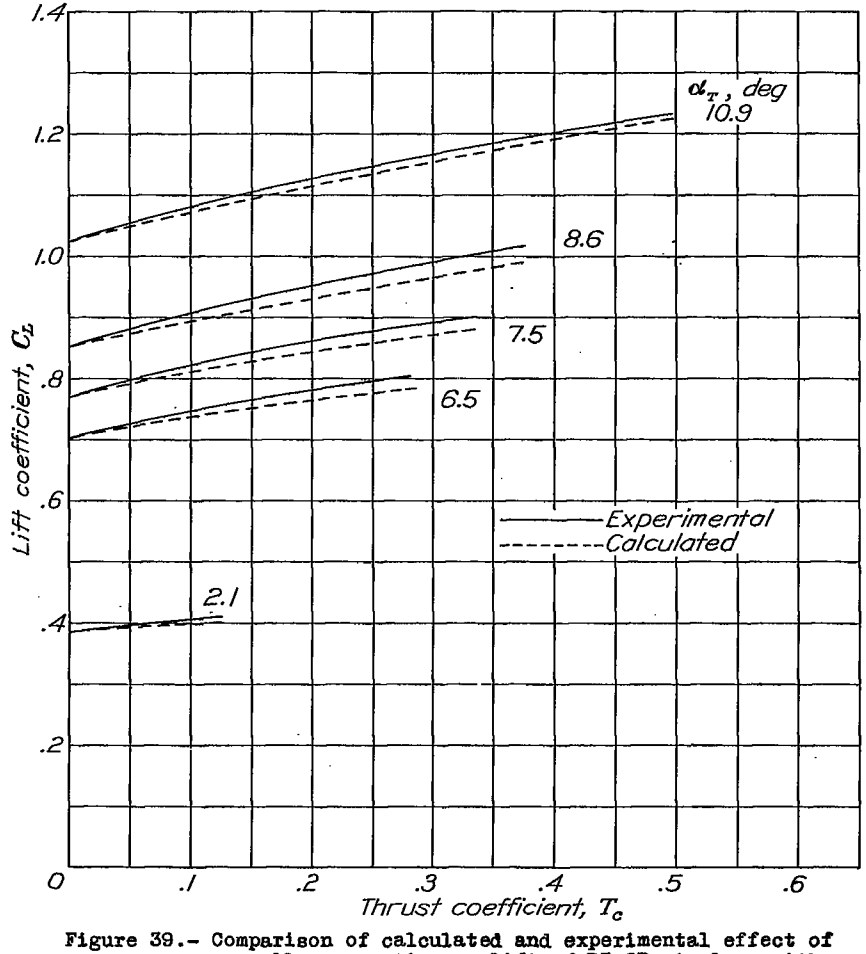

Figure 39.- Comparison of calculated and experimental effect of propeller operation on lift of BT-9B airplane with tail removed.

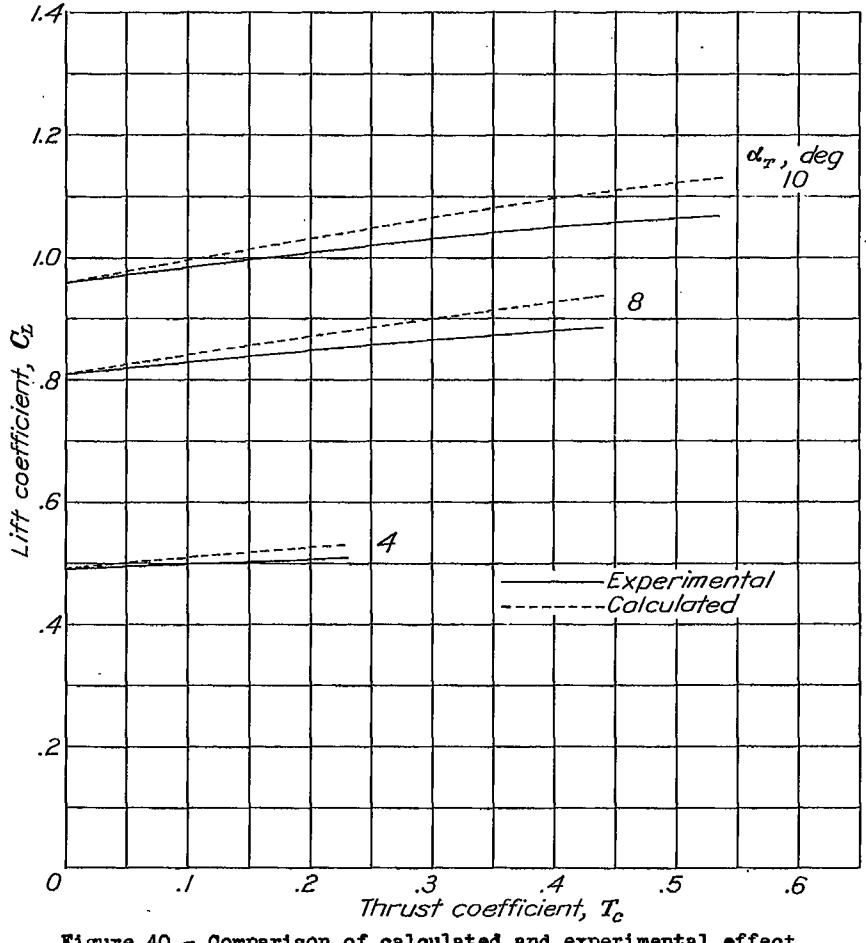

Figure 40.- Comparison of calculated and experimental effect of propeller operation on lift of P-36A airplane model with tail.(From unpublished data of 7-by 10- ft wind tunnel.)

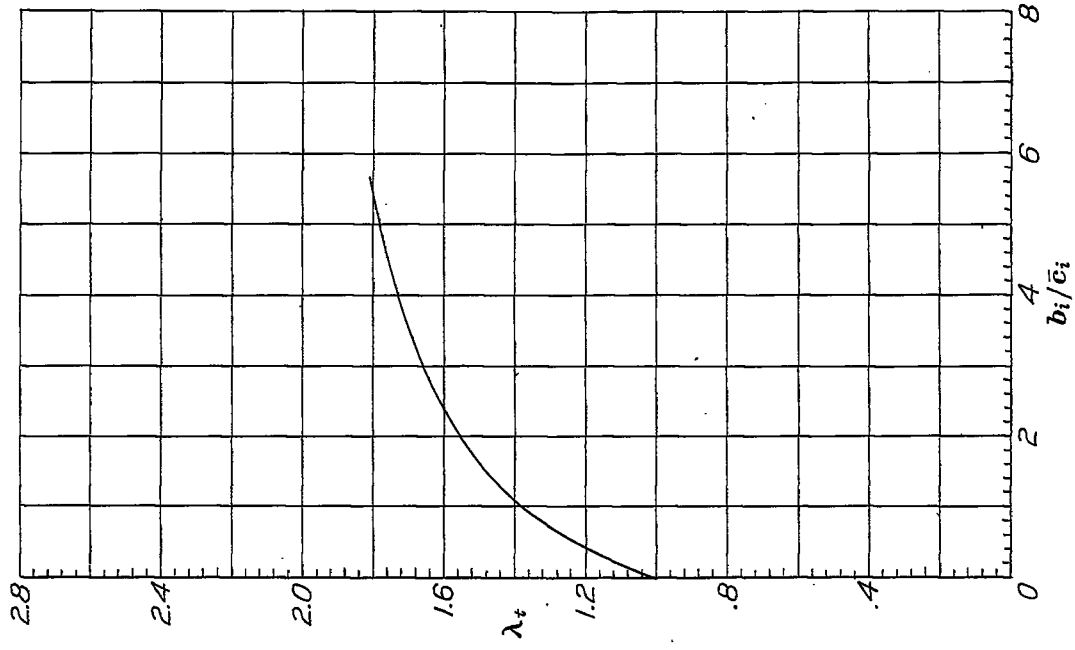

Figure 41.- Values of λ_t based on reference 15 for use with tail planes. The curve is an average one for tail aspect ratios from 2.6 to 6.4 .

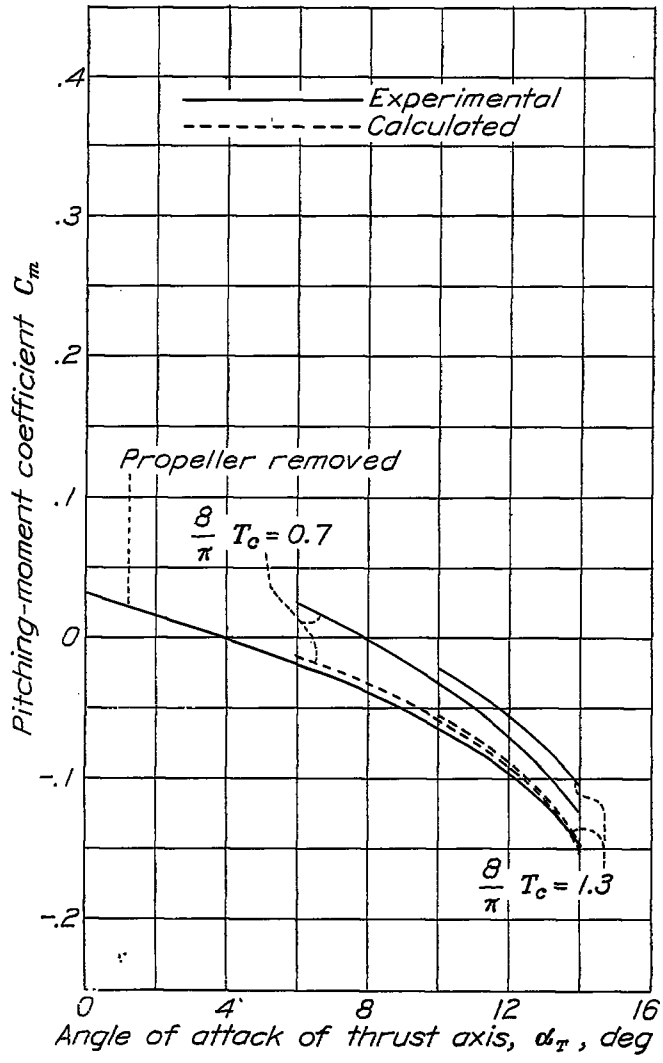

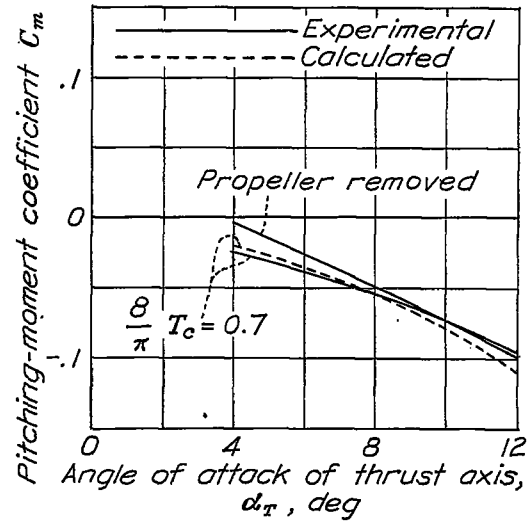

Figure 43.- Calculated and experimental variation of C_m with α_T for the BT-9B airplane.

Figure 42.- Calculated and experimental variation of C_m with α_T for the XSBA-1 airplane.

L-761

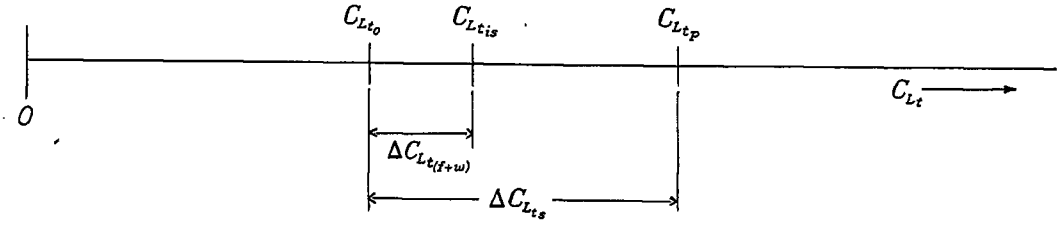

$$\Delta C_{L_{t_{(f+w)}}} = \frac{2(R_f+\delta)\bar{c}_{t_i}}{S_t}\lambda\,(S_f+S_w)C_{L_{t_{is}}}$$

$$\Delta C_{L_{t_s}} = \frac{b_{t_i}\bar{c}_{t_i}}{S_t}S_s\,(C_{L_{t_{is}}}\lambda_t - \frac{S_t}{S_w}\lambda' a_o \Delta\epsilon)$$

Figure 44.- Graphical representation of tail lift increments.

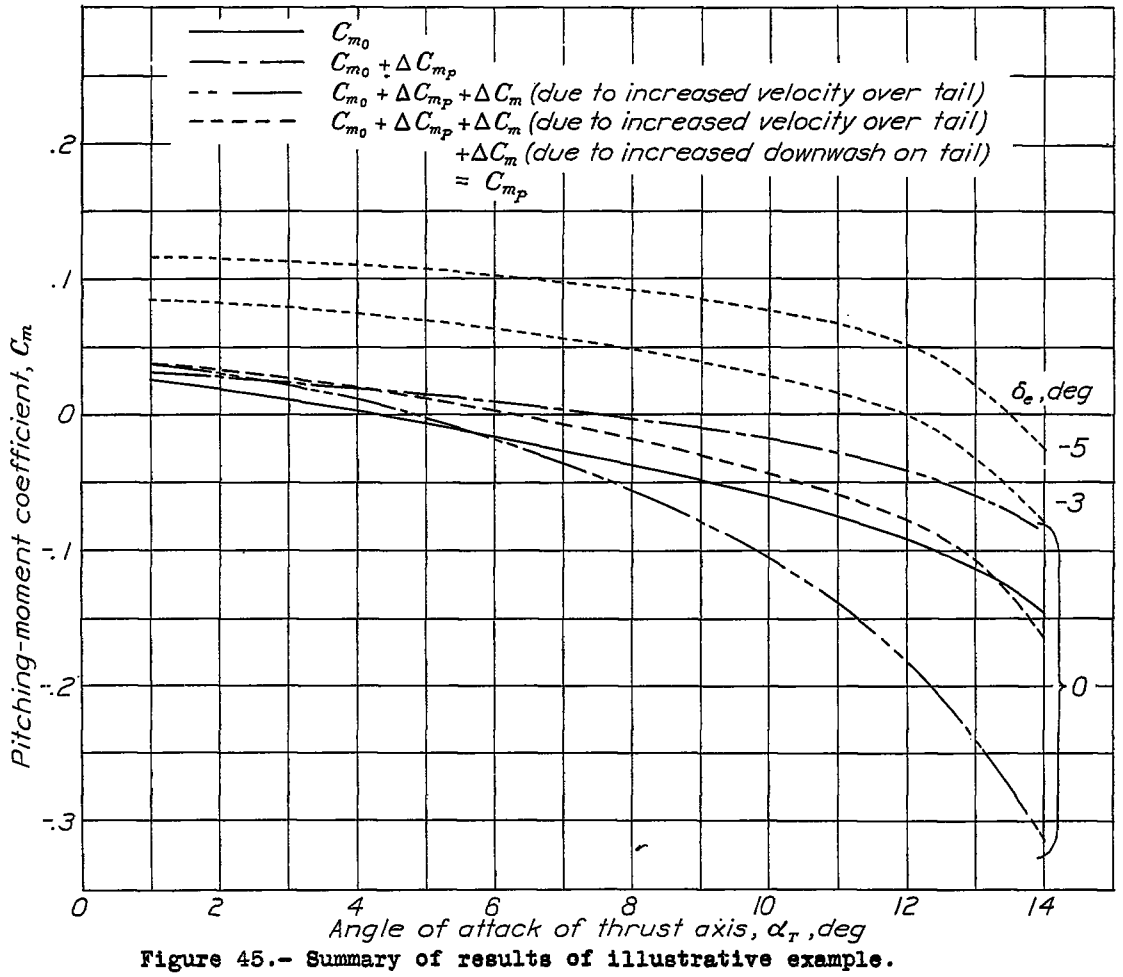

Figure 45.- Summary of results of illustrative example.